POLYHYDROXYALKANOATES FOR INNOVATIVE ELECTRODES AND PROTON EXCHANGE MEMBRANE MODIFICATION IN MICROBIAL FUEL CELL

SIRAJUDEEN, ABDUL AZEEZ OLAYIWOLA

FACULTY OF SCIENCE
UNIVERSITY OF MALAYA
KUALA LUMPUR

2020

POLYHYDROXYALKANOATES FOR INNOVATIVE ELECTRODES AND PROTON EXCHANGE MEMBRANE MODIFICATION IN MICROBIAL FUEL CELL

SIRAJUDEEN, ABDUL AZEEZ OLAYIWOLA

THESIS SUBMITTED IN FULFILMENT OF THE REQUIREMENTS FOR THE DEGREE OF DOCTOR OF PHILOSOPHY

INSTITUTE OF BIOLOGICAL SCIENCE
FACULTY OF SCIENCE
UNIVERSITI MALAYA
KUALA LUMPUR

2020

UNIVERSITI MALAYA

ORIGINAL LITERARY WORK DECLARATION

Name of Candidate: **SIRAJUDEEN, ABDUL AZEEZ OLAYIWOLA**

Registration/Matric No: **SVA170048**

Name of Degree: **DOCTOR OF PHILOSOPHY**

Title of Thesis: **POLYHYDROXYALKANOATES FOR INNOVATIVE ELECTRODES AND PROTON EXCHANGE MEMBRANE MODIFICATION IN MICROBIAL FUEL CELL**

Field of Study: **BIOTECHNOLOGY**

I do solemnly and sincerely declare that:

(1) I am the sole author/writer of this Work;
(2) This Work is original;
(3) Any use of any work in which copyright exists was done by way of fair dealing and for permitted purposes and any excerpt or extract from, or reference to or reproduction of any copyright work has been disclosed expressly and sufficiently and the title of the Work and its authorship have been acknowledged in this Work;
(4) I do not have any actual knowledge nor do I ought reasonably to know that the making of this work constitutes an infringement of any copyright work;
(5) I hereby assign all and every rights in the copyright to this Work to the University of Malaya ("UM"), who henceforth shall be owner of the copyright in this Work and that any reproduction or use in any form or by any means whatsoever is prohibited without the written consent of UM having been first had and obtained;
(6) I am fully aware that if in the course of making this Work I have infringed any copyright whether intentionally or otherwise, I may be subject to legal action or any other action as may be determined by UM.

Candidate's Signature   Date: 15/07/2020

Subscribed and solemnly decl

Witness's Signature   Date:

Name

Desig

POLYHYDROXYALKANOATES FOR INNOVATIVE ELECTRODES AND PROTON EXCHANGE MEMBRANE MODIFICATION IN MICROBIAL FUEL CELL

ABSTRACT

The increase in global energy demand due to increasing population and industrialization demands renewable and environmental-friendly alternatives. Energy from fossil fuel are non-renewable, depleting and detrimental from environmental perspectives. Alternative energy, green and renewable such as hydrogen fuel, biodiesel, bioethanol, microbial fuel cell and many more have been extensively investigated. One possible solution lies with non-combustion method such as microbial fuel cell. A microbial fuel cell is a sustainable and environmental-friendly device that combines electricity generation and wastewater treatment through metabolic activities of microorganisms. However, low power output from inadequate electron transfer to the anode electrode hampers its practical implementation. Nanocomposite of oxidized carbon nanotubes and medium-chain-length polyhydroxyalkanoates (mcl-PHA) grafted with methyl acrylate monomers enhances anode-cathode electrodes electrochemical function in microbial fuel cell. Extensive polymerization of methyl acrylate monomers within mcl-PHA matrix, and homogenous dispersion of carbon nanotubes within the graft matrix are responsible for the enhancement. Modified electrodes exhibit high conductivities, enhanced redox peak and reduction of cell internal resistance up to 76 %. A stable voltage output at almost 700 mV running for 225 hours generating maximum power and current density of 351 mW/m^2 and 765 mA/m^2 respectively. Superior biofilm growth on modified anode surface as well as enhanced redox peak of modified cathode are responsible for improved electron transfer to the anode and efficient oxygen reduction rate at cathode, hence stable and elevated power output generation. Polyhydroxybutyrate (PHB) as an integrated component of ion exchange membrane in microbial fuel cell (MFC) was also investigated. PHB crystals ranging from 5-15 % (*w/w*) were thermally dispersed and composited within

iii

medium-chain-length polyhydroxyalkanoate (PHA) matrix as shown by spectroscopic analyses. The composite membranes were juxtaposed with Nafion membrane for improved ion conduction. Membrane with 10 % and 15 % (*w/w*) PHB recorded two-fold maximum voltage potential compared to Nafion membrane alone. A power density of 601 mW/m^2 was recorded for PHB 15% membrane, which was superior to Nafion membrane (520 mW/m^2). In operation with real wastewater, maximum voltage potential, water uptake, power and current densities, chemical oxygen demand (COD) removal, ammoniacal nitrogen (NH$_3$-N) removal, as well as coulombic efficiency (CE) recovery of the composite membrane are superior to Nafion; attributed primarily to high resistivity to oxygen molecules diffusion from cathode to anode compartments, which subsequently improved the overall MFC performance.

Keywords: Polyhydroxyalkanoates; Microbial fuel cell; Electrode modification; Ion permeability; Proton exchange membrane

POLIHIDROKSIALKANOAT UNTUK MODIFIKASI MEMBRANE PERIHAL ELEKTROD DAN PROTON DALAM MESIN FUEL MICROBIAL

ABSTRAK

Peningkatan permintaan tenaga global rentetat daripada peningkatan populasi dan perindustrian telah mewujudkan alternatif bagi tenaga yang boleh diperbaharui dan mesra alam sekitar. Tenaga dari bahan api fosil adalah tidak boleh diperbaharui, semakin berkurang dan merosakkan alam sekitar. Tenaga alternatif, hijau dan boleh diperbaharui seperti bahan api hidrogen, biodiesel, bioethanol, sel bahan bakar mikrob dan banyak lagi telah diperkenalkan. Salah satu daripada penyelesaian-penyelesaian yang terletak pada kaedah bukan pembakaran adalah seperti sel bahan bakar mikrob. Sel bahan bakar mikrob adalah peranti mesra alam yang menggabungkan usaha penjanaan elektrik dan rawatan air sisa melalui aktiviti metabolik mikroorganisma. Walau bagaimanapun, keluaran kuasa yang rendah daripada pemindahan elektron yang tidak mencukupi kepada elektrod anod menghalang pelaksanaan secara praktikal. Komposit nano tiub nano karbon teroksida dan polihidroksialkanoat berrantaian sederhana panjang (mcl-PHA) yang dicantum dengan monomer metil akrilat meningkatkan fungsi elektrokimia elektrod dalam sel bahan bakar mikrob. Pempolimeran monomer metal akrilat yang meluas dan penyebaran homogen tiub nano karbon dalam matriks dalam matriks mcl-PHA bertanggungjawab dalam peningkatan ini. Elektrod yang diubahsuai menunjukkan daya konduktiviti yang tinggi, puncak redoks yang lebih baik dan pengurangan rintangan dalaman sel sehingga 76%. Keluaran voltan yang stabil pada hampir 700 mV selama 225 jam menghasilkan kuasa maksimum dan ketumpatan arus yang baik, masing-masing 351 mW/m^2 dan 765 mA/m^2. Pertumbuhan biofilem yang unggul pada permukaan yang diubahsuai juga bertanggungjawab untuk pemindahan elektron yang lebih baik ke anod, justeru menjana keluaran kuasa yang stabil dan tinggi. Polihidroksibutirat (PHB) sebagai komponen bersepadu bagi membran pertukaran ion dalam sel bahan bakar mikrob (MFC) telah

dikaji. 5-15% (w/w) kristal PHB disebarkan secara termal dan digabungkan dalam matriks mcl-PHA seperti yang ditunjukkan dalam analisis spektroskopi. Membran komposit telah dibandingkan dengan membran Nafion untuk konduksi ion yang lebih baik. Membran dengan 10% dan 15% (w/w) PHB mencatatkan potensi voltan maksimum dua kali ganda berbanding membran Nafion sahaja. Ketumpatan kuasa 601 mW/m^2 dicatatkan untuk membran PHB sebanyak 15%, yang lebih tinggi daripada membran Nafion (520 mW/m^2). Dalam operasi dengan air kumbahan sebenar, potensi voltan maksimum, pengambilan air, kepadatan kuasa dan arus, penghapusan permintaan oksigen kimia (COD), penyingkiran nitrogen ammoniak (NH$_3$-N), serta pemulihan kecekapan Coulomb (CE) bagi membran komposit adalah lebih baik daripada Nafion; disebabkan oleh rintangan yang tinggi terhadap penyebaran oksigen daripada katod ke anod, seterusnya meningkatkan prestasi keseluruhan MFC.

Kata kunci: Polihidroksialkanoat; Sel bahan bakar mikrob; Pengubahsuaian elektrod; Kebolehtelapan ion; Membran pertukaran Proton

ACKNOWLEDGEMENTS

All praises and thanks be to Almighty Allah, the beneficient, the merciful for giving me the strength, courage, perseverance, wisdom and sustenance during the course of the study. I pray for HIS endless blessings and mercies on the acquired knowledge and the degree, Aameen.

I wish to express my profound and sincere gratitude to my supervisor, Prof. Dr. Mohamad Suffian Mohamad Annuar for his guidance, encouragement, tolerance, close supervision, simplicity, devotion and tireless efforts in making this project a reality despite his busy schedules. His immense knowledge helped me throughout the period of my study and in writing of this thesis. I could not have imagined having a better supervisor and mentor to gain so much experience and knowledge from. May the Almighty grant you all your desires.

My sincere appreciation goes to my colleagues in bioprocess and enzyme technology lab especially Syed Mohamad Daniel, Dr. Cha, Dr. Naziz, Haziq, Shafiq, Suhaiyati, Ali, Peyling, Fadli and Afiqah for their technical supports, stimulating discussions, enlightenments and wonderful moments during the course of my study. In particular, I am grateful to Dr. Hindatu Yusuf for enlightening me the first glance of research.

My everlasting appreciation goes to my parents, and siblings for supporting me finantially, spiritually, emotionally and morally since my existence in life. Most importantly, my boundless appreciation goes to my wonderful, awesome, beloved and dearest wife, Nafeesah Olamide Nasirudeen and to my beautiful, lovely, adorable little daughter, Leen Adesewa Abdul Azeez for their sacrifice, prayers, patience, love and understanding throughout the course of the study. May Allah bless you all and grant all your heart desires, Aameen. I love you all!!!

TABLE OF CONTENTS

LIST OF FIGURES

LIST OF TABLES

LIST OF SYMBOLS AND ABBREVIATIONS

Symbols

%	:	Percent
±	:	Plus and minus
μ	:	Micro
μL	:	Microliter
e^-	:	Electron
ºC	:	Degree Celsius
α	:	Alpha
β	:	Beta
δ	:	Conductivity
θ	:	Theta
Ω	:	Ohm
cm	:	Centimeter
cm^2	:	Centimeter squared
$CaCl_2 \cdot 2H_2O$:		Calcium chloride dehydrate
Co	:	Cobalt
CO_2	:	Carbon dioxide
Cu	:	Copper
Fe_2O_4	:	Ferric oxide
g/L	:	Gram per liter
H^+	:	Hydrogen ion
H_2O	:	Water
H_2O_2	:	Hydrogen peroxide
H_2SO_4	:	Sulphuric acid
Hz	:	Hertz

HCl	:	Hydrochloric acid
I	:	Current
K_2HPO_4	:	Dipotassium phosphate hydrogen phosphate
$K_3Fe(CN)_6$	:	Potassium hexacyanoferrate III
KH_2PO_4	:	Monopotassium phosphate hydrogen phosphate
KHz	:	Kilohertz
KOH	:	Caustic potash
mA/m^2	:	Milliampere per meter squared
mg	:	Milligram
$MgSO_4$	:	Magnesium sulfate
$MgSO_4 \cdot 7H_2O$:		Magnesium sulfate heptahydrate
mL	:	Milliliter
mM	:	Millimolar
M_n	:	Number-averaged molecular weight
MnO_2	:	Manganese dioxide
mV	:	Millivoltage
M_w	:	Weight-averaged molecular weight
mW/m^2	:	Milliwatts per meter squared
Na_2HPO_4	:	Disodium hydrogen phosphate
NaCl	:	Sodium chloride
NaH_2PO_4	:	Sodium dihydrogen phosphate
$NaHCO_3$	:	Sodium bicarbonate
NH_3	:	Ammonia
NH_3N	:	Ammoniacal nitrogen
NH_4Cl	:	Ammonium chloride
Ni	:	Nickel

nm	:	Nanometer
O$_2$	:	Oxygen
Pt	:	Platinum
SiO$_2$	:	Silicon dioxide
S-SiO$_2$	:	Sulfonated silicon dioxide
TiO$_2$	:	Titanium dioxide
v/v	:	Volume per volume
w/w	:	Weight per weight

Abbreviations

AC	:	Activated carbon
CB	:	Carbon black
CC	:	Carbon cloth
CE	:	Coulombic efficiency
CF	:	Carbon fiber
CNT	:	Carbon nanotube
COD	:	Chemical oxygen demand
CP	:	Carbon paper
CV	:	Cyclic voltammetry
DCM	:	Dichloromethane
DMF	:	Dimethylformamide
DS	:	Degree of sulfonation
EIS	:	Electrochemical impedance spectroscopy
ESA	:	Electrode surface area
FESEM	:	Field emission scanning electron microscope
FTIR	:	Fourier transfer infrared

G	:	Graphene
GB	:	Graphite brush
GCMS	:	Gas chromatography-mass spectrometry
GO	:	Graphene oxide
GPC	:	Gel permeation chromatography
H^1 NMR	:	Proton nuclear magnetic resonance
HFP	:	Hexafluoropropylene
lcl-PHA	:	Long-chain-length polyhydroxyalkanoate
MA	:	Methyl acrylate
mcl-PHA	:	Medium-chain-length polyhydroxyalkanoate
MFC	:	Microbial fuel cell
MWCNT	:	Multi-walled carbon nanotube
OCV	:	Open circuit voltage
OD	:	Optical density
ORR	:	Oxygen reduction reaction
P	:	Phosphorus
PAM	:	Polyacrylamide
PANI	:	Polyaniline
PANInf	:	Polyaniline nanofibers
PBI	:	Polybenzimidazole
PCL	:	Polycaprolactone
PD	:	Power density
PDI	:	Polydispersity index
PEDOT	:	Poly(3,4-ethylenedioxythiophene)
PEEK	:	Polyether ether ketone
PEGMA	:	Polyethylene glycol methacrylate

PEM	:	Proton exchange membrane
PES	:	Polyethersulfone
PHA	:	Polyhydroxyalkanoate
PHB	:	Polyhydroxybutyrate
PHBV	:	Poly(3-hydroxybutyrate-*co*-3-hydroxyvalerate*)*
PNIPAM	:	Poly N-isopropylacrylamide
PPy	:	Polypyrrole
PS	:	Polysulfone
PVDF	:	Polyvinylidene fluoride
PVP	:	Polyvinylpyrrolidone
QPEEK	:	Quaternized polyether ether ketone
R	:	Resistance
Redox	:	Oxidation reduction reaction
rGO	:	Reduced graphene oxide
scl-PHA	:	Short-chain-length polyhydroxyalkanoate
SEM	:	Scanning electron microscope
SPANI	:	Sulfonated polyaniline
SPEEK	:	Sulfonated polyether ether ketone
SPES	:	Sulfonated polyethersulfone
SS	:	Stainless steel
SSEBS	:	Sulfonated polystyrene ethylene butylene polystyrene
SSFF	:	Stainless steel fiber felt
SSM	:	Stainless steel mesh
SSS	:	Sodium styrene sulfonate
SWCNT	:	Single-walled carbon nanotube
TGA	:	Thermogravimetric analysis

TS	:	Titanium suboxide
UPW	:	Ultra-pure water
V	:	Voltage
XRD	:	X-ray diffraction

LIST OF APPENDICES

CHAPTER 1: INTRODUCTION

The current rate of CO_2 release, mainly from non-renewable energy sources, could result in 1.5 °C increase in global warming by the year 2040 (Hoegh-Guldberg et al., 2018). Hence, the urgency to develop and improve alternative energy sources that are renewable, economical and environmental-friendly. With respect to these features, microbial fuel cell (MFC) stands out as a promising alternative green energy source. The device ability to combine electric current generation from the electrons released by metabolic activities of microorganisms, and wastewater treatment made it a unique energy source (Almatouq & Babatunde, 2018). A double-chambered MFC consists of anode and cathode chambers separated by a proton exchange membrane (PEM).

In MFC operation, the abundance and high reduction potential of oxygen has made it the most suitable and practical electron acceptor (Li et al., 2017). However, the slow oxygen reduction reaction (ORR) at the cathode electrode negatively affecting the overall power output necessitates the use of a catalyst in the cathode for balanced rate of ORR (Zhu et al., 2016). The most commonly utilized catalyst as cathode modifier is platinum (Pt) due to its longevity, stability and high catalytic potential. Unfortunately, its rarity makes it an expensive option (Jafary et al., 2018), and being classified as a heavy metal, the exposure to its salts could pose adverse health effects. Carbon based nanomaterials such as activated carbon (AC), carbon black (CB), graphene, single-walled and multi-walled carbon nanotube among others are seen as viable alternatives to Pt (Ahmed et al., 2012; Ates et al., 2017; Li et al., 2012). In order to lower the cost of cathode catalyst and at the same time increase its ORR potential, researchers have focused mainly on the nanocomposition of alternative catalysts. These include Ni/AC composite (Luo & He, 2016), AC/CB composite (Merino-Jimenez et al., 2016), reduced graphene oxide composited with MnO_2 (MnO_2/rGO) (Rout et al., 2018), ferric nitrate/AC nanocomposite

(Tofighi et al., 2018), and polyaniline nanofiber (PANInf) composited with CB. Recently, Papiya et al. (2018) developed a novel polymeric cathode electrode composed of Ni:Co (1:1) supported sulfonated polyaniline (Ni:Co/SPAni) for a single chamber MFC application. The maximum power density of ~ 659.79 mW/m^2 was observed which was greater than that of Pt/C cathode electrode (~ 483.48 mW/m^2). The superior performance in ORR observed by the polymeric-metal catalysts is the results of higher catalytic activity, uniform dispersion of the nanoparticles and good chemical stability of the composited electrodes.

Among major challenges hindering the practical application of MFC is inadequate transfer of electrons released from metabolism to the anode electrode (Yusuf et al., 2018). The encumbrance in the electron transfer has been attributed to over-potential of anode electrodes which arise due to loss in; initiation of oxidation reaction (activation), bacterial metabolism, and concentration gradient (mass transport) (Logan, 2008). Conventional anode electrodes such as stainless steel fiber felt (SSFF), carbon cloth (CC) and carbon paper (CP) amongst others have been modified with catalysts for better activation, low internal resistance for improved electron transfer (Yusuf et al., 2018) and ideal size compatibility for maximum internal colonization by electrogens (Hu & Cui, 2012). A recent review detailing various improvements to anode electrode needed to circumvent the loss in electron transfer, and for overall improvement of MFC power generation efficiency was presented by Hindatu et al. (2017a). This includes modification of anode electrode with graphite-based material (Chou et al., 2014), metal oxide nanocomposition (Alatraktchi et al., 2014), chemical and electrochemical modifications (Liu et al., 2014) and polymeric modification (Hindatu et al., 2017b). The latter has been reported to improve extracellular transfer of electron, thereby reducing the internal resistance and concomitantly improved power output (Cui et al., 2015; Kang et al., 2015; Wang et al., 2014).

Considering the architecture of anode electrode in MFC, the physical integrity of the electrode is of great importance as the anode is exposed to aqueous environment consisting of electrogens and substrate. The electrode must be hydrophobic enough to prevent early damage to the electrode due to swelling effect (Sarathi & Nahm, 2013). Conducting polymers such as polyaniline (PANI) (Cui et al., 2015; Gao et al., 2012; Hou et al., 2015; Wang et al., 2014), polypyrrole (Kumar et al., 2014; Roh & Woo, 2015), and poly(3,4-ethylenedioxythiophene) (Chou et al., 2014; Kang et al., 2015; Liu et al., 2015) have been extensively utilized in MFC with improved performance when doped with composites of nanomaterial. However, stability and longevity of the power output are limited to 710 mV for 6 days (Kang et al., 2015). High internal resistance resulting in reduced power density has also been reported (Hou et al., 2015; Wang et al., 2014). On the other hand, the potential of biodegradable, biocompatible, piezoelectric polymer such as medium-chain-length polyhydroxyalkanoates (mcl-PHA) has not been fully explored for its direct use as carbon composites in anode modification (Hindatu et al., 2017b; Luckarift et al., 2012). Under certain deficiency conditions, specific bacteria synthesize mcl-PHA as intracellular storage material. Therefore, efficient microbial colonization in the form of biofilm is expected in mcl-PHA modified materials than other conducting polymer materials since it is cellular by-product. The previous work has demonstrated the mcl-PHA potential utility in enhancing the MFC anode performance when it was grafted with hydrophilic polyethylene glycol methacrylate (PEGMA) and composited with carbon nanotubes (Yusuf et al., 2018). The amphiphilic product resulted in higher current and power densities, improved electron transfer and reduced internal resistance attributed to superior biofilm colonization of mcl-PHA modified electrodes.

The PEM alone could disrupt the overall performance of MFC as it is responsible for the amount of protons transferred to the cathode chamber, which could be hindered as a result of biofouling, oxygen crossover and substrate loss (Daud et al., 2015; Zhou et al.,

2013). An ideal membrane should be cheap, resistant to biofouling, prevent oxygen crossover, and allow fast, uninterrupted passage of H^+ to the cathode chamber (Angioni et al., 2017; Angioni et al., 2016). The most commonly utilized PEM in MFC is Nafion due to its high proton conductivity and low internal resistance (Sevda et al., 2013). However, non-biodegradable nature of Nafion as well as it chemical and biochemical biofouling has prompted the search for alternative and innovative membranes in MFC. The application of semi-crystalline thermoplastic polymer polyether ether ketone (PEEK) as membrane separator in MFC has been investigated. Ayyaru and Dharmalingam (2011) developed a single chambered MFC using sulphonated PEEK (SPEEK) as the PEM. When compared with Nafion 117, the power density of SPEEK membrane MFC increased by 55 %, and showed improved oxygen mass transfer coefficient and increased coulombic efficiency. Further modification of the membrane with composite of sulphonated TiO_2 nanoparticles doubled its power density compared to pristine SPEEK. Chae et al. (2014) impregnated the conventional SPEEK with polyimide nanofiber for better dimensional stability of the membrane. The novel composite showed improved proton conductivity and reduced oxygen crossover.

The utilization of biodegradable polymers as PEM has been the recent focus in MFC technology due to their biocompatibility and environmental-friendly nature. The use of biodegradable ceramic and natural rubber was investigated previously (Winfield et al., 2013a; Winfield et al., 2013b). It was evident that the biodegradable PEM could easily outperformed the commercially available ion exchange membranes (IEMs). The gradual increase in the performance of the biodegradable PEM with MFC operation time is attributed to the increased biofilm colonization, and slow (bio)degradation of the PEM which subsequently resulted in micro-pores, thereby enhancing ion permeability. Hence, biofouling in biodegradable PEM could be beneficial to the MFC rather than a disadvantage as seen in non-biodegradable PEMs. Biodegradable and biocompatible

microbial polymer such as medium-chain-length polyhydroxyalkanoates (mcl-PHA) is another potential candidate for such role in PEM.

Despite the ability of PHA to generate electrical charges in response to mechanical stress, literatures on its utilization as MFC component is extremely limited (Hindatu et al., 2017b; Luckarift et al., 2012b; Yusuf et al., 2018). To date, radical polymerization of mcl-PHA with methyl acrylate (MA) monomers, composited with carbon nanotube as anode and cathode electrode modifier have not been reported. The current work reported the synthesis, characterization and utilization in MFC, highly stable, conductive, and active anode/cathode electrode modifier based on mcl-PHA radically-grafted with MA, and composited with functionalized multi-walled carbon nanotube. The novel composite was characterized by Fourier-Transform Infrared (FTIR) spectroscopy, X-ray diffraction (XRD), field emission scanning electron microscopy (FESEM), and proton nuclear magnetic resonance (^{1}H-NMR). Electrochemical characterization of the nanocomposite was carried out using cyclic voltammetry (CV) and electrochemical impedance spectroscopy (EIS). Furthermore, investigation on solvent blending of mcl-PHA and polyhydroxybutyrate (PHB), and its utilization as PEM in MFC for wastewater treatment was carried out. The study is first of its kind, which utilizes mcl-PHA as a supporting matrix for PHB to facilitate ion transport in MFC. Spectroscopic analyses, electrochemical characterization, as well as its application in double-chambered MFC utilizing real wastewater are discussed. The objectives of the research are:

1.1 Research objectives

1) To produce medium-chain-length polyhydroxyalkanoates (mcl-PHA) from renewable substrate *via* bacterial fermentation with lauric acid as sole carbon source;

2)   To impart amphiphilicity, conductivity and crystallinity properties to neat mcl-PHA by radical polymerization with methyl acrylate monomers, and composition with functionalized multi-walled carbon nanotube (MA-PHA/MWCNT);

3)   To investigate the electrochemical activities and power generation potentials of anode and cathode electrodes modified with nanocomposites of MA-PHA/MWCNT in microbial fuel cell (MFC);

4)   To investigate mcl PHA-PHB crystal composite as alternative proton exchange membrane (PEM) in MFC utilizing real wastewater for electricity generation.

CHAPTER 2: LITERATURE REVIEW

The increase in global energy demand due to increasing population and industrialization has resulted in the search for alternative energy sources that are renewable and environmental-friendly. Energy from fossil fuel are non-renewable, depleting and detrimental from environmental perspectives. Alternative energy sources, which are green and renewable such as hydrogen fuel (Jie et al., 2017), biodiesel (Kanimozhi & Perinbam, 2013), bioethanol (Parmar et al., 2011), microbial fuel cell (MFC) (Hindatu et al., 2017a) and many more have been proposed. One of the many possible solutions lies with non-combustion method such as microbial fuel cell. A microbial fuel cell (MFC) is a sustainable, promising and nascent energy generation device that combines electricity generation and wastewater treatment through metabolic activities of microorganisms (Almatouq & Babatunde, 2018; Yu et al., 2016). Its basic design is a two-chambered MFC consists of anode and cathode chambers, and a selective membrane known as proton exchange membrane (PEM) (Figure 2.1). At anode compartment, electrons and hydrogen ions (H^+) are generated by the electrogens through biological oxidation of organic matters (Logan, 2009). The electrons are transferred to the cathode chamber *via* electrical circuit and the protons (H^+) pass through PEM for oxygen reduction reaction on the cathode surface, thus completing the redox reaction process (Logan, 2009; Xiao & He, 2015). Besides treating wastewater and generating electricity in the process, the technology also produce some important products at the cathode chamber such as hydrogen peroxide (H_2O_2) (Fu et al., 2010) and caustic potash (KOH) (Gajda et al., 2015; Gajda, et al., 2016).

Modification of the anode electrode with polymeric nanocomposites has been reported to be more efficient as a result of improved extracellular transfer of electrons to the anode surface, resulting in reduced internal resistance and improved overall MFC performance

(Cui et al., 2015; Kang et al., 2015; Wang et al., 2014). Recent anode modifications with polymeric nanomaterials are reported herewith.
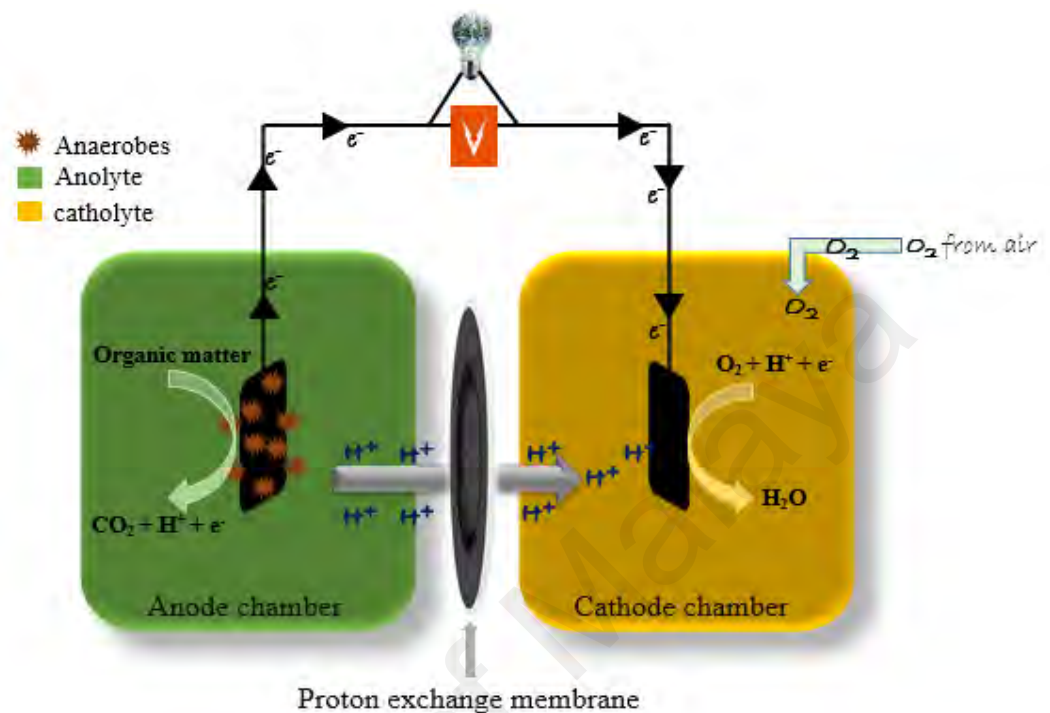
Figure 2.1: Schematic overview of a double-chambered MFC

2.1 Anode modification with polymeric nanomaterials

The anode chamber structure and function is a vital part of MFC set-up. Electrochemically active bacteria oxidize organic matter releasing electrons and protons in the process. Efficient transfer of electrons to anode surface is crucial to the power output generated and to overall MFC performance. An efficient anode electrode supports for maximum biofilm colonization thereby acting as an electron sink. Electrical conductivity, durability and stability, large surface area and porosity amongst others are the ideal characteristics of anode electrode in MFC (Baudler et al., 2015; Huggins et al., 2014; Lee et al., 2016). Carbon-based nanomaterials have been known to meet these characteristics to some extent. However, the hydrophobic nature of these materials prevent for maximum bacterial colonization of anode electrode (Jafary et al., 2018; Shuang et al., 2017). As such, polymeric nanocomposites of polyesters, conducting

polymers and polysaccharides have been used as anode electrode modifier to some degree of success as discussed in the following sections.

2.1.1 Nanocomposites of conducting polymers

2.1.1.1 Polypyrrole (PPy)

Among the most studied conducting polymers in MFC is PPy. Kaur et al. (2014) modified the surface of carbon paper with both pristine and functionalized PPy. The PPy+ modified electrode improved the voltage output, the start-up time and stability of maximum voltage potential. Further modification of PPy with reduced graphene oxide (rGO) nanocomposites (Figure 2.2) doubled the power density and recorded a maximum voltage potential of 400 mV for 75 hours (Kumar et al., 2014). One step electrochemical method was recently employed by Li et al. (2018) to synthesize PPy nanowires and composited it with graphene oxide (GO). The modified anode electrode exhibited superior surface area, improved power density and better open circuit voltage (OCV). The performance of stainless steel (SS) was significantly enhanced when layered with PPy (Pu et al., 2018). It resulted in an increase in power density 29 times higher than bare SS anode electrode. Enhancement in the generation of maximum voltage up to seven-fold was also recorded (Pu et al., 2018).
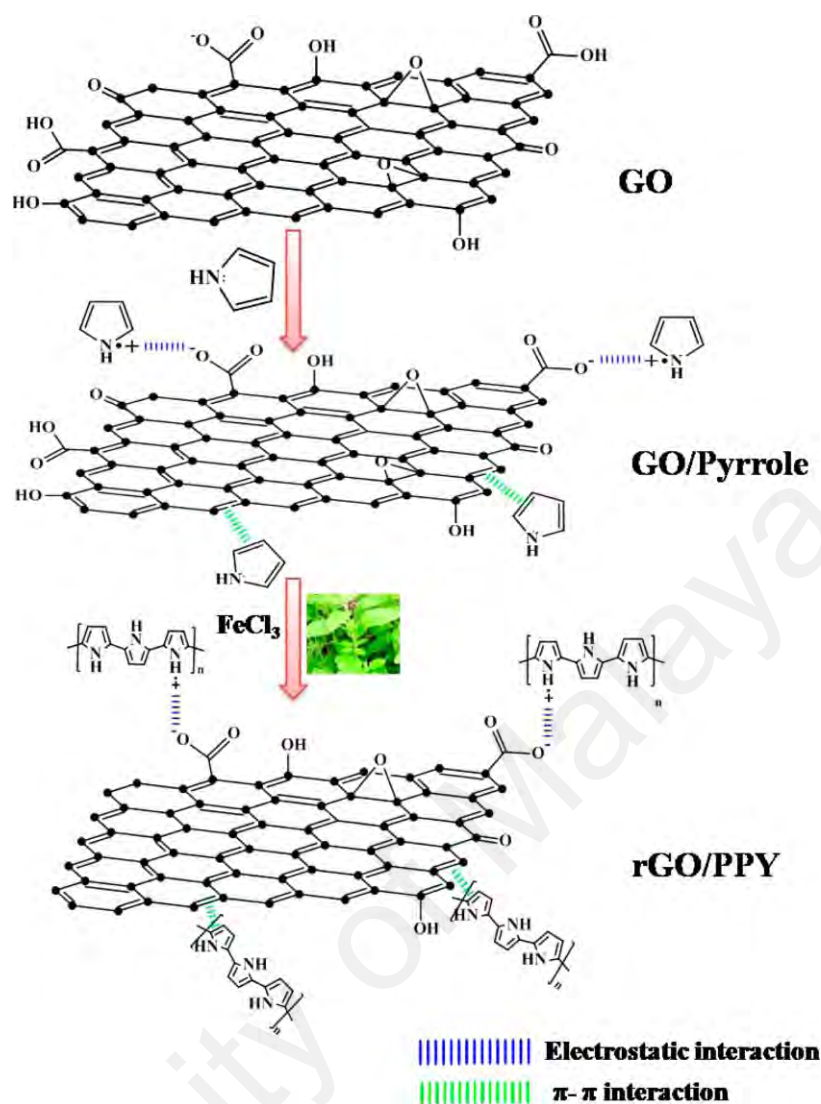
Figure 2.2: Proposed mechanism for the preparation of the rGO/PPy composite (reproduced from (Kumar et al., 2014), with permission from American Chemical Society)

2.1.1.2 Polyaniline (PANI)

PANI is another conducting polymer widely utilized as anode modifier. Cyclic voltammetry (CV) method was employed in preparing PANI composited with multi-walled carbon nanotube (MWCNT) through electroplating (Wang et al., 2014). Maximum voltage potential of almost one volt was recorded and a power density of 286 mW/m². Bifunctional catalyst of graphene (G) and TiO_2 with PANI on carbon paper (CP) enhanced the performance of MFC (Han et al., 2018). The modified electrode showed 2.7 times higher power density than plain CP. The internal resistance was found to be reduced

by half with modified electrode set-up. The superiority was attributed to efficient extracellular electron transfer to anode due to successful colonization of the anode by the bacteria (Figure 2.3). Recently, Li et al. (2019) modified carbon cloth (CC) electrode surface *in situ* with PANI composited with titanium suboxide (TS) and G nanoparticles. Longevity in maximum voltage output in modified electrode was evidenced with 13-fold increase in power density compared to bare CC. About 70 % decrease in internal resistance was recorded in PTSG/CC electrode set-up. Similarly, Yellappa et al. (2019) synthesized PANI and PANI/CNT nanoparticles through *in situ* oxidative chemical polymerization and spread on stainless steel mesh (SSM) for wastewater treatment. PANI/CNT-SSM electrode recorded 80 % chemical oxygen demand (COD) removal while 65 % was recorded for PANI-SSM and 58 % for bare SSM. Higher OCV was also recorded for polymeric modified electrodes compared to bare SSM. The superiority in PANI/CNT-SSM electrode was attributed to enhanced charge transfer due to CNT incorporation which subsequently increased the conductivity between the biocatalyst and the anode surface. The studies of Yin et al. (2019) showed a synergistic effect of TiO_2 nanosheets (TiN) and PANI through electrochemical deposition of PANI onto TiN, at different CV cycles. Maximum power density up to 63.6 % increase was recorded for PANI deposited through 20 CV cycles. Lowest charge transfer resistance was also recorded by the modified electrode with 20 CV cycles.
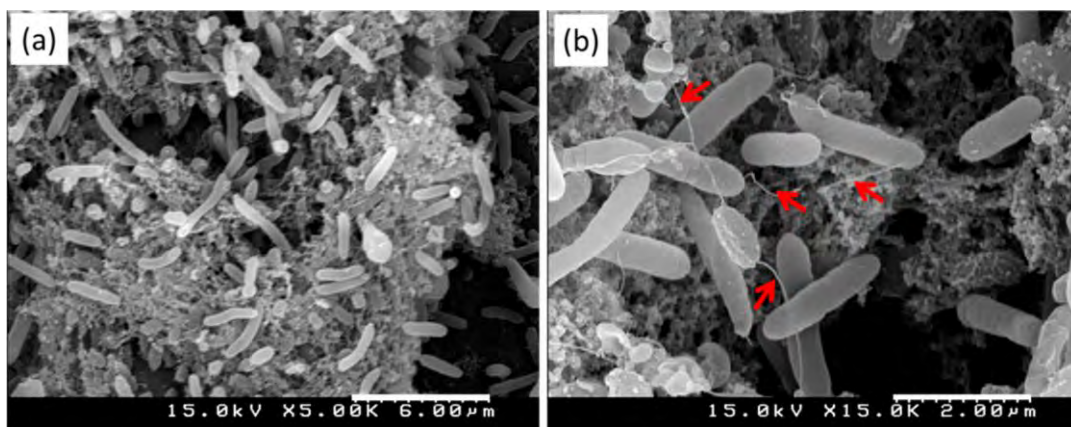
Figure 2.3: (*a,b*) Morphology of *Shewanella oneidensis* MR1 embedded in the matrix of the PANI-TiO$_2$-GN catalyst. The red arrows in panel *b* indicate the nanowires (pili) of *Shewanella oneidensis* MR1 (reproduced from (Han et al., 2018), with permission from American Chemical Society)

2.1.1.3 Poly(3,4-ethylene dioxythiophene) (PEDOT)

PEDOT is a derivative of polythiophene with superior conductivity compared to PPy and PANI (Abidin et al., 2018). This resulted in its utilization as electrode modifier in MFC. Ma et al. (2018) modified the surface of SS with PEDOT through electrochemical polymerization method. PEDOT/SS electrode recorded six-fold increase in power density compared to bare SS electrode. The current density recorded during MFC operation leveled off at 1150 mA/m^2 for PEDOT/SS compared to 210 mA/m^2 for SS electrode (Figure 2.4). The efficiency of PEDOT/SS electrode was ascribed to dense and conductive film formed on SS plate which not only prevent SS base from biogenic and chemical corrosion, but also improved the electron transport rate to anode. Recently, Senthikumar et al. (2019) modified PEDOT with nickel ferrite nano-rod on biochar as a free-standing electrode. A maximum power density of 1200 mW/m^2 was recorded which was about five times higher than control (ferric oxide on biochar). Further modification of PEDOT polymer matrix with nanoparticles of nickel and rGO (PEDOT/Ni/rGO) resulted in a power density up to 3200 mW/m^2 and improved internal resistance and OCV (Hernandez et al., 2019). The improved performance of modified electrode was attributed to homogenous dispersion of the nanoparticles within PEDOT matrix and enhanced

biocompatibility between biocatalyst (*Escherichia coli*) and PEDOT/Ni/rGO electrode surface
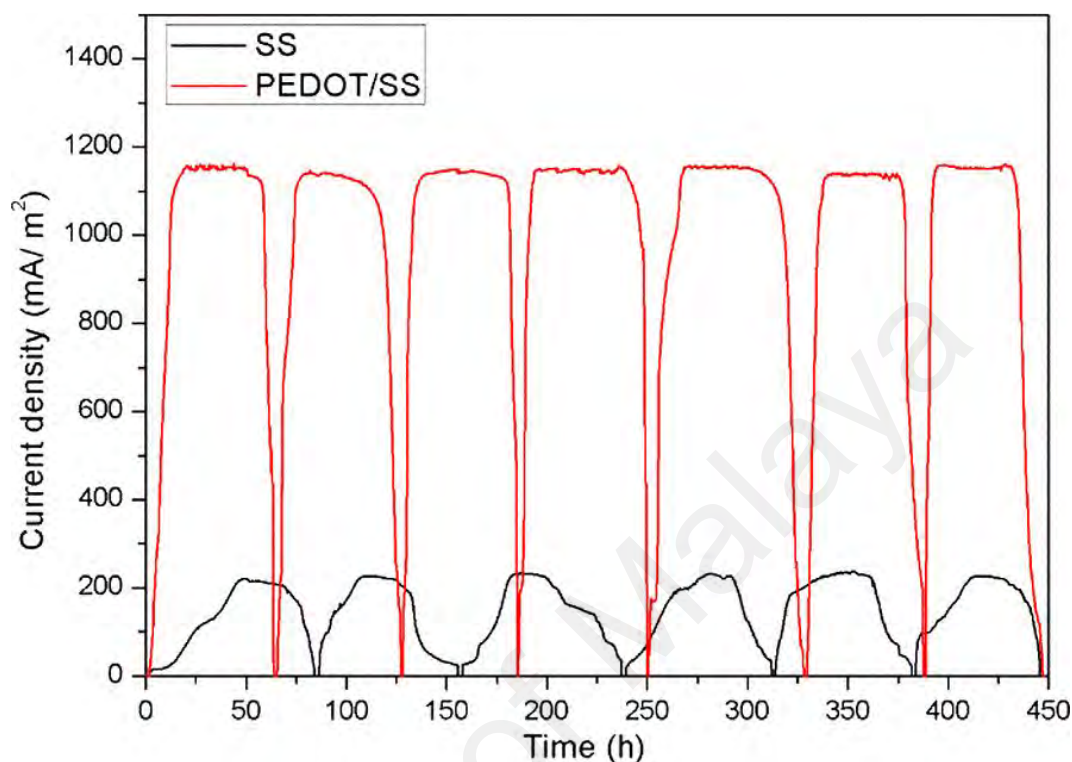
Figure 2.4: Power generation in MFCs with an external resistance of 1000 Ω (reproduced from (Ma et al., 2018), with permission from American Chemical Society)

2.1.2 Nanocomposites of polyesters

Polymers with ester functional groups in their main chain are regarded as polyesters. Due to their biocompatibility, biodegradability, piezoelectricity, elasticity, durability and resistivity to most chemicals, polyesters have been recently used as anode electrode modifier. Its first utilization in MFC was reported by Luckarift et al. (2012) when 3-polyhydroxybutyrate-*co*-3-hydroxyvalerate (PHBV) was composited with carbon nanofiber by solvent casting method (Figure 2.5). Superior biofilm colonization of the modified anode surface resulted in efficient bioelectrocatalysis, stability and reproducibility in electrolyte with significant power density generation compared with previously reported graphite felt electrode. Hindatu et al. (2017b) reported the utilization

of elastic medium-chain-length polyhydroxyalkanoates (mcl-PHA) composited with multi-walled carbon nanotube (MWCNT) as CC surface modifier. Maximum power density up to 53 % increase, internal resistance reduction of 31 % and improved maximum voltage potential of 50 % were recorded for mcl PHA-MWCNT composite modified electrode compared to pristine CC electrode. Interestingly, further modification of CC surface with amphiphilic mcl-PHA-*co*-polyethylene glycol methacrylate / MWCNT composite (mcl-PHA-*co*-PEGMA/MWCNT) further reduced the internal resistance by 97 %, improved the maximum voltage potential by 75 %, and 74 % enhancement in maximum power density was also reported (Yusuf et al., 2018). It was hypothesized that the superiority in mcl-PHA-*co*-PEGMA/MWCNT electrode stemmed from better biocompatibility and synergistic relationship between the biocatalyst (*Escherichia coli*) and the modified anode surface (Yusuf et al., 2018). Polycaprolactone (PCL) nano-fibers and micro-fibers were composited with gold particles and utilized as anode modifier (Fraiwan et al., 2014). Although, high activation loss and high internal resistance were reported, the modifier electrode nevertheless showed an improved stability of maximum voltage potential of 600 mV up to 10 days MFC operation. Also, the micro-fiber composite exhibited two-fold increase in power and current densities compared to nano-fiber composite.
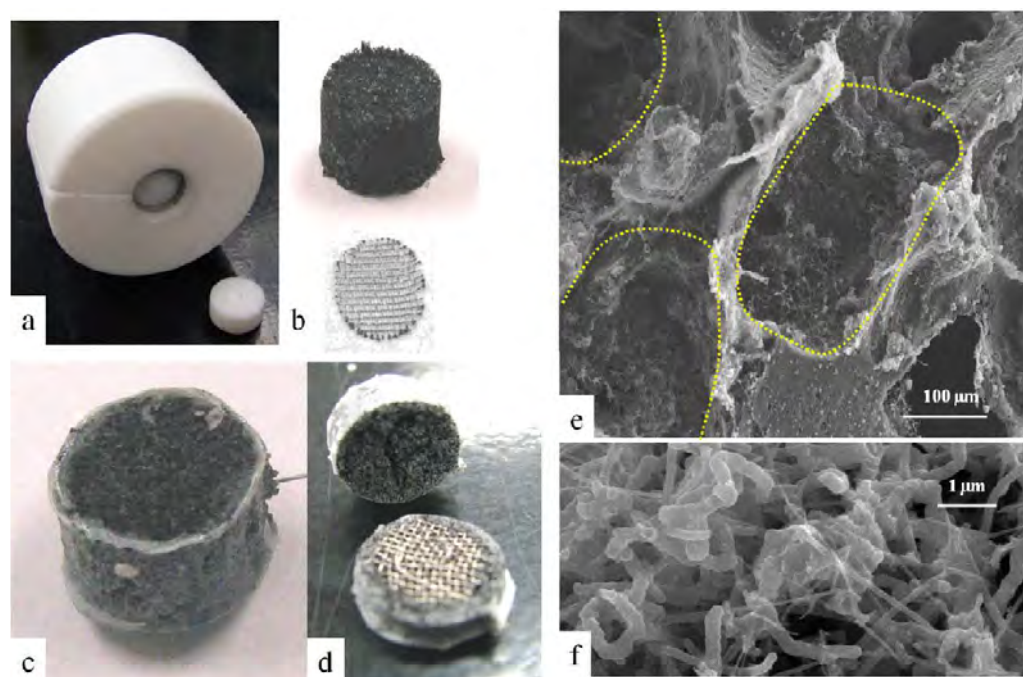
Figure 2.5: Visual representation of polymer/carbon (PHBV/CF) composite fabrication. (a) A die is used to (b) pack sucrose/CF around a nickel mesh. (c) The resulting sucrose/CF scaffold is intercalated with polymer and (d) the sucrose removed to form a porous scaffold. Final electrode cut to show the interior nickel mesh. (e) The sucrose dissolves and leaves a hole of a size comparable to the original particles (yellow dashed lines) that is (f) interconnected with carbon fibers (reproduced from (Luckarift et al., 2012), with permission from American Chemical Society)

2.1.3   Nanocomposites of polysaccharides

Polysaccharides nanocomposite as anode modifier has been exploited since they are made up of polymeric carbohydrate molecules. The effects of different nanocomposites *viz.* magnesium and graphite composed alongside chitin particles were investigated as anode electrode modifier (Jung et al., 2014). Maximum power density peak of 1872 mW/m^2 was recorded in magnesium/chitin composite. Chitin supplement was responsible for 121 % increase in magnesium anode, and 164 % increase in graphite anode. The improvement showed by chitin-supplemented anode was attributed to the simplicity active growth of bacterial communities on anode surface encouraged by the saturated carbon source. A conductive carbon nanotube hydrogel composited with chitosan was layered on carbon paper (CP) electrode (Figure 2.6) (Liu et al., 2014). A

current density peak of 500 mA/m^2 was recorded for hydrogel modified electrode at a power density of 132 mW/m^2, compared to raw CP electrode (150 mA/m2 of current density). Coulombic efficiency (CE) of 32 % was reported for CNT-hydrogel modified electrode while 19 % CE for the control. It was discovered that the presence of oxygen-containing functional groups of C=O and C=OH were responsible for high conductivity of the modified electrode (Liu et al., 2014). Similarly, Mottet et al. (2018) constructed a conductive composite hydrogel made up of alginate and carbon nanotube. The new electrode recorded high compatibility with biocatalyst and better conductivity.
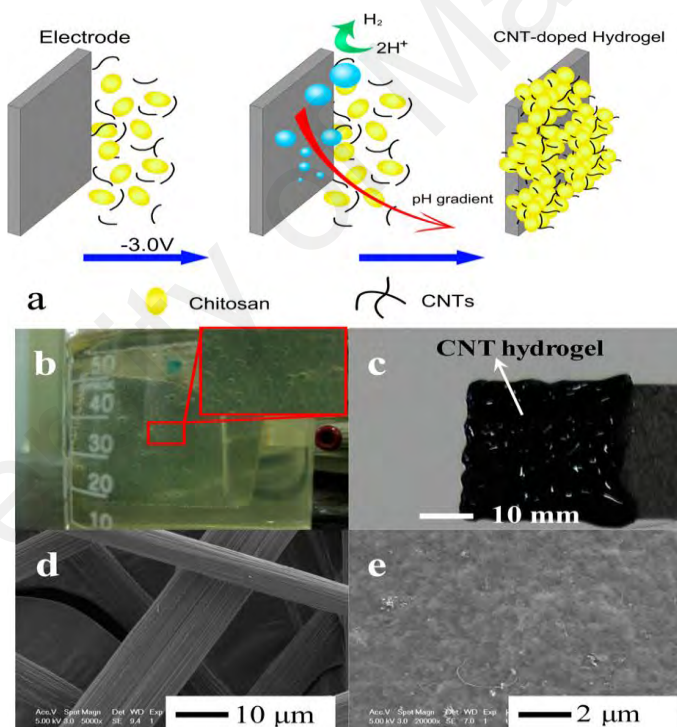
Figure 2.6: Visual representation of the CNT-hydrogel electrode preparation (a), hydrogen gas bubbles produced as template in the deposition process (b), CNT-hydrogel on carbon paper (c), SEM images of carbon paper (d), and CNT-hydrogel modified carbon paper (e) (reproduced from (Liu et al., 2014), with permission from American Chemical Society)

2.1.4 Nanocomposites of other polymers

Temperature responsive polymer of poly-N-isopropylacrylamide (PNIPAM) was investigated by Kumar et al. (2014a) as anode modifier. PNIPAM was composited with CNT and GO nanoparticles and subsequently structured into hydrogel. Pristine PNIPAM electrode recorded a power density peak of 43 mW/m^2 at a current density of 453 mA/m^2. The incorporation of CNT into PNIPAM matrix resulted in six-fold increase of power density *viz.* 264 mW/m^2 at a current density of 2502 mA/m^2. Further modification with GO nanoparticles resulted in significant increase in both power and current densities at 434 mW/m^2 and 3603 mA/m^2, respectively. The decrease in charge transfer resistance of PNIPAM was attributed to synergistic interaction between two highly conductive nanoparticles of CNT and GO which subsequently improved the MFC performance with a longevity of more than 300 hours. Recently, Chen et al. (2019) reported hydrogel formation of polyacrylamide (PAM) with rGO and graphite brush (GB) as current collector through *in situ* polymerization method, followed by reduction with ascorbic acid. The PAM/rGO/GB electrode recorded 34.8 % increase in maximum power density compared to GB anode. Superiority in CE was observed for PAM/rGO/GB electrode at 35.6 % compared to GB electrode (21.1 %). The close proximity of the biofilm to anode as well as the large surface area of modified electrode were responsible for enhanced MFC performance. Polymeric derived ceramics (PDC) route was employed in making a highly conductive hydrophilic polymeric nanocomposite of poly(methylsilsesquioxane) and poly(methyl phenyl silsesquioxane) composited with graphite and carbon black (Silva et al., 2019). The novel anode material recorded two-fold increase in power density (211 mW/m^2) compared to carbon felt anode (111 mW/m^2). When the MFC system is applied for wastewater treatment, similar COD removal rate and CE were recorded for modified and pristine anode electrodes. Nevertheless, high specific area in the modified anode as well as its porous structure resulted in superior biocompatibility as confirmed

by improved biofilm growth on the electrode surface, hence better electron transfer (Silva et al., 2019).

2.2 Cathode modification

Although, MFC is clean, sustainable, renewable and earth-friendly, which are the characteristics needed in an alternative energy source, the low power output generated by this technology is of major concern for its widespread practical applications (Hindatu et al., 2017a). To tackle this issue, the cathode electrode which determines the catalytic activities of the terminal electron acceptors needs to be modified accordingly. The difficulty in fabricating the cathode electrode lies with the three-phase reaction of the protons, electrons and oxygen meeting at a catalyst. The catalyst must be on a conductive surface and at the same time exposed to water and air for easy contact with protons and electrons (Logan, 2008). A good cathode electrode should be inexpensive and readily available (Ortiz-Martínez et al., 2015), easy to fabricate (Kim et al., 2009; Liu & Logan, 2004), effective in electrocatalysis (Gajda et al., 2018; Lu & Li, 2012; Xia et al., 2016), and stable in catholyte (Dicks & Rand, 2018; Rabaey & Verstraete, 2005; Wei et al., 2011). Factors such as pH (He et al., 2008; Mani et al., 2017), concentration of protons (Zhao et al., 2009), electrode spacing (Cheng et al., 2006), and electrode surface area (Lianhua et al., 2011; Liu et al., 2011; Oh & Logan, 2006) have been known to affect the electrocatalytic activities of the cathode electrode. An extensive review detailing the carbon-based polymer nanocomposites as cathode electrode material for MFC was presented by Jafary et al. (2018). Significant improvements were evidenced in polymeric modified cathode electrodes compared to bare electrode materials. The development of a stable, efficient, polymeric cathode electrode that boost the chemical reaction meeting at a tri-phase reaction (water, air and solid catalyst) will significantly increase the power output of MFC, and a step closer towards its adoption in various applications.

2.2.1 Cathode modification with polymeric nanomaterials

Ahmad et al. (2012) set-up an MFC with PANI nanofibers composited with carbon black. Higher electrochemical activities with power density improvement up to 2.7-fold increase with composite cathode electrode compared to pristine PANI (control). Although the power density is still lower than Pt-based electrode, the environmental-friendly polymeric composite is economically feasible when considering large-scale applications. Further doping of the conducting polymer PANI to form sulfonated PANI (SPANI), and composited with highly efficient bimetallic nanocomposites of 1:1 nickel and cobalt was investigated by Papiya et al. (2018) for cathode electrode modifier. Spectroscopic analyses showed equal distribution of the nanocomposites on the supporting matrix. When compared with controls, the highest catalytic activity was observed in SPANI/Ni-Co electrode with a maximum power density of 659 mW/m^2 relative to Pt-based electrode at 483 mW/m^2. Highly functional nanoparticles of graphene and TiO$_2$ were incorporated into PANI matrix to enhance the reduction of oxygen at cathode (Han et al., 2018). The ternary nanocomposite exhibited superior oxygen reduction reaction activity compared to controls (pristine PANI and PANI/TiO$_2$ electrodes).

Polypyrrole (PPy) is another conducting polymer that has been utilized as cathode modifier. A solvothermal method was employed to synthesize a novel composite of manganese, PPy and carbon nanotube (Lu et al., 2013). The composite demonstrated efficiency and stability as cathode catalyst for oxygen reduction reaction. A power density peak of 213 mW/m^2 at a material loading rate of 2 mg/cm^2 was recorded, comparable to platinum/carbon black composite electrode. Further modification of PPy polymer matrix with MnO$_2$/CNT composite through cost-effective hydrothermal method resulted in an improved maximum power density of 721 mW/m^2 (Yuan et al., 2015). Improved long-

term stability of the composite electrode compared to Pt/C electrode was also reported, making the electrode an alternative to Pt/C electrode for sustainable energy generation.

A single-chambered MFC was developed by coating the air facing side with poly(dimethylsiloxane) composited with nitrogen doped nickel nanoparticles and carbon nanofibers. The polymer-metal-carbon nanocomposite showed high efficiency in oxygen reduction reaction in MFC, serving as an ideal alternative to poisonous Pt-based and Nafion electrode (Modi et al., 2017). Ong et al. (2018) recently synthesize a polymeric cathode composed of polyvinylpyrrolidone/carbon nanotube/manganese oxide (P/MnO_2/CNT) for air cathode MFC. Electrochemical analyses revealed higher oxygen reduction reaction activities with low charge transfer resistance compared to control electrodes of MnO_2 and MnO_2/CNT. When utilized in MFC, a maximum power density of 91 mW/m^2 was recorded, which was significantly higher than MnO_2/CNT catalyst (72 mW/m^2), MnO_2 catalyst (36 mW/m^2) and CNT catalyst (29 mW/m^2). Also, higher COD removal percentage of 74 % was recorded for P/MnO_2/CNT electrode.

Among the most recent modification involving polymeric cathode nanocomposite utilizes polysaccharide-carbon composite. A bacterial cellulose doped with particles of phosphorus (P) and copper (Cu) was used as cathode catalyst in MFC (Li et al., 2019) (Figure 2.7). A three-dimensional structure with extensive large surface area was obtained. Improvement in the catalytic activity of the polymeric nanocomposite was attributed to increase active sites from Cu and P doping. A maximum power density of 1177 mW/m^2 at a current density of 6730 mA/m^2 was recorded, which was significantly higher than Pt-based electrode (1044 mW/m^2 at a current density of 6020 mA/m^2). A five-fold increase in power density was observed when a cathode electrode was modified with a dual-doped carbon derived from chitosan (Liang et al., 2019). Improved internal resistance, high open circuit voltage potential as well as large surface area of about 982

m^2/g, which resulted in better oxygen mass transfer were attributed to better performance in the nitrogen- and phosphorus-doped electrode.
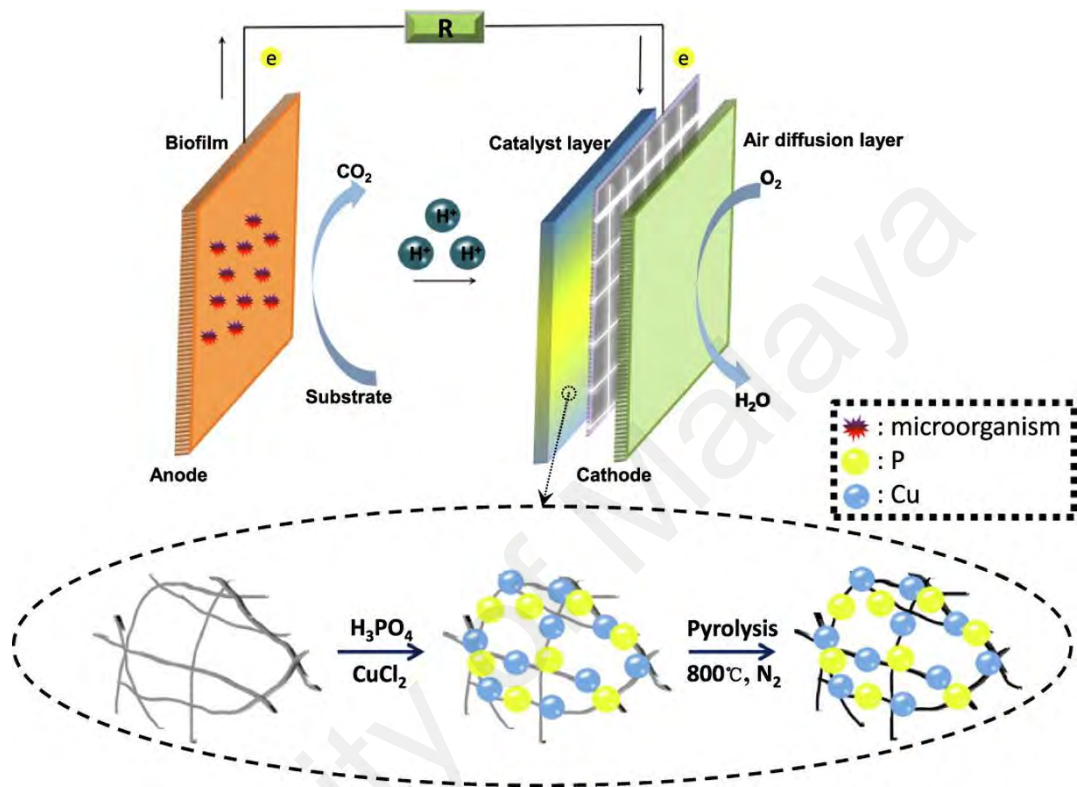
Figure 2.7:   Schematic diagram of bacterial cellulose doped with phosphorus and copper *via* freeze-drying and high-temperature pyrolysis (reproduced from (Li et al., 2019), with permission from Elsevier)

2.3   Proton exchange membrane (PEM)

The primary function of a PEM in MFC is to separate the anode and cathode electrolytes and simultaneously allow for maximum proton (H^+) passage from anode to cathode chamber. However, high cost and non environmental-friendly nature of some widely utilized PEM warrant for the development of efficient, readily available, cheap, and environmental-friendly PEMs. The recent advancements in PEM fabrication for MFC application are discussed hereafter.

21

2.3.1 Polyether ether ketone (PEEK) nanocomposites as PEM

Quaternized PEEK (QPEEK) and sulfonated PEEK (SPEEK) were fabricated and respectively utilized as anion and cation exchange membranes (Elangovan & Dharmalingam, 2016). Superiority in QPEEK were observed with maximum power density of 603 mW/m^2 and CE of 76 % compared to SPEEK (458 mW/m^2 and 61 %). SPEEK allowed for more cation transport instead of protons, and exhibited high pH gradient. This resulted in chemical precipitate formation on cathode surface and subsequently, high internal resistance and MFC deterioration. SPEEK membrane was fabricated with different degree of sulfonation (DS) (20.8 %, 41 %, 63.6 % and 76 %) for MFC application (Ghasemi et al., 2016a). SPEEK with 63.3 % DS exhibited the highest power density (68.64 mW/m^2), COD removal (91 %) and CE (26 %). Although, the power density generated was still lower than Nafion membrane (74.8 mW/m^2), cost estimation suggested the utilization of SPEEK with 63 % DS as feasible alternative due to high power generation per cost. Further modification of the SPEEK membrane with hybridization of polysulfone (PS) at lower and higher DS for desalination and power generation was investigated (Ghasemi et al., 2016b). The degree of porosity of the modified membrane was in direct proportion to DS as illustrated in Figure 2.8. The amphiphilic hybrid membrane with 29 % DS exhibited the highest power density and a significantly high NaCl (62 %) and MgSO$_4$ (68 %) rejection rate albeit lower than PS/SPEEK (76 %) for NaCl (67 %) and MgSO$_4$ (81 %) rejection rate. Particles of silicotungstic acid were entrapped into the matrix of SPEEK through phase inversion method (Venkatesan & Dharmalingam, 2017). The hybrid composite membrane showed reduced oxygen gas crossover, which resulted in four-fold increase in the generation of maximum power density compared to Nafion membrane.
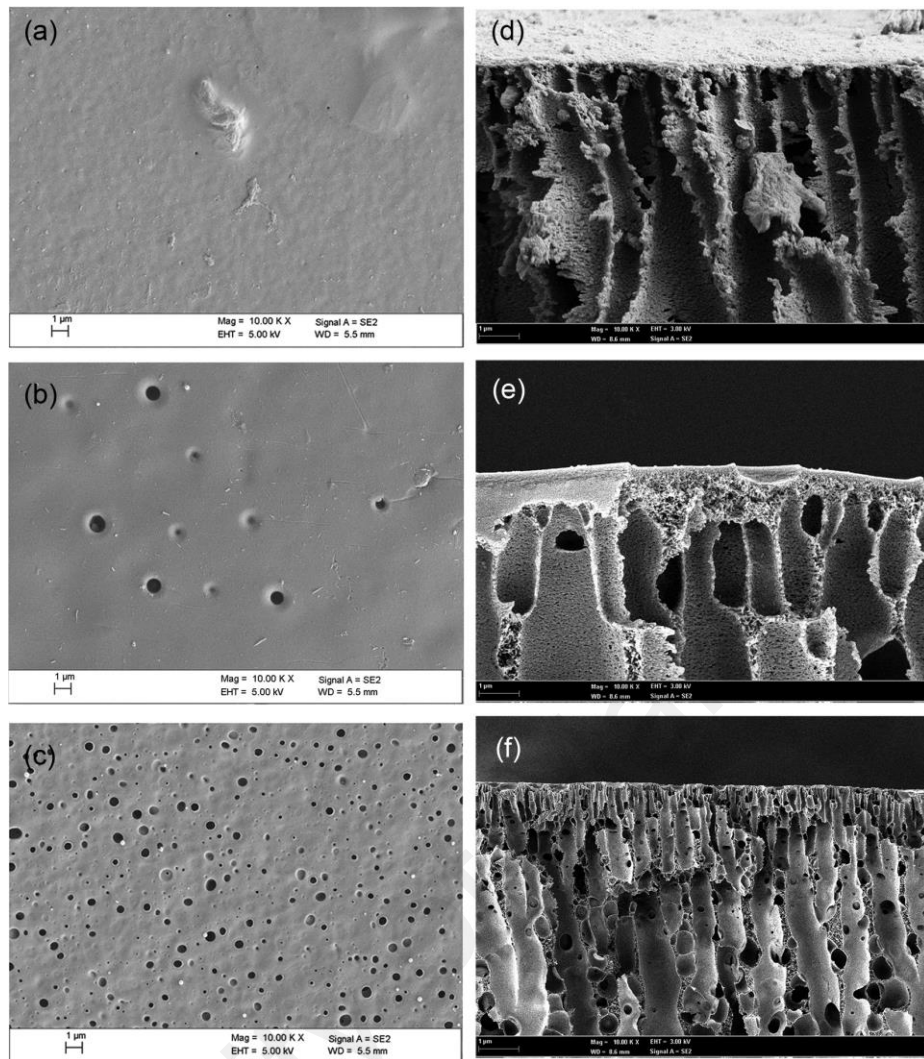
Figure 2.8: SEM image of the cross section of *a*) surface of PS, *b*) surface of PS/SPEEK (29 %), *c*) surface of PS/SPEEK (76 %), *d*) cross section of PS, *e*) cross section of PS/SPEEK (29 %), *f*) cross section of PS/SPEEK (76 %) (reproduced from (Ghasemi et al., 2016b), with permission from Elsevier)

2.3.2 Nafion nanocomposites as PEM

While neat Nafion is the most utilized PEM in MFC, enhancement of its performance through composites of nanoparticles have also been investigated. Angioni et al. (2016) modified Nafion membrane with functionalized SB-15 silica. Functionalization was done with SO_3H group and utilized as PEM in a prolonged MFC operation. Nafion-based SB-15 composite of 15 % *w/w* was found to exhibit maximum power density, three times higher than neat Nafion after three months of MFC operation. The same membrane offered high resistivity to biofouling, high COD removal of 95 %

after 14 days and improved CE recovery of 34 %. The efficiency of the modified PEM was attributed to the presence of the silica-based SO_3H functionalized filler. Bajestani et al. (2016) investigated the effects of different solvents on Nafion composited with TiO_2 through solvent casting method. Nafion composite with dimethylformamide (DMF) solvent exhibited the highest OCV, proton conductivity and highest membrane porosity. Alumina nanoparticles (Al_2O_3) ranging from 5-20 % (*w/w*) were incorporated within the matrix of sulfonated poly-(vinylidene fluoride-hexafluoropropylene) (PVDF-*co*-HFP) blended with Nafion at different molar ratios (Kumar et al., 2016a). Increase in water uptake was observed with an increase in Al_2O_3 nanoparticles. Membrane with 5 % *w/w* nano Al_2O_3 showed superior proton conductivity and improved maximum power and current densities of 48 and 11 % respectively. Hernandez et al. (2016) developed membranes of agar composited with Nafion liquid and tested against Nafion 117 membrane. Reduced internal resistance was observed in all modified membranes from incorporation of agar. Although the power densities were lower than the control i.e. Nafion 117 membrane, higher power/cost ratio was more advantageous in agar composite membranes than Nafion membrane.

2.3.3 Chitosan and polyester nanocomposites as PEM

A low cost polyester cloth (PC) with varying layers were utilized as PEM in MFC and compared with Nafion membrane (Kim et al., 2016). Higher mass transfer and reduced diffusion coefficient of oxygen were observed in PC membranes compared to Nafion. A comparable internal resistance, power and current densities were observed in PC membranes and Nafion membrane, indicating a possible alternative to poisonous Nafion. Yusuf et al. (2018) for the first time utilized biodegradable microbial polyester i.e. medium-chain-length polyhydroxyalkanoates composited with functionalized multi-walled carbon nanotubes (mcl-PHA/MWCNT) at varying amount of the nanoparticles (5-20 % *w/w*) through ultrasound dispersion blending method. Comparable power density to

Nafion membrane was recorded. However, membrane with 10 % MWCNT was superior in COD removal percentage, CE, conductivity and reduced internal resistance over Nafion membrane. Harewood et al. (2017) investigated the thermal condensation of malic and citric acid in ratio 3:1 and blended with chitosan. The copolymer was utilized as PEM in MFC. The maximum power and current densities generated were comparable to Nafion 117 membrane. The copolymer is biodegradable and environmental-friendly, which makes it another alternative to Nafion membrane. Furthermore, the effects of applying different cross-linkers were investigated by Holder et al. (2017). Graphene oxide nanoparticles were incorporated into the matrix of chitosan and cross-linked with either phosphoric or sulfuric acid. Phosphoric acid cross-linked PEM showed 135 % increase in power density compared to sulfuric acid cross-linked PEM.

2.3.4 Ceramics and polyethersulfone (PES) nanocomposites

Polyethersulfone (PES) was sulfonated with chlorosulfonic acid (SPES) and finally blended with pristine PES (PES/SPES) (Zinadini et al., 2017). The PES/SPES membrane showed superiority in COD removal percentage, CE, oxygen permeability, biofouling and power generation compared to Nafion membrane. Di Palma et al. (2018) recently developed a membrane of PES composited with different concentration of Fe_3O_4 nanoparticles through melt-blend method. PES with 20 % Fe_3O_4 nanoparticles generated maximum power density of 9.59 mW/m^2 and current density of 38 mA/m^2. Incorporation of the nanoparticles of more than 20 % (*w/w*) led to cracking of the membrane. Similar observation was also reported by Yusuf et al. (2018). Ceramic membranes with different pore sizes were investigated as PEM in MFC and compared with cation exchange membranes and Nafion membrane (Daud et al., 2018). Ceramic membrane with the largest pore size (13.8 %) showed improved power density, better CE and reduced internal resistance compared to other membranes. Furthermore, the surface wall of ceramics was fabricated with composite layered films composed of chitosan and montmorillonite

minerals (Yousefi et al., 2018). Membranes with six layers and above of the composites recorded a decrease of six-fold in the oxygen gas crossover. This resulted in two-fold maximum power density in membrane with seven bi-layers compared to pristine ceramic membrane.

2.3.5 Nanocomposites of other material as PEM

Hernandez et al. (2016) developed a polymer inclusion membrane based on different weight percent ionic liquid as PEM in MFC application. Ionic liquid of 1-octyl-3-methylimidazolium hexafluorophosphate and methyl trioctil ammonium chloride were utilized. Maximum power density of up to 30 mW/m^2 and COD removal efficiency of 80 % were recorded for membrane with 70 % (*w/w*) ionic liquid supported with ammonium. The increase in ionic liquid concentration resulted in an increase in power density. A synthetic fiber of polybenzimidazole (PBI) was fabricated with different amount of polyvinylpyrrolidone (PVP) and utilized as PEM in MFC (Kumar et al., 2016b). About 81 % increase in power output and superior COD removal percentage were observed in composite membrane with 70:30 % (PVP:PBI) over pure PBI membrane, indicating the efficacy of PVP as composite membrane in MFC. Similarly, PBI was fabricated with mesostructure of SB-15 silica as PEM in a long term MFC operation for wastewater treatment (Angioni et al., 2017). The cost-efficient composite membrane showed an order magnitude increase in maximum power density compared to Nafion, and about 31 % CE and 90 % COD removal were observed.

Blending of sulfonated SiO$_2$ (S-SiO$_2$) with sulfonated polystyrene ethylene butylene polystyrene (SSEBS) was investigated as yet another alternative to Nafion membrane. Various percentages of S-SiO$_2$ ranging from 2.5-10 % (*w/w*) were studied (Sivasankaran et al., 2016). The modified membranes showed superior power density over Nafion, with 7.5 % S-SiO$_2$ membrane exhibiting four-fold increase in power density (1209 mW/m^2)

over Nafion (290 mW/m^2). S-SiO$_2$ incorporation was responsible for improve proton conductivity. Li et al. (2017) thermally grafted an ozone-pretreated poly(vinylidene fluoride) (PVDF) with sodium styrene sulfonate (SSS) as illustrated in Figure 2.9. Solvent evaporation method was employed for the preparation of sulfonic acid PEM. Better in COD removal percentage was observed in the cost-efficient copolymer with comparable maximum power density to Nafion membrane.
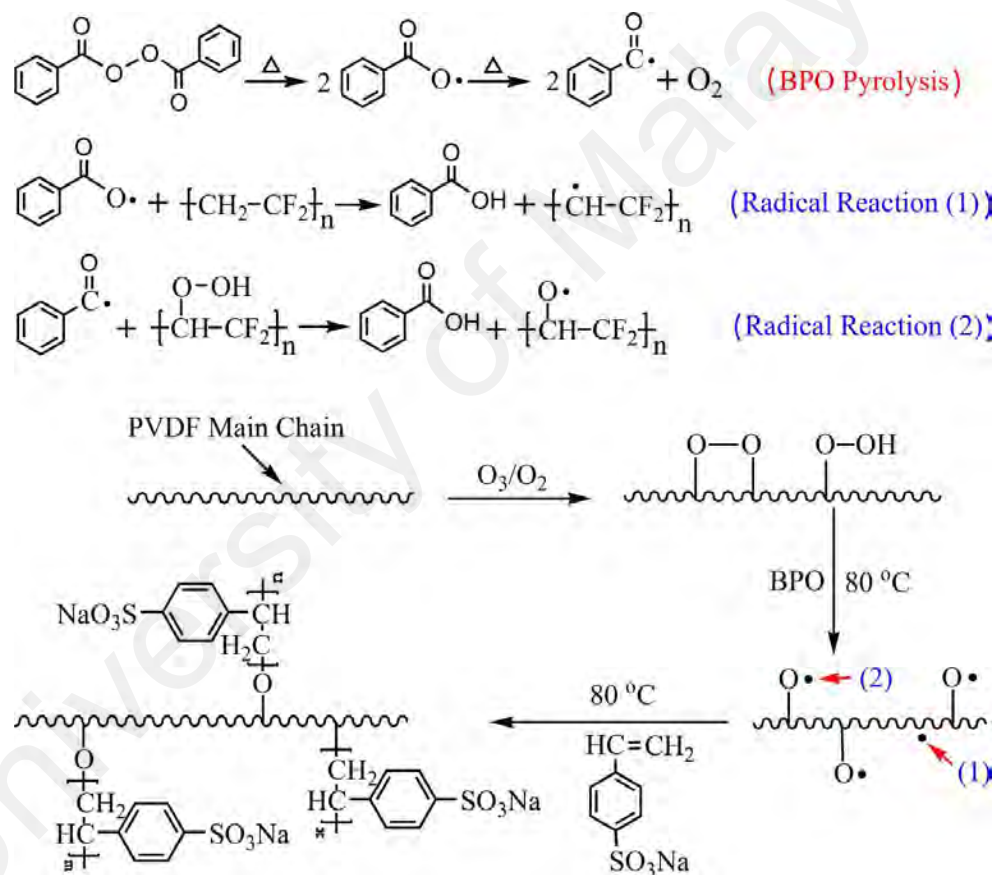
Figure 2.9: Schematic representation of ozone pretreatment of PVDF and graft copolymerization of SSS (reproduced from (Li et al., 2017), with permission from Elsevier)

2.4 Polyhydroxyalkanoates (PHA)

Polyhydroxyalkanoates (PHA) are natural polyesters synthesized by specific groups of bacteria under certain nutrient-deprived conditions. They are widely utilized in medical, industrial and environmental applications due to their biodegradability, biocompatibility and piezoelectric nature (Gumel et al., 2012). In 1926, *Bacillus megaterium* was the first bacterium reported by a French microbiologist to accumulate PHA (Prieto, 2007). Subsequently, various organisms were reported to accumulate PHA either intracellular (Ni et al., 2010; Prieto, 2007; Wong et al., 2011) or extracellular (Abu-Elreesh et al., 2011; Sabirova et al., 2014). The early extraction method using hot alcohol and subsequent purification process by diethyl ether and chloroform resulted in saponified PHA (Lemoigne, 1926). Since then, efficient methods for extraction and purification have been proposed such as extraction through refluxing at 60 ºC in organic solvent such as chloroform for 4 hours and purification using excess cold methanol (Gumel et al., 2012).

PHA are classified into three main groups on the basis of their carbon side chain length. Short-chain-length PHA (scl-PHA) contains 3-5 carbon atoms and are mostly homopolymers, whereas, medium-chain-length PHA (mcl-PHA) contains 6-12 carbon atoms, and are heteropolymers of 3-hydroxyhexanoate, 3-hydroxyoctanoate, 3-hydroxydecanoate and 3-hydroxydodecanoate (Zhang et al., 2009). PHA with more than 14 carbon atoms are considered long-chain-length PHA (lcl-PHA). The structural properties of PHA are determined by the bacterial species and the carbon source(s) utilized during production (Berezina & Martelli, 2014). Figure 2.10 shows mcl-PHA inclusion in cells, extracted and purified mcl-PHA and mcl-PHA chemical structure.
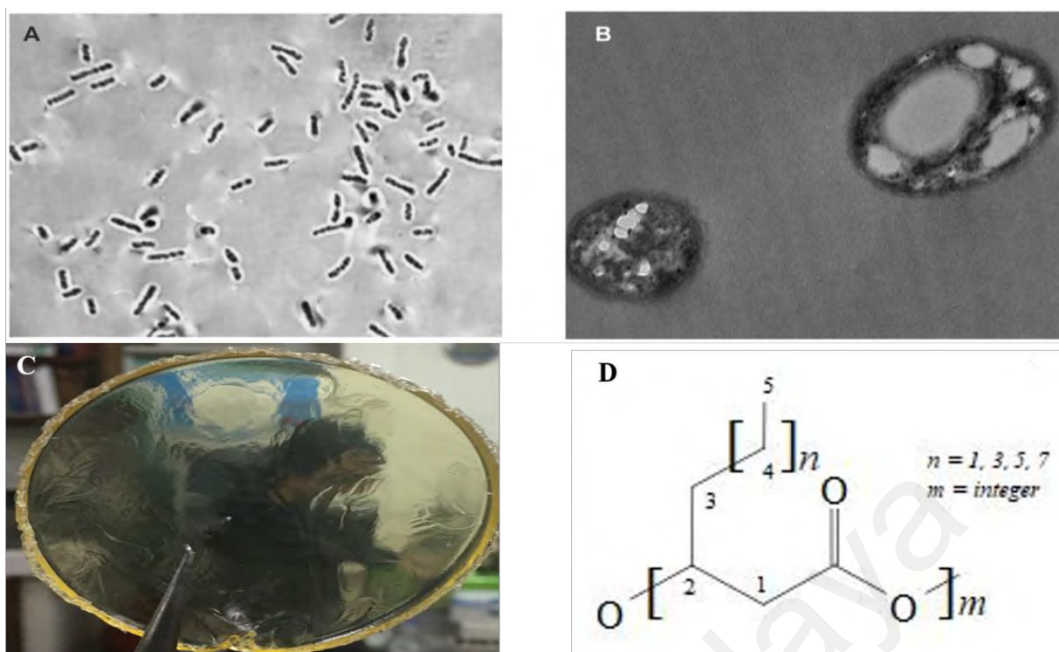
Figure 2.10: (A) phase contrast (× 100 magnification) and (B) transmission electron microscope (× 5000 magnification) micrographs of *Pseudomonas putida* Bet001 cells with PHA inclusion (Gumel et al., 2012), (C) extracted and purified mcl-PHA film, and (D) mcl-PHA basic structure

2.4.1 Biosynthetic pathway of PHA

For maximum polymer yield and specificity in the PHA type and properties, metabolic engineering of PHA pathways have been reported (Filippou et al., 2011; Jian et al., 2010; Theodorou et al., 2011). Three pathways are utilized by bacteria for PHA production (Figure 2.11). The first and common pathway begins with breaking down of sugar to form pyruvic acid through glycolysis pathway (Figure 2.11). Pyruvic acid is then converted to acetyl-CoA *via* pyruvate dehydrogenase oxidation pathway. This process is followed by condensation of acetyl-Co-A molecules to form acetoacetyl-Co-A *via* β-ketothiolase enzyme. Acetoacetyl-CoA reductase enzyme further reduces acetoacetyl-CoA to form the building blocks of PHAs ((*R*)-3-hydroxyacyl-CoA). Polymerization of (*R*)-3-hydroxyacyl-CoA monomers is finally carried out by PHA synthase to form polyhydroxyalkanoates (Figure 2.11) (Gumel et al., 2013).
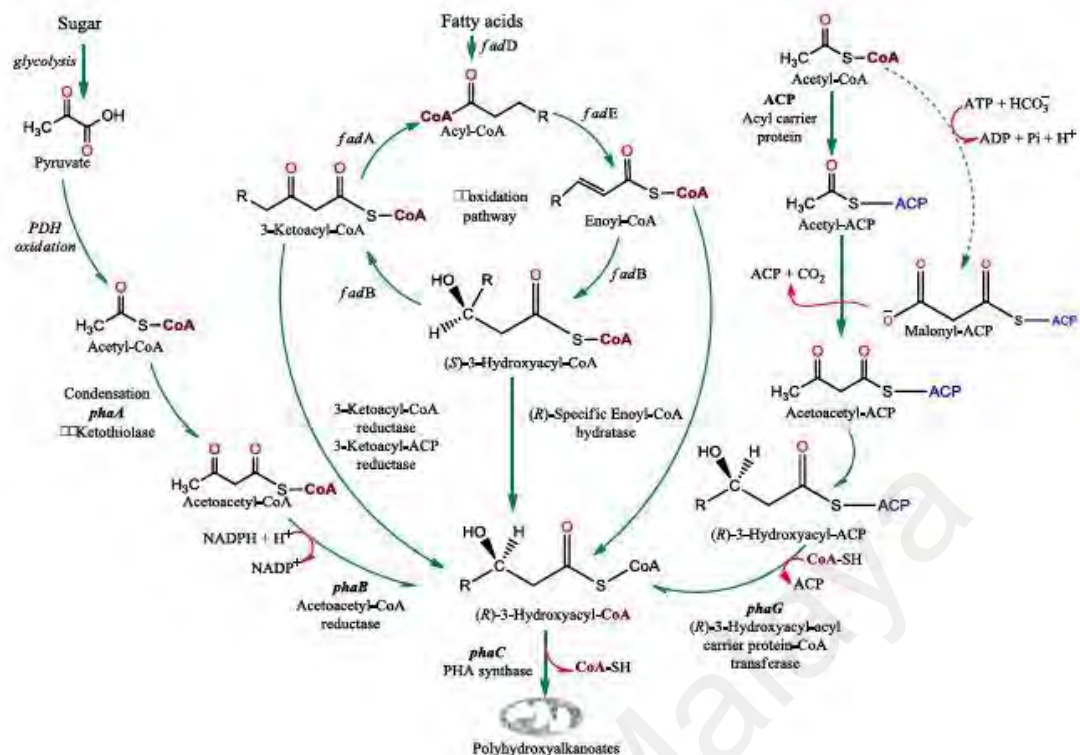
Figure 2.11: Metabolic pathways for PHA biosynthesis *via* sugar catabolism, fatty acid β-oxidation and intermediary pathways (reproduced from (Gumel et al., 2013) with permission from Springer Nature)

The second pathway involves the synthesis of acyl-CoA from fatty acid in the presence of acyl-CoA synthetase. The acyl-CoA then enters the oxidation pathway to form (*S*)-3-hydroxyacyl-CoA (Fig. 2.11). The (*S*)-3-hydroxyacyl-CoA is either reduces to 3-ketoacyl-CoA in the presence of 3-hydroxyacyl-CoA dehydratase or forms the PHA building block monomers of (*R*)-3-hydroxyacyl-CoA *via* (*R*)-specific enoyl-CoA hydratase enzyme. Finally, PHA synthase enzyme polymerize the (*R*)-3-hydroxyacyl-CoA monomers to form polyhydroxyalkanoates.

2.4.2 Production of PHA from renewable sources

Various methods for PHA production have been reported with varying amount of polymer yield. *Cupriavidus species* USMAA2-4 was reported to produce poly-(β)-hydroxybutyric acid at 29 % yield when supplied with oleic acid and 1-pentanol as carbon source (Grothe et al., 1999). The fermentation was carried out in a fed-batch mode at 30 ºC, 200 rpm with 20 % dissolved oxygen. Similar condition with 400 rpm and higher dissolved oxygen (50 %) resulted in about 45 % yield of poly(3-hydroxybutyrate-*co*-4-hydroxybutyrate) when *Ralstonia eutropha* DSM428 was supplemented with fructose as carbon source (Chanprateep et al., 2010). Annuar et al. (2008) reported the production of mcl-PHA by *Pseudomonas putida* PGA1 cultivated on saponified palm kernel oil as the sole carbon source with the yield of 70 % of total biomass weight.

A two-stage continuous fed-batch mode of fermentation was employed for the synthesis of complexed poly(3-hydroxybutyrate-*co*-4-hydroxybutyrate) by *Pseudomonas putida* KTOY06ΔC (PhaPCJac) supplied with mixed fatty acids as carbon source (Theodorou et al., 2011). The system was controlled at 30 ºC, 200 rpm, and pH of 6.5 for 2 days. Sugar molasses was supplied to mixed culture in continuous stirred tank reactor at 400 rpm (Albuquerque et al., 2010). Copolymer of hydroxybutyrate and hydroxyvalerate were synthesized at maximum polymer yield of 61 % by the mixed culture. This process of PHA production opens up a new view in simultaneous production of PHA during wastewater treatment.

2.4.3 Applications of PHA

The rapid increase in utilization of PHA in numerous field has given rise to its mass production. Among the current commercial producers of PHA are Kaneka (Japan); Biomatera, (Italy); Lianyi Biotech (China); Tellas (USA); and Biomer Biotechnology Co. (Germany) (Bugnicourt et al., 2014).

2.4.3.1 Biomedical applications of PHA

PHB brittle nature limited its applications in some fields. Nevertheless, its utilization in biomedical field has been widely reported due to its biocompatibility with cells, supporting role for cell growth, guiding and organizing the cells, allowing tissue in-growth, and degradation to non-toxic products (Williams et al., 1999). Both PHB and PHBV have been reported to respond to both acute and chronic inflammation when applied *in vivo* (Akhtar, 1990). The composites also facilitated healing of muscle-fascial wound (Shishatskaya et al., 2002; Shishatskaya et al., 2004). PHBV alone sustained cell proliferation up to 35 days when incorporated with fibroblast cells (Williams et al., 1999). The blends of PHB and hydroxyapatite were reported for the treatment of bone defects (Doyle et al., 1991; Knowles et al., 1992; Luklinska & Bonfield, 1997). Polyhydroxyalkanoates (PHA) was synthesized by *Bacillus circulans* (MTCC 8167) and used in enhancing the stability of colloidal silver nanoparticles (Phukon et al., 2011). The copolymer of PHA and polycaprolactone (PCL) has been used as scaffolds for cardiovascular tissue engineering (Bouten et al., 2011). Fig. 2.12 shows the applications of various PHA types in biomedical field (Zhang et al., 2018).
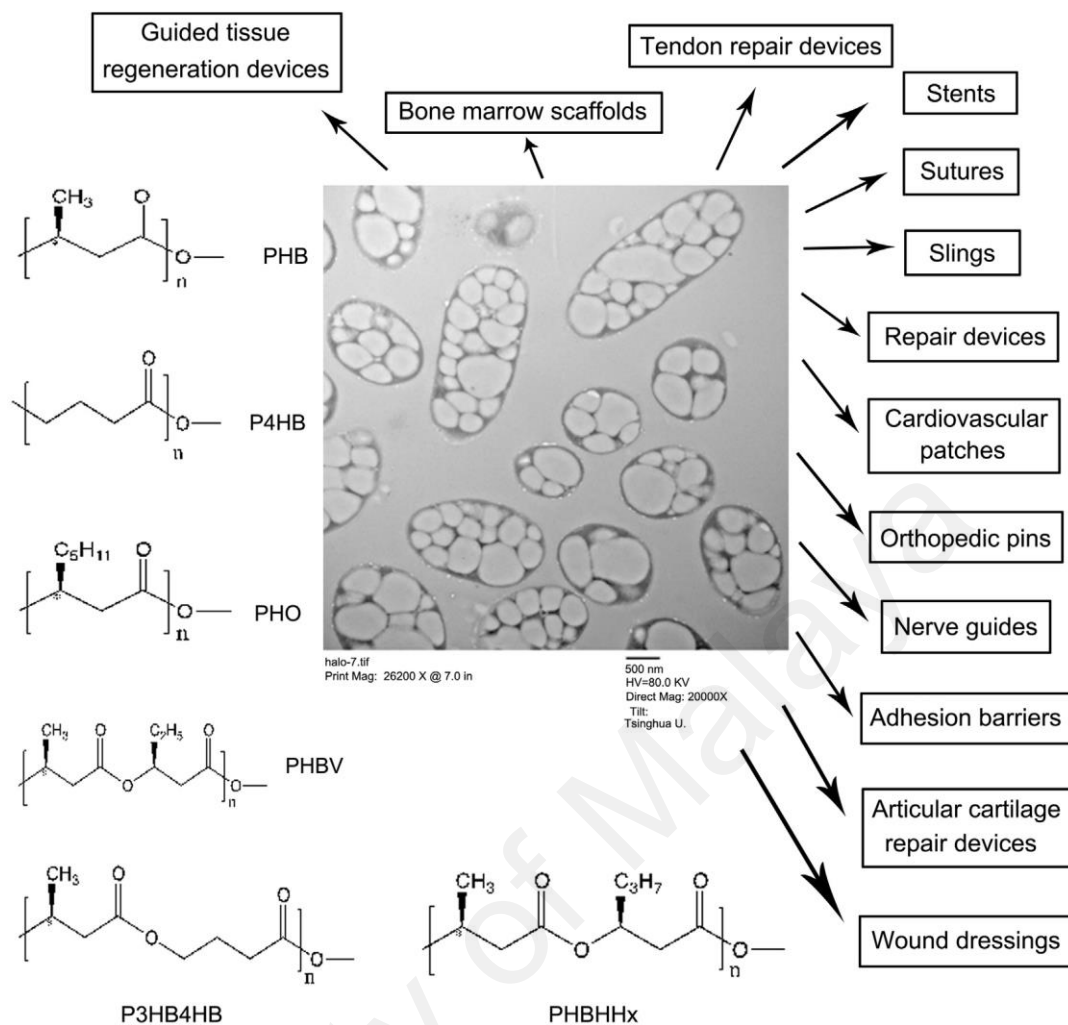
Figure 2.12: Applications of different PHA types in biomedicine. PHB: poly-(*R*)-3-hydroxybutyrate; P4HB: poly-4-hydroxybutyrate; PHO: poly-3-hydroxyoctanoate; PHBV: copolymers of (*R*)-3-hydroxybutyrate and (*R*)-3-hydroxyvalerate; PHBHHx: copolymers of (*R*)-3-hydroxybutyrate and (*R*)-3-hydroxyhexanoate; P3HB4HB: copolymers of (*R*)-3-hydroxybutyrate and 4-hydroxybutyrate (reproduced from (Zhang et al., 2018) with permission from Elsevier)

2.4.3.2 Industrial applications of PHA

Zhang et al. (2009) proposed a novel biofuel containing esterified PHB and mcl-PHA with methanol *via* acid-catalyzed hydrolysis. The copolymer with purity of about 97 % showed combustion heat of 30 KJ/g, slightly lower than ethanol (27 KJ/g). Blending of the copolymer with diesel or gasoline significantly lowered the combustion heat compared to pure diesel or gasoline. Manipulation of PHB synthesis pathway with other metabolic pathways resulted in a new biofuel of butanol, produced from glucose (Bond-

Watts et al., 2011). Also, the monomer chiral centers of PHA and the functional groups of carboxyl and hydroxyl groups in each monomer pave way for its utilization as precursors or intermediates for production of antibiotics, pheromones, aromatics and vitamins (Gao et al., 2011; Ren et al., 2010).

PHB granules in fish-feed have been shown to inhibit the growth of pathogenic bacteria in aquaculture, serving as an alternative to antibiotics (De Schryver et al., 2011; Defoirdt et al., 2011; Nhan et al., 2010). The successful encapsulation of ametryn in PHB was reported by Grillo et al. (2011) to improve herbicidal action and reduce environmental pollution. PHB was successfully utilized as a biomimetic adsorbent material for chlorobenzene and *o*-nitrochlorobenzene removal (Zhang et al., 2010). The glass transition and melting temperatures of PHB were reduced when synthesized with copolymer of poly(3-hydroxyvalerate) for packaging potential (Modi et al., 2011). The glass transition temperature of the copolymer ranged between -10 ºC and 20 ºC making it suitable for packaging.

CHAPTER 3: MATERIALS AND METHODS

3.1   Materials

Ammonium chloride (NH_4Cl), magnesium sulfate heptahydrate ($MgSO_4.7H_2O$), sodium chloride ($NaCl$), monopotassium phosphate hydrogen phosphate (KH_2PO_4), dipotassium phosphate hydrogen phosphate (K_2HPO_4), hydrogen peroxide (H_2O_2), potassium hexacyanoferrate III ($K_3Fe(CN)_6$), sodium dihydrogen phosphate (NaH_2PO_4), disodium hydrogen phosphate (Na_2HPO_4) were purchased from SYSTERM (Malaysia). Sodium bicarbonate ($NaHCO_3$) and calcium chloride dihydrate ($CaCl_2.2H_2O$) were purchased from BDH Chemicals (England). *n*-hexane and methanol were obtained from Lichrosolv (Germany). Methyl acrylate, dichloromethane and benzoyl peroxide were supplied by Merck Millipore (Germany). Sulphuric acid (H_2SO_4, 98 %) was obtained from Fisher Chemicals (Malaysia). Poly-(*R*)-3-hydroxybutyrate was purchased from Sigma-Aldrich (Germany) while Nafion 117 membrane was supplied by Dupont (U.S.A), and activated prior usage by soaking in H_2O_2 (30 %), ultrapure water and sulphuric acid (0.5 M) at 60 ºC for an hour each. Carbon cloth (CC) was sourced from Fuel Cell (Texas, U.S.A), and cleaned *via* ultrasonication in ultrapure water at 35 ºC, 35 kHz for 30 minutes (Qiao et al., 2014). Polytetrafluoroethelene (PTFE) binder was purchased from Sigma-Aldrich (U.S.A) while Nafion 117 solution (binder) was obtained from Fluka (USA). Multi walled carbon nanotube, CNT ($\geq$ 98 % carbon basis, O.D $\times$ I.D $\times$ L 10 nm $\pm$ 1 nm $\times$ 4.5 nm $\pm$ 0.5 nm $\times$ 3 to ~6 μm) was purchased from Sigma-Aldrich (USA).

The oxidation of (CNT) with slight modification to earlier report (Gumel et al., 2014) was carried out. In brief, an appropriate amount of CNT was transferred into a Schott bottle containing a mixture of H_2SO_4 and H_2O_2 in 3:1 volume ratio. The solution was stirred at room temperature (25 $\pm$ 1 °C) for 24 hours and followed by sonication at 40 ºC, 40 kHz for 120 minutes at a power output of 100 % (Elma, P30H, Germany). The sonicated CNT was recovered by filtration using fritted glass. The cake containing the

CNT was washed several times with ultrapure water until the pH of the filtrate became neutral. Finally, it was washed with absolute ethanol. The functionalized CNT cake was dried in an oven at 70 ºC until constant weight. The final yield was approximately 93 %. All experiments were conducted using ultrapure water of 18.2 MΩ/cm resistivity while the reagents are of analytical grades and used as received.

3.2 Methods

3.2.1 Cultivation of medium-chain-length polyhydroxyalkanoate (mcl-PHA)

Mcl-PHA was synthesized by *Pseudomonas putida* BET001 using shaking incubator (DAIHAN LABTECH Co. Ltd., LSI-3016R, Korea). The bacteria culture was grown in a sterilized 30 mL nutrient broth medium contained in 100 mL conical flask shaken at 200 rpm for 24 hours. The culture was further cultivated in rich medium (RM) containing (g/L): yeast extract (10), nutrient broth (15), and ammonium sulphate (5) (Table 3.1). Then, 1 mL of the culture was transferred aseptically into sterilized 200 mL RM contained in 500 mL conical flask, and incubated at 200 rpm for 24 hours at 25 ± 1°C. The cells were concentrated in a 50 mL centrifuge tube by centrifugation (8000 rpm, 3 min, 4 ºC) (SORVALL RC5C PLUS, Thermo Scientific, U.S.A). Residual debris was removed from the cell by washing twice with normal saline (0.9 g/l) prior to optical density determination at 600 nm (OD_{600nm}) using spectrophotometer (UNICO 2100, Vis spectrophotometer). Subsequently, an appropriate volume of the cell was transferred aseptically into 200 mL of polymer production medium (E2) contained in 500 mL conical flask. The E2 medium contained (g/L): 5.6 lauric acid as the sole carbon and energy source, 5.7 K_2HPO_4, 3.7 KH_2PO_4 and 3.5 $NaNH_4HPO_4.4H_2O$ (Table 3.1). After sterilization of E2 medium, a separate solution of 0.1 M $MgSO_4.7H_2O$ (10 mL/L) and trace element solution (1mL/ L) were aseptically added prior to inoculation. Incubation was carried out at 200 rpm for 48 hours (Gumel et al., 2012). The culture containing the cells and the polymer was harvested by centrifugation at 8000 rpm, 3 min, 4 ºC. The

recovered pellet was washed twice with normal saline and finally with *n*-hexane to remove residual fatty acid. Then, the separated biomass was dried using vacuum drier (SCANVAC CoolSafe, 110-4, Denmark) and its weight recorded.

3.2.2   Extraction and purification of synthesized polymer (mcl-PHA)

Mcl-PHA was extracted from the dried biomass using acetone. The biomass was ground using mortar and pestle into fine powder and poured into 1 liter Schott bottle containing excess acetone. The mixture was stirred at room temperature for 24 hours at 200 rpm. This was followed by filtration using Ross 44a filter paper (125 mm in diameter) and the filtrate containing the polymer was concentrated using rotatory evaporator (Yamato Scientific Co. LTD, RE300, Japan). The concentrated mcl-PHA was purified by precipitating the polymer in excess cold methanol (1:5 *v/v* of acetone to methanol) followed by centrifugation at 2500 rpm for 30 min. The process was repeated several times prior to casting of the purified mcl-PHA in PTFE petri-dish (5.5 cm diameter). The polymer was kept at room temperature until it solidify completely. It was finally dried under *vacuo* over P_2O_5 prior to characterization.

Table 3.1: Composition of nutrient rich (NR), fermentation medium (E2), mineral solution and trace element

Media	Composition	Weight per liter (g/L) in UPW
Nutrient rich (NR)	Nutrient broth	15.0
	Yeast extract	10.0
	Ammonium sulphate	5.0
Fermentation medium (E2)	$NaNH_4HPO_4.4H_2O$	3.5
	K_2HPO_4	5.7
	KH_2PO_4	3.7

Mineral solution	Volume in E2 (% v/v)
$MgSO_4.7H_2O$ (0.1M)	1.0
Trace element	0.1

Trace element	Weight per liter (g/L) in 1 M HCl
$CoCl_2.6H_2O$	2.4
$CuCl_2.2H_2O$	0.2
$CaCl_2.2H_2O$	1.5
$FeSO_4.7H_2O$	3.0
$MnCl_2.4H_2O$	2.0
$ZnSO_4.7H_2O$	0.3

3.2.3 Gas chromatography (GC)

GC (Trace GC Ultra, Thermo Scientific, Italy) was employed to determine the concentration and monomer composition of the purified mcl-PHA. The machine was fitted with a fused silica capillary column of 30 m length × 0.32 mm internal diameter with 0.25 μM film (Supelco SPBTM-1, USA). About 10 mg of the sample was dissolved in 2 mL chloroform contained in a vial. Then, methanol and sulphuric acid mixture (85 : 15 % *v/v*) at 2 mL was added to the vial followed by uniform heating in a metal block at 100 ºC for 2 hours. Then, 1 mL of ultrapure water was added to the mixture and vortexed thoroughly. The solution was left overnight for adequate separation. The lower organic solvent layer containing the hydrolysed polymer was separated and analyzed by GC. Benzoic acid methyl ester was used as internal standard to mark the beginning of sample

elution in the column. Methyl 3-hydroxyalkanoates monomer standards (Larodan, Sweden and Aldrich, Germany) were used to determine the retention time and amount of each monomer present (Anis et al., 2017).

3.2.4 Gel permeation chromatography (GPC)

The GPC analysis was carried out using Agilent Technologies 1220 infinity LC instrument (Agilent, USA) with gel column of 7.8 mm internal diameter × 300 mm length and equipped with refractive index detector (Model 1260) (Aris et al., 2016). About 1 mg of the sample was dissolved in 1 mL of tetrahydrofuran (THF) solvent and filtered through PTFE membrane filter (nominal pore size 0.22 μm.) The filtered sample 0.1 mL aliquot was injected at 40 ºC with a flow rate of 0.4 mL / minute using THF as a mobile phase.

3.3 Radical grafting of mcl-PHA with methyl acrylate (MA)

The grafting of mcl-PHA with MA was carried out using thermal method (Figure 3.1). About 200 mg of neat mcl-PHA was dissolved in 4 mL acetone in a trident vial. Benzoyl peroxide (5 mg) was added as the radical initiator and finally, 200 mg of MA was added to the mixture. The solution was sparged with nitrogen gas for 10 minutes to provide O_2-free reaction medium. Then, the reaction vials were immediately sealed and incubated at 80 ºC for 120 minutes in a metal heating block (WiseTherm®, HB48, Korea). After incubation, the vials were allowed to cool to room temperature, and subsequently poured into a glass petri dish and allowed to solidify. The grafted polymer was purified by dissolution in acetone followed by precipitation in excess cold methanol. This process was repeated thrice, and the graft material was re-casted in a glass petri dish. Finally, it was dried *in vacuo* over P_2O_5 at 30 ºC. The purified grafted copolymer was designated as MA-PHA and showed 71.2 % increase in mass.
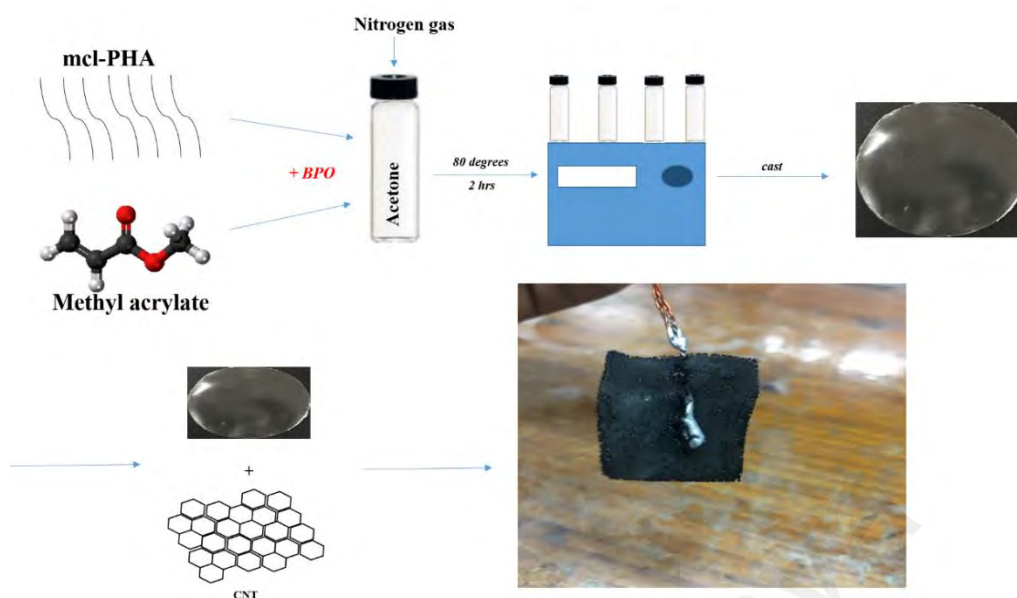
Figure 3.1: Schematic diagram of MA-PHA copolymerization and its subsequent composite with oxidized CNT

3.3.1 Preparation of electrodes

For cathode electrodes, purified carbon cloth (CC) was modified with either CNT (designated as CC-CNT) or composite of CNT and MA-PHA (designated as CC-CNT/MA-PHA). For CC-CNT cathode electrode, about 20 mg of functionalized CNT was added into a vial containing 2 mL ultrapure water. The mixture was vortexed and sonicated at 40 kHz, 35 °C for 30 minutes at 100 % power output. Thereafter, 100 µL of Nafion 117 solution was added and vortexed rigorously. Using 100 µL micro pipette, the mixture was evenly spread on purified CC and allowed to dry at room temperature. For CC-CNT/MA-PHA cathode electrode, about 5 mg of the grafted polymer was dissolved in 2 mL acetone. Approximately 20 mg of CNT was added and vortexed prior to ultrasonication as previously explained without the addition of a binder.

The anode electrodes were modified with either CNT (CC-CNT) as explained above or with CC-CNT/MA-PHA containing 20 mg of the grafted polymer. All electrodes were dried for 48 hours at room temperature before undergoing further preparation steps by

soaking in ultrapure water for 4 hours to remove residual debris prior to application in MFC. The surface area of each electrode is approximately 2×3 cm^2. The loading of CNT on the CC was approximately 3 mg/cm^2 while that of MA-PHA and CNT composite was 6 mg/cm^2 and 3 mg/cm^2 for anode and cathode electrode respectively. The material loading was calculated according to equation (3.1):

$$\text{Material loading rate} = \frac{FW_{cc} - IW_{cc}}{ESA} \qquad\qquad (3.1)$$

where FW_{cc} and IW_{cc} are the final and initial weight of CC (mg), and ESA is the electrode surface area (cm^2).

3.3.2   Characterization of electrodes

Functionalized CNT, neat mcl-PHA, carbon cloth and modified electrodes were subjected to Perkin-Elmer (Wellesley, MA, USA) FTIR spectrometer at a scan range of 4000-400 cm^{-1} (Gumel & Annuar, 2014). The crystallinity of pristine and modified electrodes was determined using XRD (Bruker, Smart Apex II) at 25 ºC ranging between $5º \leq 2\theta \leq 70º$ with a step size of 0.0260 s^{-1} (Yusuf et al., 2018). The morphologies of the electrodes before and after biofilm formation were analyzed using FESEM (FEI Quanta 450 FEG) and coated with platinum prior viewing. Electrode samples with biofilm attached after MFC operation were prepared by soaking in 2.5 % glutaraldehyde for 12 hours, followed by washing with sodium chloride (0.9 % w/v) and with ethanol solution of 30, 50, 70, 85 and 95 % for an interval of 10 minutes (Liu et al., 2014). Proton nuclear magnetic resonance (H^1 NMR) spectra of plain PHA and MA-PHA were recorded on JEOL (FT-NMR ECA400) machine (Gumel & Annuar, 2014).

3.3.3   Electrochemical analyses

Electrochemical impedance spectroscopy (EIS), cyclic voltammetry (CV) and electrode conductivity (δ) measurement were performed on the electrodes applied in MFC

using Gamry Interface 1000 (Warminister, PA, USA). The CV of each anode electrode in 100 mL of fresh anolyte was recorded at a scan rate of 5 mV/s between -600 mV and +600 mV, while the cathode electrode in 100 mL of fresh catholyte was recorded at scan rate of 5 mV/s from 0 to 1000 mV. The working electrode was either the anode or cathode electrode while the reference and counter electrodes were Ag/AgCl and platinum wire respectively.

At a stable and maximum cell potential, the EIS of the device was measured at an open circuit potential mode with frequency ranging from 10^{-8} to 1 MHz at alternate current (AC) amplitude signal of 10 mV. Prior to MFC operation, different amounts of MA-PHA ranging from 5 mg to 100 mg was composited with a fixed amount of CNT (20 mg) and loaded onto CC to determine the appropriate amount for MFC operation. The electrodes were subjected to CV and conductivity tests. The conductivity (δ) of dried electrodes was measured by placing the electrode between metal electrode of 3.142 cm^2 surface area and the resistance (R) from 100 Hz to 1 MHz measured at AC of 10 mV. The δ was calculated according to equation (3.2):

$$\delta(S/cm) = \frac{T_e}{R \times A} \tag{3.2}$$

where T_e is the electrode thickness (cm) and A is the electrode cross-sectional area (cm^2).

3.3.4 MFC fabrication and operation

3.3.4.1 Inoculum preparation

The anode chamber of the doubled-chambered MFC was inoculated with *Escherichia coli* as biocatalyst. *Escherichia coli* was chosen because it is a facultative anaerobe, and oxygen cross-over effects on the strain will be minimal, compared to other biocatalysts such as *Geobacter sulfurreducens*, which is an obligate anaerobe. The

bacteria preparation was activated aseptically from freeze dried samples kept at -20 °C in glycerol. The activation was performed in Luria-Bertani (LB) broth at 30 °C, 200 rpm for 24 hours. The bacteria was concentrated by centrifugation at 8000 rpm, 4 °C for 3 minutes, followed by three times washing with phosphate buffer solution (PBS, pH 7). The concentrate was finally re-suspended in 10 mL PBS and used as biocatalyst in MFC operation at 10 % *v/v*.

3.3.4.2 MFC assembly and operation

The MFC operation was carried-out using a double-chambered, H-shaped cylindrical glass vessel (Adams and Chittenden Scientific Glass, Berkeley, USA). The use of toxic and expensive platinum at the cathode for efficient oxygen reduction rate in most single-chambered MFC favors the application of inexpensive double-chambered MFC in this study. In addition, the steps involved in assembling air cathode single-chambered MFC are relatively less simple compared to the double-chambered MFC. More importantly, the rate of oxygen diffusion from membraneless single-chambered MFC is about 2.7 times higher than the double-chambered MFC. Consequently, it results in low coulombic efficiency (CE) and low power output (Luo et al., 2009; Saravanan & Karthikeyan, 2017).

The chambers were separated by purified Nafion membrane (3.5 cm diameter). The total volume for each of the anode and cathode compartment was 90 mL. The anode chamber was inoculated with 10 % *v/v* biocatalyst together with laboratory prepared anolyte containing (g L^{-1}) in ultrapure water: K_2HPO_4 (10.7), KH_2PO_4 (5.3), NaCl (1), $MaHCO_3$ (0.2), NH_4Cl (0.3), $MgSO_4.7H_2O$ (0.3), $CaCl_2.2H_2O$ (0.04) and 0.1 % (v/v) of trace element (Table 3.1). The cathode chamber was filled with 50 mM [$K_3Fe(CN)_6$] in 100 mM PBS (pH 7). Since the biocatalyst is a facultative anaerobe microorganism, the anode chamber was sparged with nitrogen for 15 minutes and immediately sealed for

oxygen-free environment. The prepared electrodes were utilized in three different MFC setups. MFC 1 consisted of CC-CNT anode and CC-CNT cathode, MFC 2 consisted of CC-CNT anode and CC-CNT/MA-PHA cathode, while MFC 3 consisted of CC-CNT/MA-PHA anode and CC-CNT/MA-PHA cathode. The three MFC setups were operated at 30 °C in an incubator (Hotech, Model 624, Taiwan) for 30 days across 1 kΩ external resistor. The voltage was recorded hourly using a digital multimeter (VICTOR, 86B, RuoShui Yitensen®). Fed-batch mode of operation was employed and the anolyte was replaced when the voltage reading decreased below 40 mV. The catholyte was sparged continuously during 30 days operation with filtered air using air pump (FISCO, Model AP-348T, Singapore). Resistors between 0.33 kΩ - 10 kΩ were applied during stable and maximum power output and the polarization data was recorded (Logan, 2008). The current (*I*) and power density (PD) were calculated according to the equations (3.3) and (3.4), respectively;

$$I = \frac{V}{R}$$
(3.3)

where *R* is the resistance (Ω) and *V* is the voltage recorded (V); and

$$PD = \frac{I \times V}{ESA}$$
(3.4)

where *ESA* is electrode surface area (cm^2).

3.3.5   Stability of polymeric electrode in MFC

The anode electrode containing MA-PHA nanocomposites was tested for copolymer (bio)degradability at day 0, 30 and 60 of MFC operation. The reduction in the molecular weight of the copolymer indicated its (bio)degradability rate.

3.3.5.1 Gel Permeation Chromatography (GPC)

At the end of 0-, 30- and 60 days MFC operation, a small piece (1×1 cm^2) of the electrode containing MA-PHA was cut out and immersed in dichloromethane (DCM). The copolymer was extracted, purified and analyzed as previously reported in *section 3.2.4*, and the changes in molecular weight were recorded.

3.4 Preparation of polymeric membrane (mcl PHA-PHB composite)

Mcl PHA-PHB membrane was prepared through solvent blending method (Figure 3.2). An appropriate amount of purified mcl-PHA was dissolved in 5 mL chloroform in a vial. Different percentages of commercially sourced PHB ranging from $5 - 15$ % (*w/w*) were added to the solution. The mixture was stirred at room temperature for 30 min and subsequently kept in 50 ºC oven for 12 hours. The blend was stirred once more for 30 min prior to casting in PTFE petri-dish (5.5 cm diameter). The membrane was kept at room temperature until constant weight. Residual solvent was removed under *vacuo* over P$_2$O$_5$ before characterization and utilization in MFC. Pristine mcl-PHA was prepared in parallel following the above steps to be applied as reference membrane.
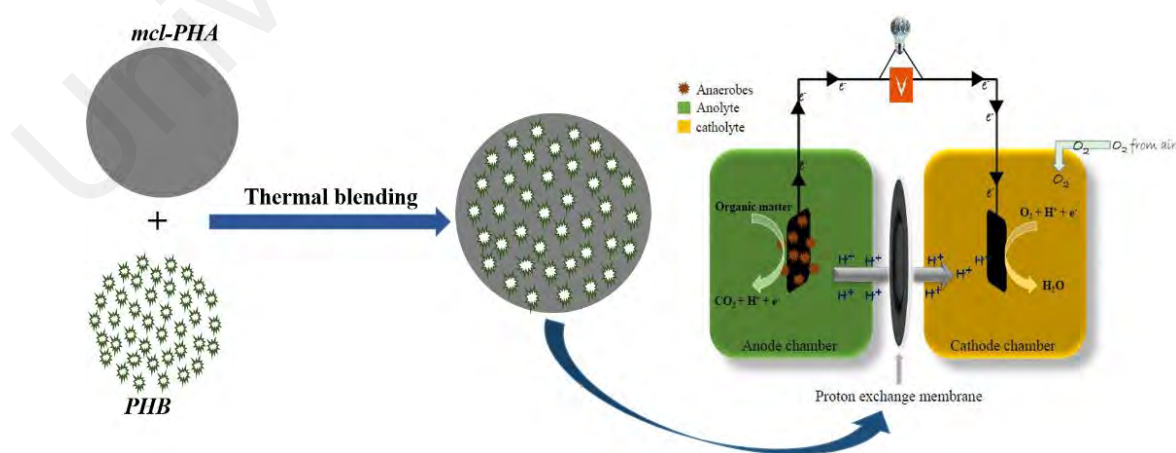
Figure 3.2: Schematic diagram of mcl PHA-PHB nanocomposite membrane formation

3.4.1 Characterization of membranes

3.4.1.1 FTIR and XRD Analyses

The functional groups of the membranes were determined using FTIR spectrometer (Perkin-Elmer, Wellesley, MA, USA) as described in *section 3.2.2*. The degree of crystallinity of neat and modified membranes were evidenced by XRD (Bruker, Smart Apex II) as previously described in *section 3.2.2*.

3.4.1.2 Field Emission Scanning Electron Microscopy (FESEM)

About 1×1 cm^2 of each membrane sample was subjected to both surface and cross-sectional morphology using FESEM (FEI Quanta 450 FEG) (details in *section 3.2.2*)

3.4.1.3 Oxygen Diffusion Test

The amount of oxygen seeping from aerobic cathode to anaerobic anode over time was determined according to earlier reports (Kim et al., 2007; Yusuf et al., 2018). In brief, both the anode and cathode chambers were filled with 100 mL of sterilized ultra-pure water (UPW) of 18.2 Ω/cm^2 resistivity. The cathode was sparged with purified oxygen until 100 % saturation while the anode was sparged with purified nitrogen gas until 0 % oxygen content. The oxygen diffusivity rate was measured with oxygen probe sensor (Mettler Toledo, Greitensce, Switzerland). The measurements were used to determine diffusion coefficient (D_o) and mass transfer coefficient of oxygen (K_o) as reported by (Kim et al., 2007);

$$K_o = -\frac{V}{C_s \cdot t} \cdot ln\left[\frac{C_1 - C_2(t)}{C_1}\right] \tag{3.5}$$

where V is the volume of UPW in the anode chamber (100 mL), C_s is the membrane cross-sectional area, C_1 is the concentration of dissolved oxygen at the cathode chamber and $C_2(t)$ is the dissolved oxygen at the anode at time t.

The D_o was calculated using the following equation;

$$D_o = K_o \cdot M_t \tag{3.6}$$

where M_t is the membrane thickness (cm).

3.4.1.4 Water uptake by membrane

About 50 mg of each membrane was dried under *vacuo* over P_2O_5 overnight and the weight recorded as weight initial (W_i). The membrane was then immersed in 50 mL UPW and allow to stand for 24 hours at room temperature. The wet membrane was blotted to remove excess water and the weight was recorded as weight final (W_f). The percentage water uptake (% *WU*) was determined according to equation 3.7:

$$\% \, WU = \frac{W_f - W_i}{W_i} \cdot 100 \tag{3.7}$$

3.4.2 MFC fabrication and operation

3.4.2.1 Wastewater characterization

Food wastewater was obtained from Euro Cafeteria, Student Complex Center, University of Malaya, Malaysia and kept in -20 ºC freezer (Protech, Chest Freezer, CF-300, Malaysia). Table 3.2 showed the raw and supplemented pH, conductivity, chemical oxygen demand (COD), and ammoniacal nitrogen (NH_3-N) of the wastewater. To increase the conductivity of the wastewater, the following supplements were added (g/L): 10.7 K_2HPO_4, 5.3 KH_2PO_4, 1 glucose and 0.1 % (*v/v*) trace element.

Table 3.2:   Food wastewater parameters before and after the addition of supplements

Parameters	Raw wastewater	Wastewater with supplements
Conductivity (µS/cm)	208.8	1500
pH	4.20	7.00
COD (mg/L)	780	1005
NH$_3$-N (mg/L)	6.3	8.2

3.4.2.2 Preparation of inoculum

Escherichia coli was utilized as the biocatalyst. The bacteria preparation was cultivated aseptically as previously reported in *section 3.2.4.1*. Separated bacterial cells were re-suspended in 10 mL phosphate buffer solution (PBS, pH 7) and used in MFC operation at 10 % *v/v*. The acclimatized anolyte containing *E. coli* and wastewater was used as inoculum at 10 % *v/v* as described in the following sections.

3.4.2.3 Electrode preparation

Carbon cloth (CC) of 2×3 cm^2 surface area was utilized as base material for both anode and cathode electrodes, and modified with functionalized MWCNT with PTFE as binder. The anode electrode was activated with biofilm colonization by dipping it for a month in an MFC set-up with wastewater and *E. coli* mixture as anolyte. The electrode with prominent microbial growth and biofilm attachment was utilized in a batch mode MFC operation.

3.4.2.4 MFC operation

A double-chambered, H-shaped cylindrical glass vessel (Adam and Chittenden Scientific Glass, Berkeley, U.S.A) was used throughout the experiment. The working volume of the anode was 100 mL containing 90 mL of wastewater and 10 mL of

acclimatized inoculum. The cathode chamber was filled with 100 mL of 50 mM [$K_3Fe(CN)_6$] in 100 mM PBS (pH 7) (Figure 3.3). An oxygen-free environment was created in the anode chamber by sparging with nitrogen gas for 15 min and then immediately sealed. The cathode chamber was sparged with purified oxygen gas. The modified membranes were utilized in six different MFC set-ups. MFC 1 consisted of Nafion 117 as the control membrane, and designated as Nafion, MFC 2 consisted of 5 % PHB and 95 % PHA (*w/w*) and designated as PHB5%. MFC 3 consisted of 10% PHB and 90% PHA (*w/w*) and designated as PHB10%, MFC 4 consisted of 15% PHB and 85% PHA (*w/w*) and designated as PHB15%, MFC 5 consisted of 15% PHB with polymeric modified electrodes of MA-PHA as described in *section 3.3.1* and designated as mMFC (modified MFC) while MFC 6 consisted of 100% PHA as negative control and designated as PHA100%. The six MFC set-ups were operated at 30 ºC in an incubator (Hotech, 624, Taiwan) across 1000 Ω external resistor for a complete MFC cycle. Polarization data was recorded at a stable and maximum power output between 430 − 10,000 Ω resistance (Logan, 2008). The voltage was monitored at an hour interval while 5 mL of anolyte was drawn every 24 hours for the determination of OD_{600nm} (UNICO 2100, Visible spectrophotometer), pH (Mettler Toledo, FiveEasy F20, Switzerland), conductivity (Mettler Toledo, SevenCompact S20, Switzerland), ammoniacal nitrogen (NH_3-N) and chemical oxygen demand (COD) tests (Rice et al., 2012). The NH_3-N concentration was calculated from standard calibration plot prepared according to phenate method as reported by (Rice et al., 2012) (Figure 3.4) while COD content was calculated based on equation 3.8:

$$\%COD\ reduction = \frac{COD_1 - COD_2}{COD_1} \cdot 100 \qquad (3.8)$$

where COD_1 is the initial COD content while COD_2 is the final COD content of the wastewater.

The coloumbic efficiency (CE) over time *t* was determined according to equation 3.9 (Logan et al., 2006)

$$CE = \frac{M_w^{glu} \int_0^t I\,dt}{FbV\Delta COD} \tag{3.9}$$

where M_w^{glu} is the glucose molecular weight, F is Faraday's constant (96,485 C/mol), b is the number of electrons exchanged per mole of glucose (24), V is the volume of anolyte (100 mL) and ΔCOD is change in COD over time.
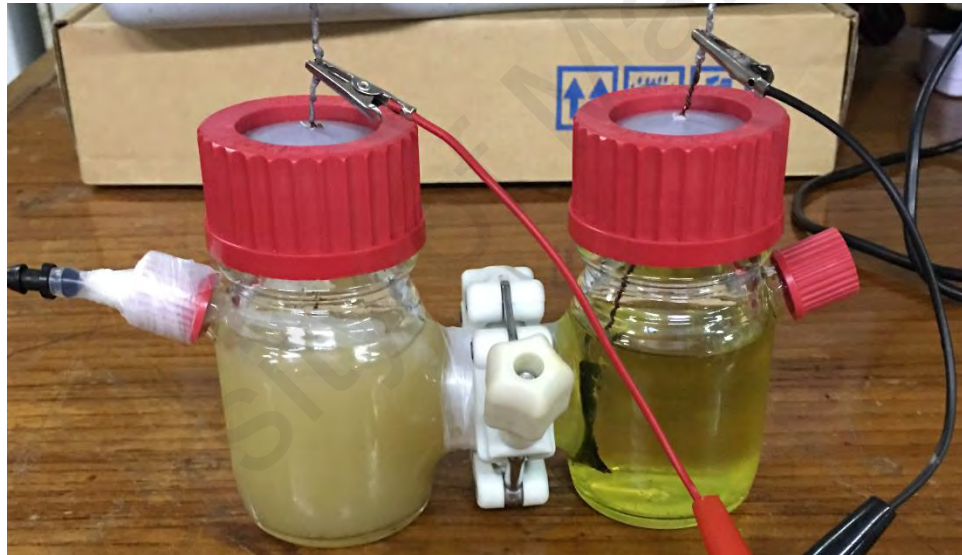
Figure 3.3:   MFC utilized for mcl PHA-PHB membrane performance

$$y = 1.3655x - 0.0619$$
$$R^2 = 0.991$$
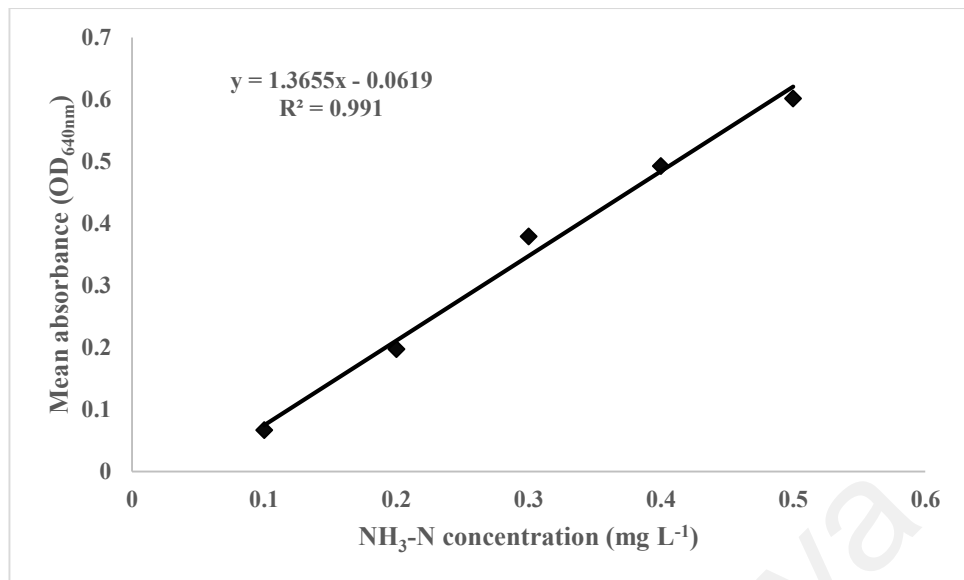
Figure 3.4: Ammoniacal nitrogen (NH$_3$-N) standard calibration

3.5 Statistical analysis

Experimental data were analyzed using SigmaPlot™ version 12.0. One-way ANOVA was utilized for determination of significant difference at $p < 0.05$ using Minitab® software version 17.

CHAPTER 4: RESULTS AND DISCUSSION

4.1   Mcl-PHA properties

Shake flask technique was employed for bacterial synthesis of mcl-PHA with lauric acid as the sole carbon and energy source. The gas chromatography-mass spectrometry analysis (GCMS) of the purified PHA revealed the following monomer composition: 3.7 mol% hydroxyhexanoate, 40.7 mol% hydroxyoctanoate, 39.5 mol% hydroxydecanoate and 16.0 mol% hydroxydodecanoate. It's composed of 136 ± 4 KDa weight-averaged molecular weight (M_w), 73 ± 2 KDa number-averaged molecular weight (M_n) and 1.9 ± 0 polydispersity index (PDI) based on gel-permeation chromatography (GPC) analysis. The extracted polymer was about 32.3% (*w/w*) from the dry biomass weight.

4.2   Characterization of MA-PHA composite electrodes

The functional groups of oxidized CNT, neat mcl-PHA, MA-PHA and its composite are shown in Figure 4.1 from FTIR spectroscopic analysis. The presence of – OH groups in functionalized CNT spectra shows successful oxidization of multi-walled carbon nanotubes. The peak was significantly reduced in CC-CNT/MA-PHA electrode as the result of dispersion of CNT within the MA-PHA polymer matrix (Gumel et al., 2014). The common observation in all samples is the symmetric and asymmetric vibration of –C-H stretch at 2928 cm^{-1} and 2860 cm^{-1} (Figure 4.1). In neat mcl-PHA polymer, the peak signal at 1736 cm^{-1} is assigned to –C=O stretch, which denotes the ester group. The same stretch is observed in the grafted polymer (MA-PHA) with a sharper peak indicating successful grafting of methyl acrylate monomers into mcl-PHA matrix. The presence of new absorption band at 827 cm^{-1} in MA-PHA polymer is assigned to the out-of-plane deformation of the C=C of acrylate groups (Salih et al., 2015). The side chain of mcl-PHA polymer characterized by the presence of –CH$_2$ is evidenced by the signal at 732 cm^{-1} for both mcl-PHA and MA-PHA samples (Sánchez et al., 2003). The signal,

although weaker, is also present in CC-CNT/MA-PHA and shifted to 724 cm^{-1} from the layered composite on the CC surface.
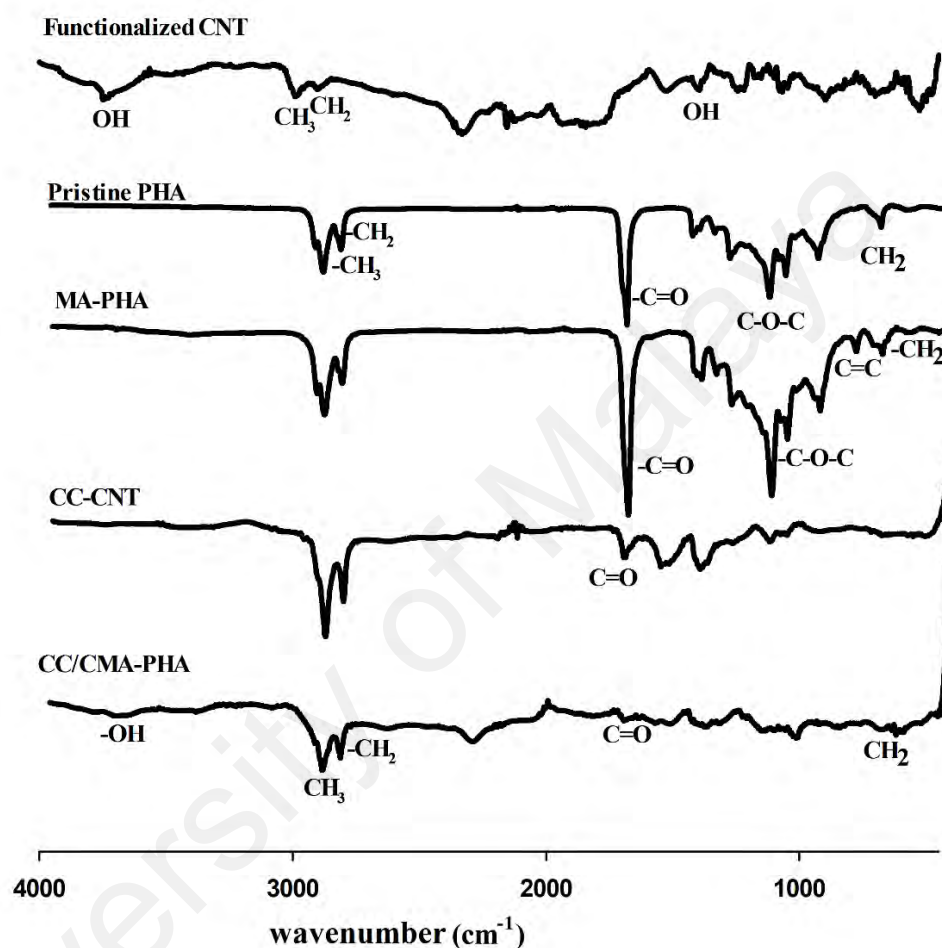
Figure 4.1: ATR-FTIR spectra of functionalized CNT, pristine mcl-PHA, MA-PHA, CC modified with CNT, and CC modified with CNT and MA-PHA

The crystallinity of grafted polymer and its composites are shown in Figure 4.2. The diffraction peaks in neat mcl-PHA which appeared at 2θ values of 19.1 and 21.3 correspond to the reflections of (110) and (111) with *d*-spacing of 0.46 and 0.42 nm respectively. These two distinct peaks represent the polymer backbone (Gumel et al., 2014; Yusuf et al., 2018) and are also present in MA-PHA graft and CC-CNT/MA-PHA composite. A new peak at 2θ of 19.9 with *d*-spacing of 0.45 nm corresponds to a reflection

of 130, a property found in crystalline polymer (Muralidhar & Pillai, 1988; Yıldırım & Seçkin, 2014). The presence of CNT within the polymer matrix and on CC is evidenced by 2θ values of 25.5 (002) and 43.4 (101) with *d*-spacing of 0.35 and 0.21 nm respectively on the composite samples (CC-CNT/MA-PHA). The increased intensity of 25.5 (002) peak in CC-CNT/MA-PHA is attributed to the crystalline nature of methyl acrylate monomers in addition to the presence of dispersed CNT mass that subsequently increased its crystallinity (Hindatu et al., 2017b).
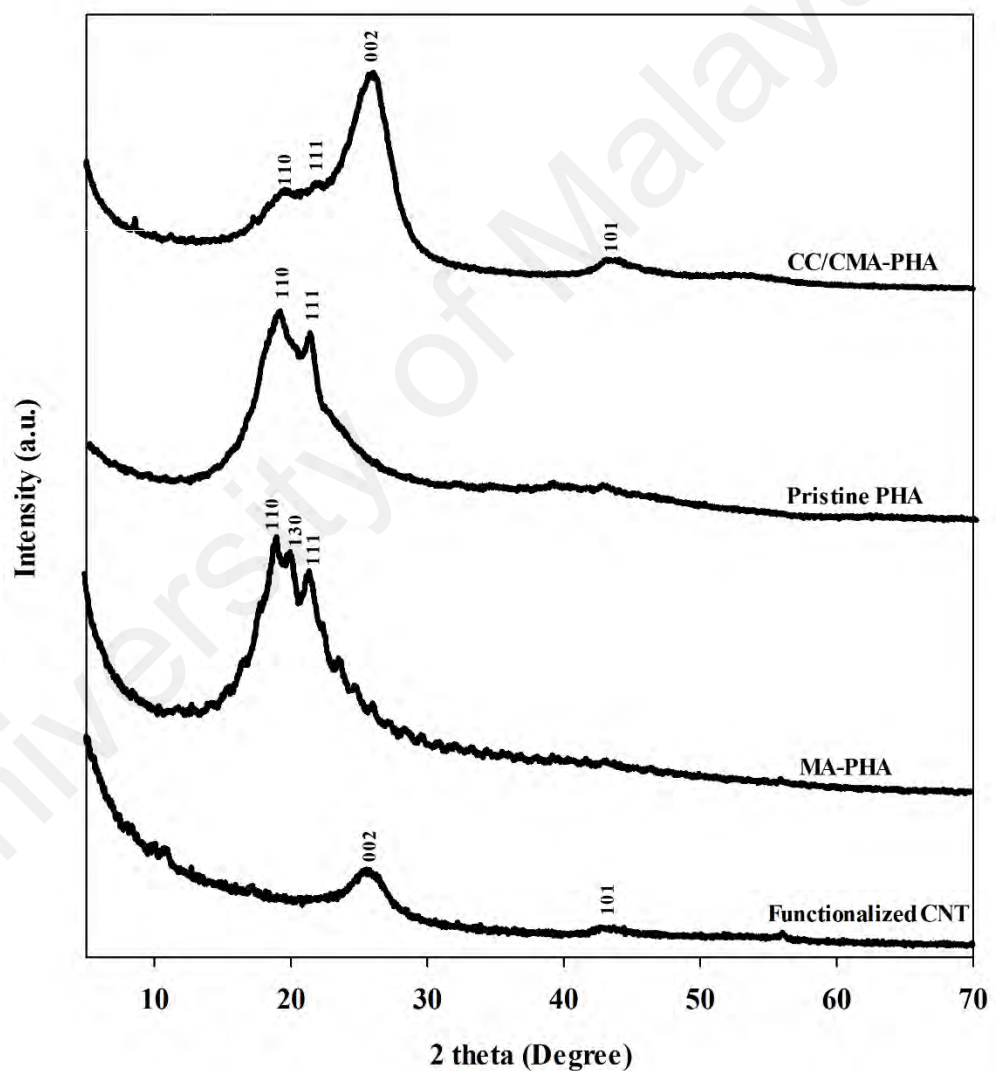
Figure 4.2: X-ray diffractograms of functionalized CNT, pristine mcl-PHA, MA-PHA, and CC modified with CNT and MA-PHA

The ^{1}H NMR spectra for both neat mcl-PHA and grafted polymer are shown in Figure 4.3 *a* and *b* respectively. Tetramethylsilane (TMS) was included as the internal standard with deuterated chloroform as the solvent. Chemical shifts 1, 2, 3, and 4 are assigned to α and β protons of CH-COO, O-CH, CH$_2$, and CH$_2$ respectively in mcl-PHA while the shift 5 represent the terminal methyl group of mcl-PHA side chain. In Figure 4.3*b*, shift *x* indicates the terminal methyl group of methyl acrylate monomer while the chemical shifts *y* and *z* represent the backbone of MA monomer *viz*. CH-COO and CH$_2$ respectively. The results are in accordance with previously reported literatures (Gumel & Annuar, 2014; Ward et al., 2015). The detection of chemical shifts *x*, *y* and *z* as shown in Figure 4.3*b* supported successful grafting of MA monomers into mcl-PHA matrix.
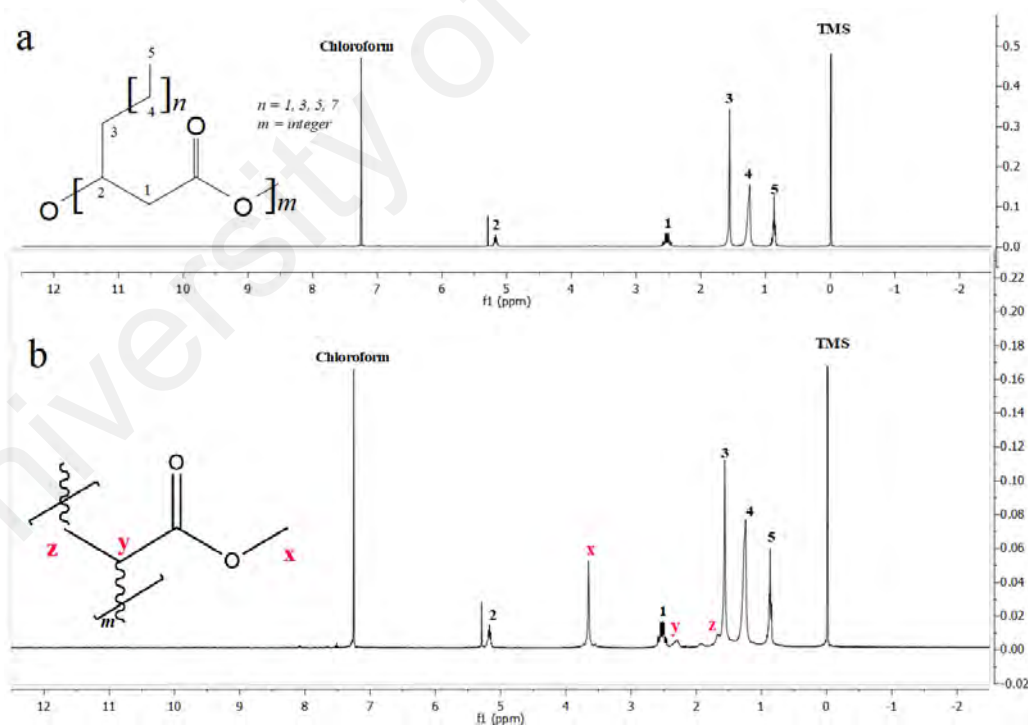
Figure 4.3: Proton NMR spectra of, *a* neat mcl-PHA, and *b* MA monomers grafted with mcl-PHA

Visual observation of the nanomaterials on the electrode was made using FESEM as shown in Figure 4.4. The pristine CC (Fig. 4.4*a*) showed the absence of foreign bulk deposit compared to Figure 4.4*b*, where CNT was layered on the CC surface aided by 100 µl Nafion 117 solution as a binder. Ultrasonication of the grafted polymer and CNT resulted in dispersion the CNT within the polymer matrix as shown in Figure 4.4*c*. Here, the more complete coverage of CC surface by the grafted material owed to the higher mass fraction of MA-PHA used i.e. 20 mg. In contrast, CC-CNT/MA-PHA-cathode (Figure 4.4*d*) electrodes appeared less complete in its surface coverage as only 5 mg of grafted material was applied. This was also the reason for the calculated material loading of CC-CNT/MA-PHA-anode (6 mg/cm^2) being twice that of CC-CNT (3 mg/cm^2) and CC-CNT/MA-PHA-cathode (3 mg/cm^2) electrodes. FESEM micrographs at lower and higher magnifications for studied electrodes before and after MFC application are presented in Figures 4.5, 4.6 and 4.7.
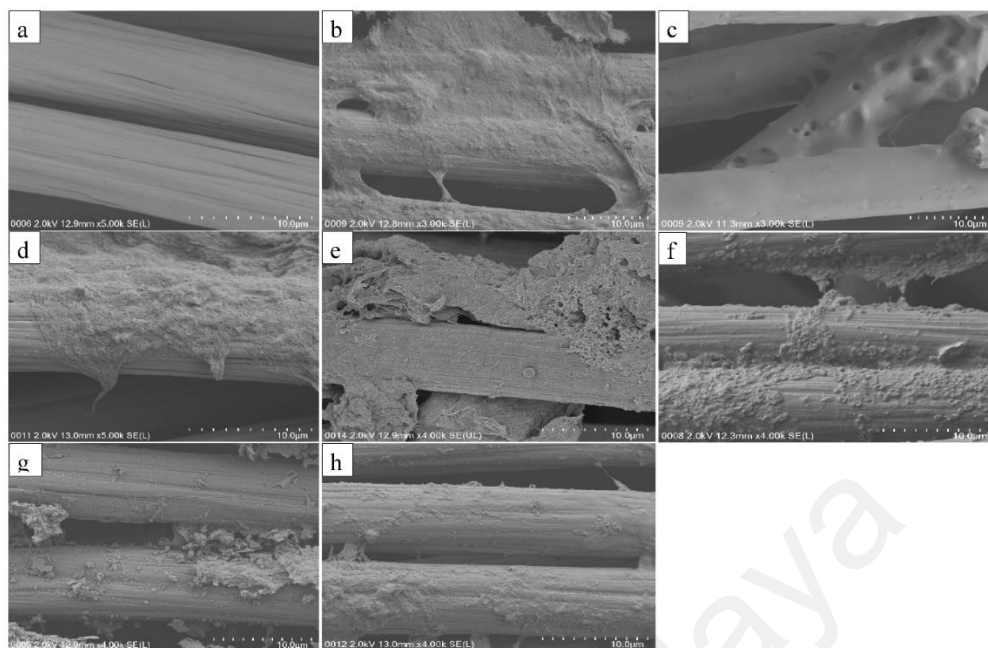
Figure 4.4: FESEM micrographs of plain electrode and modified electrodes prior to MFC analysis, *a* Pristine CC, *b* CC modified with CNT (CC-CNT), *c* CC modified with CNT (20 mg) and MA-PHA (20 mg) as anode electrode (CC-CNT/MA-PHA-anode), *d* CC modified with CNT (20 mg) and MA-PHA (5 mg) as cathode electrode (CC-CNT/MA-PHA-cathode) and biofilm formation of electrodes after MFC analysis, *e* CC-CNT-anode, *f* CC-CNT/MA-PHA-anode, *g* CC-CNT-cathode, *h* CC-CNT/MA-PHA-cathode
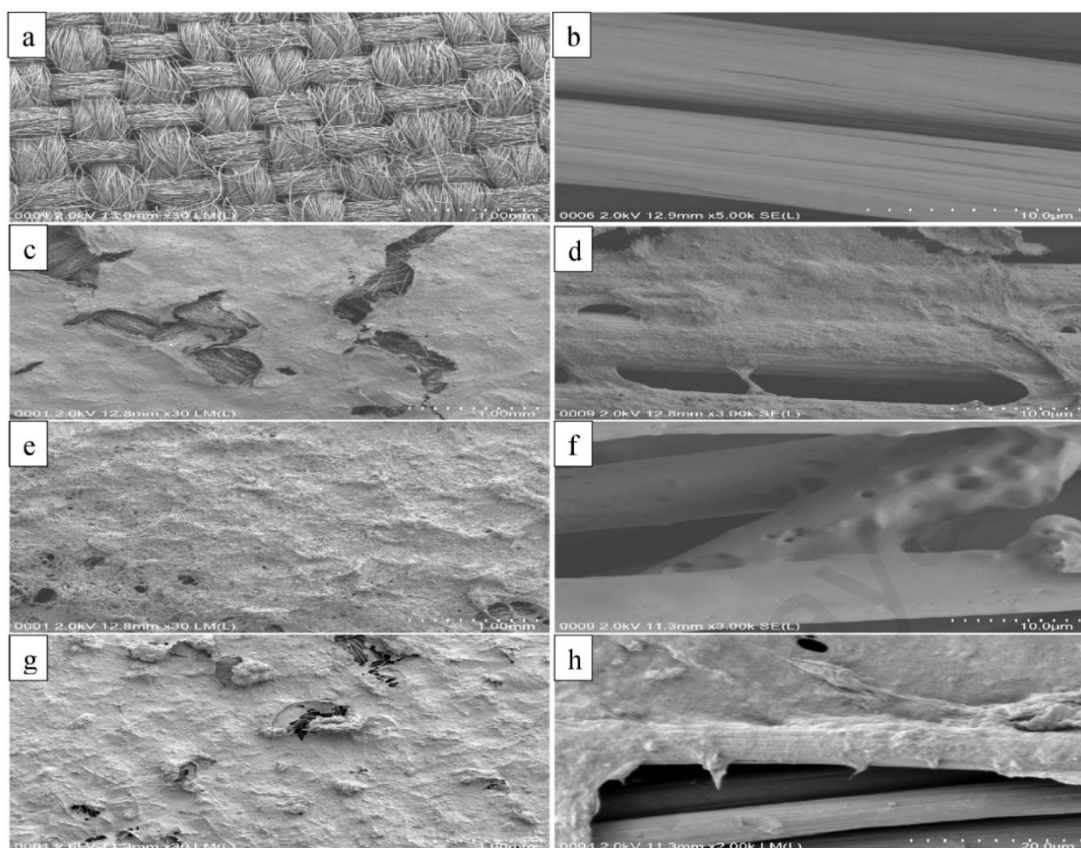
Figure 4.5: FESEM images of plain and modified electrodes prior to MFC analysis at different magnifications, *a* Pristine CC at 1.0mm, *b* Pristine CC at 10.0μm, *c* CC modified with CNT at 1.0mm, *d* CC modified with CNT at 10.0μm *e* CC modified with CNT (20 mg) and MA-PHA (20 mg) as anode electrode (CC-CNT/MA-PHA-anode) at 1.0mm, *f* CC modified with CNT (20 mg) and MA-PHA (20 mg) as anode electrode (CC-CNT/MA-PHA-anode) at 10.0μm, *g* CC modified with CNT (20 mg) and MA-PHA (5 mg) as cathode electrode (CC-CNT/MA-PHA-cathode) at 1.0mm, and *h* CC modified with CNT (20 mg) and MA-PHA (5 mg) as cathode electrode (CC-CNT/MA-PHA-cathode) at 10.0μm
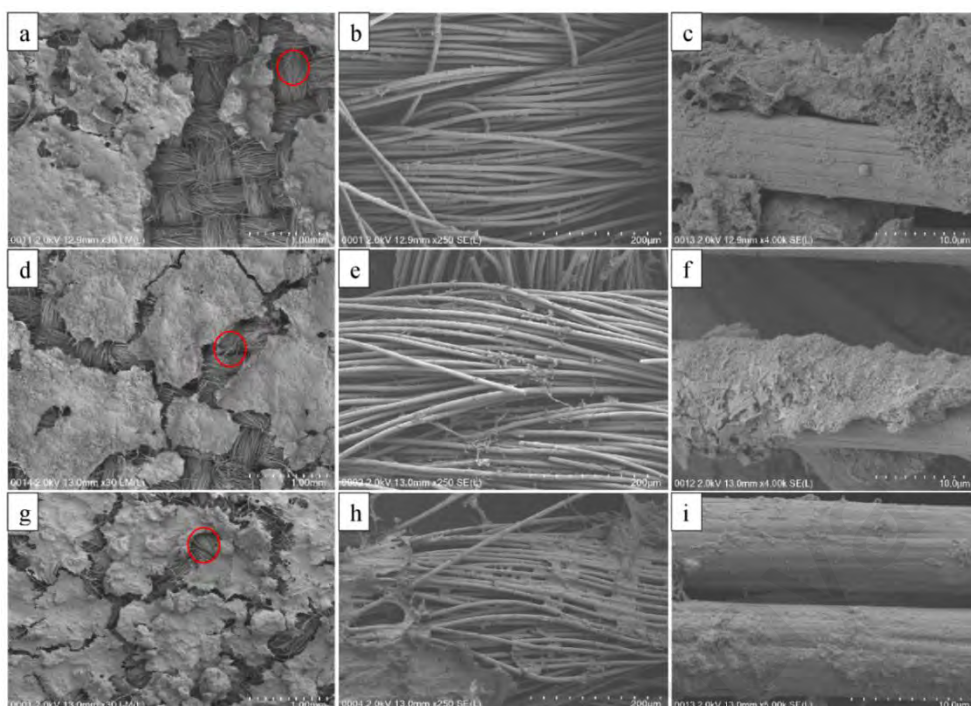
Figure 4.6: FESEM images of modified electrodes after MFC analysis at different magnifications. *a,b,c* represent anode electrode of CC modified with CNT at 1.0mm, 200μm and 10μm respectively, *d,e,f* represent cathode electrode of CC modified with CNT at 1.0mm, 200μm and 10μm respectively, while *g,h,i* represent cathode electrode of CC modified with CNT (20 mg) and MA-PHA (5 mg) at 1.0mm, 200μm and 10μm respectively
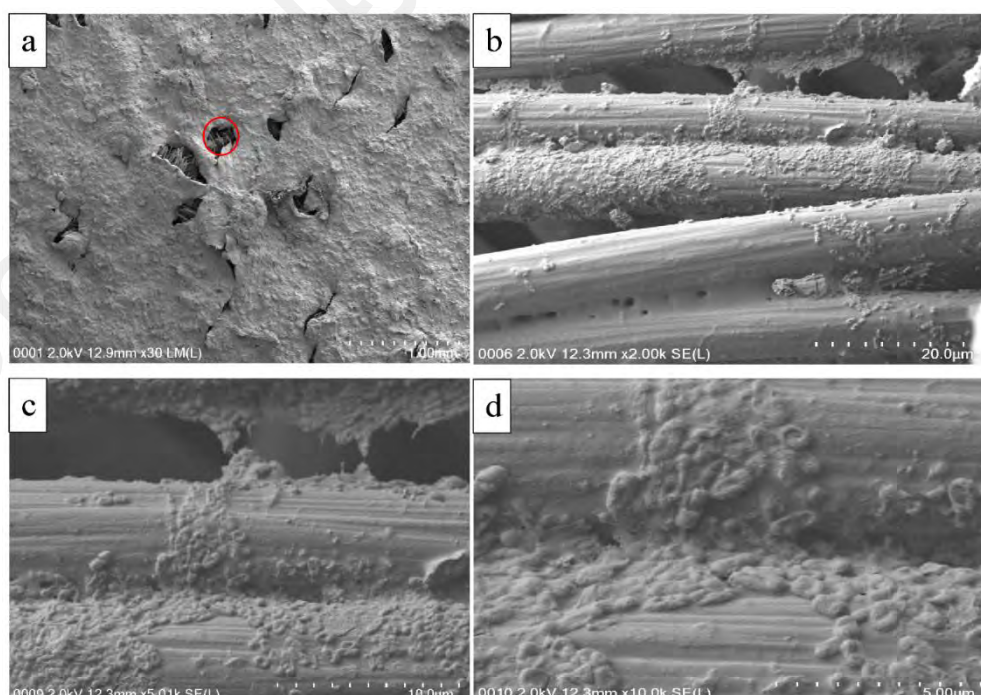
Figure 4.7: FESEM images of biofilm formation on CC-CNT/MA-PHA modified anode electrode at *a* 1.0mm, *b* 20.0μm, *c* 10.0μm, and *d* 5.0μm

4.2.1 Electrochemical performance of the electrodes

4.2.1.1 Conductivity

The neat mcl-PHA and MA-PHA graft materials showed negligible conductivity (Table 4.1) when tested as electrode modifier in the MFC. When neat mcl-PHA is composited with CNT (PHA/CNT), the conductivity recorded was 0.11 mS/cm. The reading was doubled when grafted copolymer composited with CNT was tested. Layering the PHA/CNT onto CC resulted in a significant conductivity reading at 4.20 ± 0.2 mS/cm (Table 4.1). The conductivity reading increased by two-fold to 8.48 ± 0.3 mS/cm when CNT/MA-PHA was surface-layered on CC (CC-CNT/MA-PHA). This strongly demonstrated that MA-grafted mcl-PHA composited with CNT is an efficient electrode modifier material in MFC application.

Table 4.1: Conductivities of the neat mcl-PHA and grafted copolymer composited with carbon nanotubes

Material	Conductivity (mS/cm)
mcl-PHA	0.01 ± 0.0
MA-PHA	0.02 ± 0.0
PHA/CNT	0.11 ± 0.0
CNT/MA-PHA	0.26 ± 0.0
CC-PHA/CNT	4.20 ± 0.2
CC-CNT/MA-PHA	8.48 ± 0.3

Values are average of triplicate measurements ± standard deviation

Table 4.2 shows the conductivity measurements of electrodes at different MA-PHA loading amounts. When $5 - 10$ mg was used in CC-CNT/MA-PHA modifier material, comparable conductivity readings were recorded. The highest electrode conductivity of 38.0 ± 1.5 mS/cm was achieved at 20 mg of MA-PHA. The decrease in the conductivity measurements thereafter could be due to increased thickness of modifier material on the

anode electrode that curtails electron conduction. Therefore, 1:1 *w/w* of MA-PHA to CNT (20 mg, Table 2) was chosen for subsequent studies. For cathode electrode, 0.25:1 *w/w* of MA-PHA-to-CNT (5 mg) was chosen to be applied in order to minimize biofilm colonization on its surface as it needs to be exposed to dissolved oxygen.

Table 4.2: Conductivities of the anode electrode at different MA-PHA loading amounts and constant CNT amount at 20 mg

MA-PHA in CC-CNT/MA-PHA (mg)	Apparent deposition of MA-PHA within CC-CNT/MA-PHA (%)	Conductivity (mS/cm)
5	94	17.5 ± 1.4
10	92	12.6 ± 0.1
20	96	38.0 ± 1.5
40	83	9.2 ± 0.1
60	84	5.4 ± 0.2
80	78	4.9 ± 0.9
100	82	1.9 ± 0.2

Values are average of triplicate ± standard deviation

4.2.1.2 Cyclic Voltammetry (CV)

To investigate electrochemical activities of the electrodes in MFC, they were subjected to cyclic voltammetry (CV). CV curves for different MA-PHA loading amount ranging from 20 mg to 100 mg with a fixed amount of CNT (20 mg) is shown in Figure 4.8. From the figure, 20 mg MA-PHA showed the highest electrochemical activities compared to the other loadings. Therefore, 20 mg MA-PHA loading was chosen as the anode electrode modifier. Figure 4.9a shows the CV curves of anode electrodes with

biofilm formation while Figure 4.9b shows the stability of the modified electrode in electrolyte. The anodic peak of the modified electrode (CC-CNT/MA-PHA) located at a potential of 305 mV generated a current of 5.7 mA, while the cathodic peak located at -118 mV generated about 3.6 mA of current (Figure 4.9a). The redox peaks of the control electrode were much weaker compared to modified electrode. About 2.7 mA of current was generated by the CC-CNT electrode at the anodic peak while the cathodic peak generated a current of -2.2 mA, located at a potential of -105 mV. The superiority in redox peaks of modified electrode is attributed to prominent microbial growth and film attachment to the electrode surface (see Figure 4.4*f*). The close proximity allows for higher chances of successful electron transfer *via* mediators or electrochemically active metabolites secreted by the biocatalyst to the anode (Zhang et al., 2008). The stability of the modified electrode was evidenced by subjecting the electrode material to 10 cycles (Figure 4.9b). Both the anodic and cathodic peaks of all cycles generated similar current, thereby indicating the stability of the electrode.

Figure 4.9c shows the CV curves of cathode electrodes while Figure 4.9d shows the stability of the modified cathode electrode in ferricyanide. Peak sensitivity indicates the effectiveness of the electrodes for oxygen reduction function at the cathode (Papiya et al., 2018). In comparison with control electrode (CC-CNT), the modified electrode showed a higher oxygen reduction reaction (Figure 4.9c). The CC-CNT electrode generated an anodic current of 5.6 mA at a potential of 401 mV in the absence of corresponding cathodic peak. The anodic current of modified electrode shifted to a potential of 472 mV, emitting an anodic current of 7.3 mA and recorded a cathodic potential of 451 mV, with a current of -3.2 mA. It can therefore be concluded that the modified electrode exhibited better catalytic activity than the control electrode. The proven stability of the electrode in electrolyte is evidenced in Figure 4.9d.
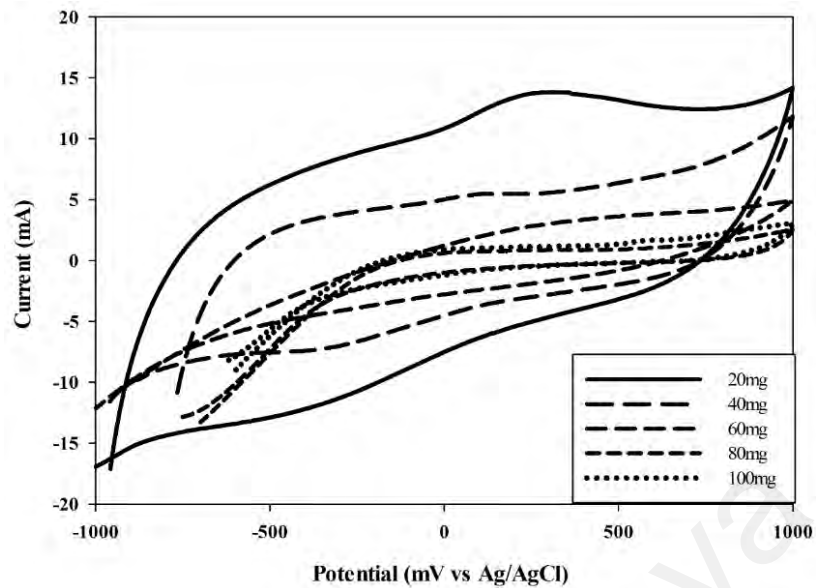
Figure 4.8: Cyclic voltammetry curves of different MA-PHA loading amount with constant CNT amount (20 mg) at 50 mV/s
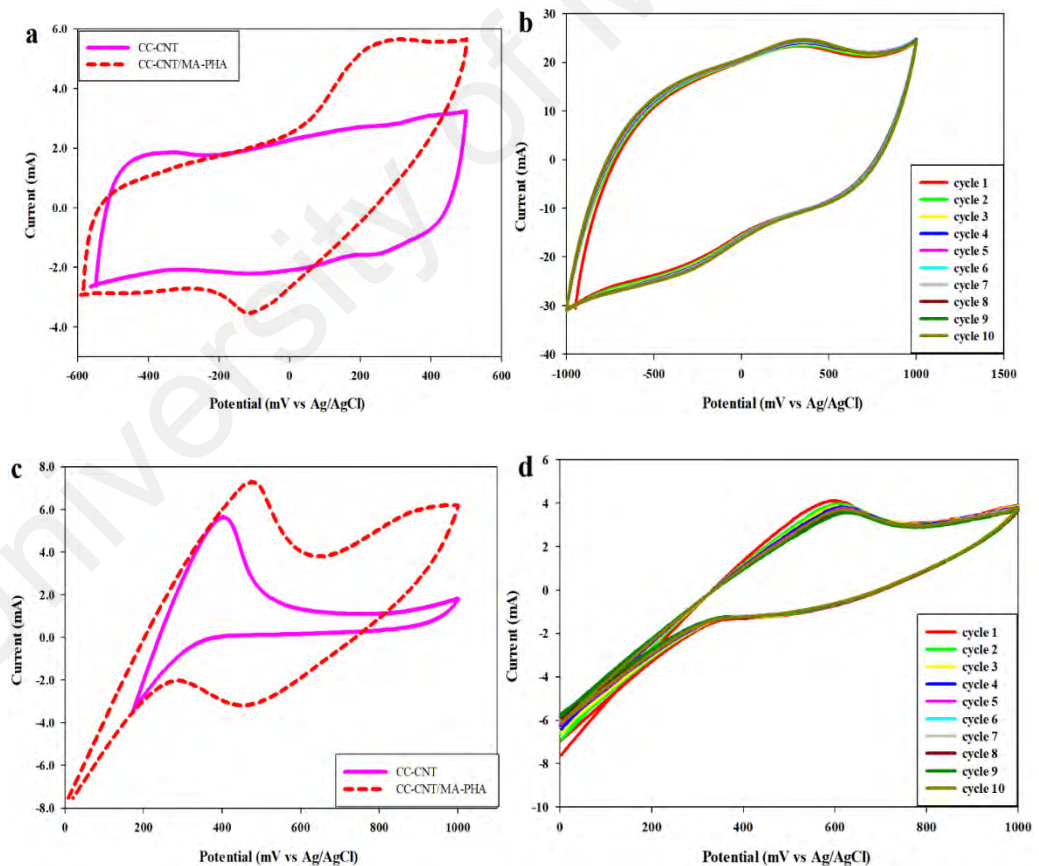
Figure 4.9: Cyclic voltammetry curves of (a) anode electrodes for CC-CNT and CC-CNT/MA-PHA-anode at 5 mV/s, (b) 10 cycles of CC-CNT/MA-PHA-anode at 50 mV/s, (c) cathode electrodes for CC-CNT and CC-CNT/MA-PHA-cathode at 5 mV/s, (d) 10 cycles of CC-CNT/MA-PHA-cathode at 50 mV/s

4.2.1.3 Internal resistance

To investigate the internal resistance of the MFC, the device operated with different electrodes were subjected to EIS as shown in Figure 4.10. The charge transfer resistance of the device operated with CC-CNT/MA-PHA-anode-cathode (MFC 3, Figure 4.10*c*) represented with a larger semi-circle was 42 Ω while the MFC operated with CC-CNT anode versus CC-CNT/MA-PHA cathode (MFC 2, Figure 4.10*b*) was 56 Ω, and 44 Ω was recorded for CC-CNT anode versus CC-CNT cathode (MFC 1, Figure 4.10*a*). Electrolyte resistance is in direct proportion to the overall internal resistance (He et al., 2006; Hindatu et al., 2017b). The higher the electrolyte resistance, the higher the internal resistance. In this experiment, the electrolyte resistance of MFC 1 was the highest at 402 Ω which gives overall internal resistance of 447 Ω, while MFC 2 and 3 showed electrolyte resistances of 131 Ω and 63 Ω, respectively, corresponding to overall internal resistance of 190 Ω and 107 Ω. The high electrolyte resistance is governed by many factors e.g. biofilm concentration, temperature, ion concentration in the electrolyte (Sekar & Ramasamy, 2013). Nevertheless, the polymeric modified electrodes (MFC 2 and 3) showed significantly lower internal resistance compared to MFC 1 (unmodified electrode). About 76 % decrease in internal resistance was observed in MFC 3 and 58 % decrease in MFC 2. The highest percentage in MFC 3 when compared with other two MFC and with earlier polymeric studies (Hindatu et al., 2017b; Hou et al., 2015; Wang et al., 2014) was attributed to the successful colonization of electrode surface by the microorganism as indicated in Figure 4.4*f* (FESEM), as well as low electrolyte impedance of un-replenished MFC 3. Both MFC 1 and 2 received nutrient replenishment as they underwent several cycles within 30 days of MFC operation, whereas MFC 3 with its single cycle did not require nutrient replenishment. Since EIS was recorded at replenished nutrient state, high electrolyte resistance was expected in MFC 1 and 2.
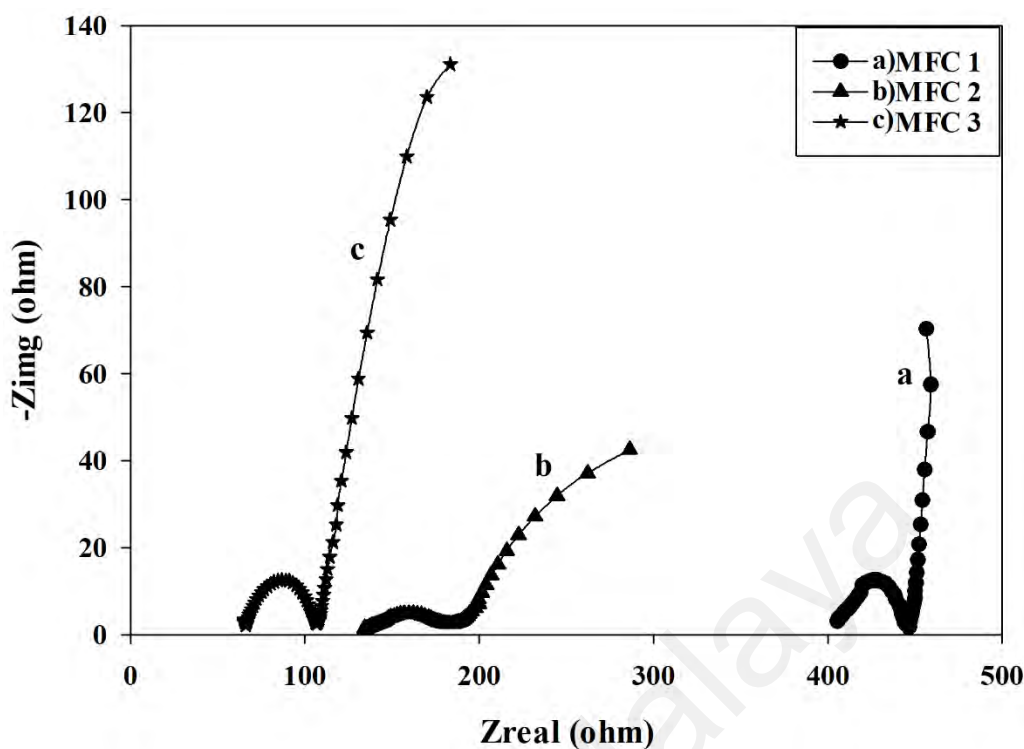
Figure 4.10: Nyquist plot for MFC set up with *a* CC-CNT-anode vs. CC-CNT-cathode (MFC 1), *b* CC-CNT-anode vs. CC-CNT/MA-PHA-cathode (MFC 2), *c* CC-CNT/MA-PHA-anode vs. CC-CNT/MA-PHA-cathode (MFC 3)

4.2.2 MFC operation

During the 30 days of MFC operation, the voltage generated was monitored every single hour. Figure 4.11 showed the voltage generated over time for the three MFC set-ups. For MFC 1 (Figure 4.11*a*), which served as a control, the initial voltage recorded (start-up time) was 15 mV at 0th hour. The voltage steadily increased to reach a maximum of 460 mV at 32nd hour of the first cycle. Similar maximum voltage of about 460 ± 20 mV was observed in the four subsequent cycles resulting in a total of five cycles during 30 days of operation. For MFC 2 (Figure 4.11*b*), the number of total cycles was reduced to four maximum voltage generation i.e. 478, 495, 493, and 729 mV in 1st, 2nd, 3rd, and 4th cycles respectively with a start-up voltage of 54 mV at 0th hour. The increase in the maximum voltage generated as the cycle progresses was attributed primarily to improved O_2 reduction by the transferred electrons at the modified cathode. More importantly, O_2 reduction activities of the modified cathode electrodes did not appear to be affected by

marginal biofilm formation on them (Figure 4.4*g* and 4.4*h*). Longevity and stability in voltage production are the most important features in making MFC a practical system. MFC 3 (Figure 4.11*c*) underwent a single cycle without nutrient replenishment requirement. The start-up voltage generated at 0th hour by MFC 3 (398 mV) was seven times higher than that of MFC 2 (54 mV) and 27 times higher than the control, MFC 1 (15 mV), primarily attributed to superior electron charge transfer at the modified anode (MFC 3). Significant increase in the voltage generation for MFC 3 was observed within the first 58 hours until a maximum and stable voltage of 685 mV was achieved. The voltage was stable for 225 hours. The longevity and stability of maximum voltage generated was ascribed to mature and established biofilm colonization on modified anode electrode, consequently translated to more efficient electron transfer relative to the unmodified anode electrode (CC-CNT) with minimal biofilm colonization (Figure 4.4*e*). It is also suggested that the amphiphilic nature of MA-PHA encourages strong biofilm growth and attachment on modified electrode (Figure 4.4*f*). Interestingly, the nutrient may have been exhausted after 18 days of MFC operation as observed from the disappearance of culture medium turbidity (data not shown). The microorganism was able to survive and sustained the voltage generation most likely by metabolizing the modifier material (grafted copolymer) on the electrode as its carbon source since it primarily comprised of a biological product (mcl-PHA). The results of this study showed superior stability and longevity in terms of generated maximum voltage compared to other studies (Cui et al., 2015; Hou et al., 2015; Kang et al., 2015; Wang et al., 2014; Yusuf et al., 2018).
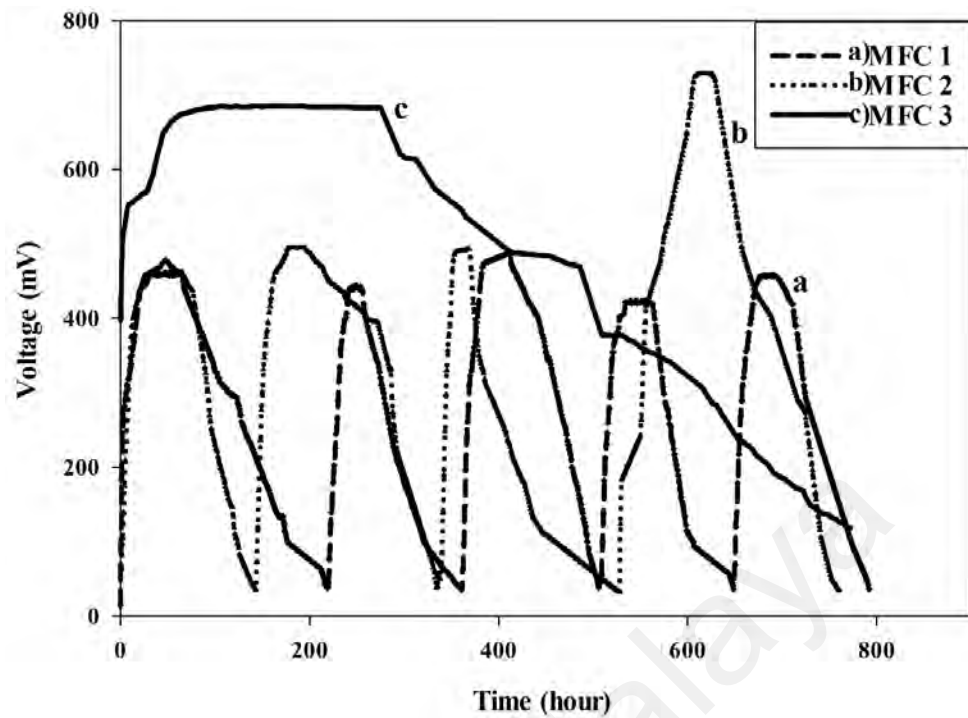
Figure 4.11: Voltage curves recorded during 30 days MFC operation for *a* CC-CNT-anode vs. CC-CNT-cathode (MFC 1), *b* CC-CNT-anode vs. CC-CNT/MA-PHA-cathode (MFC 2), *c* CC-CNT/MA-PHA-anode vs. CC-CNT/MA-PHA-cathode (MFC 3)

Voltage measurements at different external resistances provide useful information on current and power densities (Yusuf et al., 2018). These data were used in the determination of polarization curve and power density as shown in Figure 4.12. The polarization data was taken at a maximum and stable voltage. MFC 1 generated a maximum power density of 289 mW/m^2 at a current density of 695 mA/m^2. The other two modified MFC show improvement in power density *viz.* 339 mW/m^2 at current density of 751 mA/m^2 for cathode modified MFC (MFC 2). The highest power density was observed in MFC 3 containing modified anode and cathode with power density of 351 mW/m^2 at 765 mA/m^2 current density, higher than previously reported (Liu et al., 2015; Roh & Woo, 2015; Wang et al., 2014). Rapid drop in voltage generation at lower currents was observed in MFC 1 due to high activation loss. Similar loss was not observed in modified MFCs from improved O$_2$ reduction performance at the cathode electrode

(MFC 2), and improved electron transfer between the anode and the biocatalyst (MFC 3) (Logan, 2008).
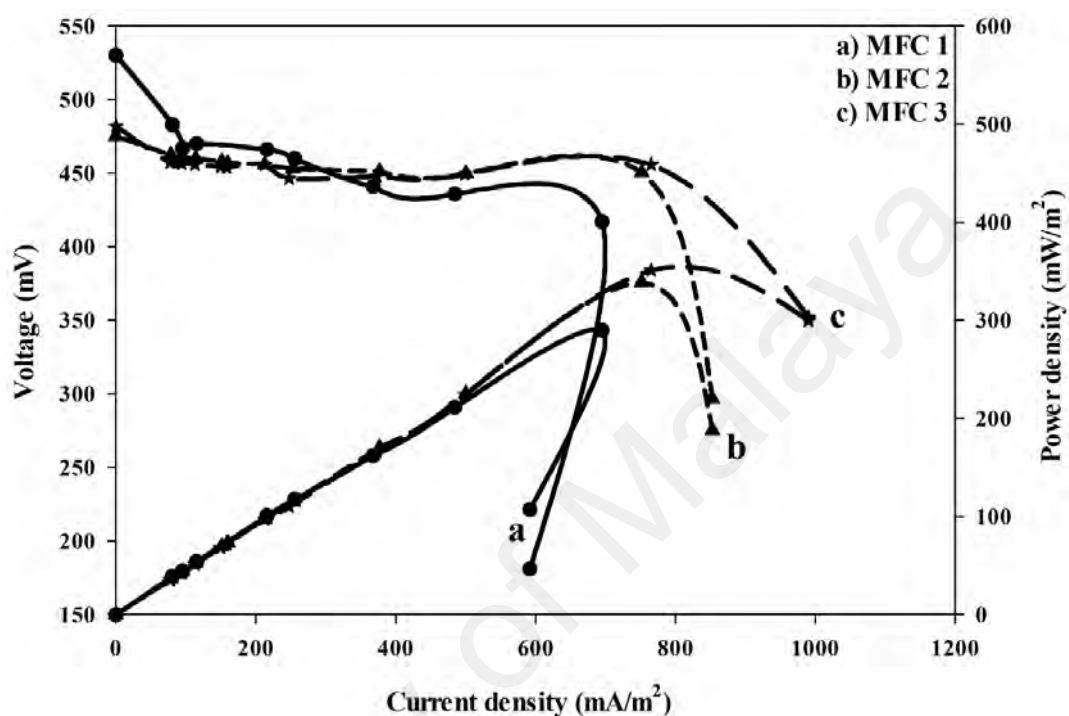
Figure 4.12: Polarization curve and power density recorded for *a* CC-CNT-anode vs. CC-CNT-cathode (MFC 1), *b* CC-CNT-anode vs. CC-CNT/MA-PHA-cathode (MFC 2), *c* CC-CNT/MA-PHA-anode vs. CC-CNT/MA-PHA-cathode (MFC 3)

4.2.3 Polymer degradability

The biodegradable nature of PHA and PHA-based materials calls for testing the susceptibility of the grafted polymer to (bio)degradation in MFC. This was examined by the change in molecular weight before and after its application as an electrode nanocomposite modifier in MFC (Table 4.3). No drastic changes were observed in the weight-averaged molecular weight (M_w) and the number-averaged molecular weight (M_n) values between neat mcl-PHA and MA-PHA. However, significant increase in the polydispersity index (PDI) was observed after grafting the MA monomers into the mcl-PHA matrix. It is suggested that the grafted copolymer exhibits wider distribution of

molecular weight (Anis et al., 2017). When applied as composite material for electrode modification, negligible difference was observed in the M_w after 30 days of MFC operation. It is suggested that the CNT incorporated in the matrix of the grafted polymer played a role in reducing the degradation rate of the polymer (Yusuf et al., 2018). The M_n after 30 days significantly increased while the PDI significantly reduced compared to neat MA-PHA. Prolonged exposure to biofilm growth and operation conditions in MFC up to 60 days resulted in significant reduction in M_w, indicating utilization of the copolymer by the attached microorganism as major carbon source. Both the M_n and PDI values at day 60 showed no significant difference corresponding values on day 30. Monomer composition, morphology and microstructure of the polymer may account for low percentage decrease (11 %) in the M_w of the copolymer even after 60 days. These factors are known to determine the degradation rate of PHA-based materials (Li & Loh, 2015).

Table 4.3: Molecular weights of neat mcl-PHA, MA-PHA prior to- and after 30 and 60 days of MFC operation

Sample	Molecular weight (kDa)		
	M_w	M_n	PDI
mcl-PHA	136 ± 4^a	$73 \pm 2^{a,b}$	1.9 ± 0.0^b
MA-PHA at day 0	$129 \pm 4^{a,b}$	60 ± 0^b	2.2 ± 0.1^a
CNT/MA-PHA at day 30	$123 \pm 2^{b,c}$	77 ± 9^a	1.6 ± 0.2^b
CNT/MA-PHA at day 60	114 ± 2^c	$70 \pm 1^{a,b}$	1.6 ± 0.0^b

Values are average of duplicate ± standard deviation

Table 4.4 shows the results of the current study and other reported studies in MFC electrode modification. While Wang et al. (2014) and Li et al. (2019) reported slightly improved maximum voltage potential compared to the current study, nonetheless, the maximum voltage recorded in this study was comparatively better than other reported studies (Table 4.4). The ability of MFC to generate stable electrical current for extended period of time is of most important in practical application of MFC technology. The current study exhibited comparable longevity in maximum voltage potential when compared with those reported by Fraiwan et al. (2014) while superior to other studies (Table 4.4). The maximum power density of the current study was within reasonable range when compared with other literatures.

Table 4.4: Comparison of results in current study with previous studies on electrode modification

Electrode	Maximum voltage potential (mV)	Longevity of maximum voltage potential (hours)	Maximum power density (mW/m^2)	References
Mcl-PHA-*co*-methyl acrylate/MWCNT	700	225	351	**Current study**
Gold/polycaprolactone microfiber	600	240	65	(Fraiwan et al., 2014)
Chitosan/CNT hydrogel	132	45	132	(Liu et al., 2014)
PANI/MWCNT	967	100	286	(Wang et al., 2014)
rGO/Polyacrylamide hydrogel	512	80	782	(Chen et al., 2019)
Titanium suboxides/graphene/PANI	980	72	2073	(Li et al., 2019)
PANI/CNT	450	210	48	(Yellappa et al., 2019)
PANI/TiO2	555	168	813	(Yin et al., 2019)
Mcl-PHA-*co*-PEGMA/MWCNT	678	87	466	(Yusuf et al., 2018)
Mcl-PHA/MWCNT	409	60	254	(Hindatu et al., 2017)

4.3   Characterization of membranes

4.3.1   FTIR and XRD

Both the synthesized mcl-PHA and commercially sourced PHB belong to polyhydroxyalkanoates family, representing medium chain length- and short chain length polyhydroxyalkanaotes, respectively. This resulted in similar FTIR spectra as shown in Figure 4.13. The successful composition of PHB into PHA matrix was confirmed by the increase in peak intensities in mcl PHA-PHB composites (Figure 4.13). The presence of symmetric and asymmetric vibration of –C-H stretch at 2930 cm^{-1} and 2854 cm^{-1} were evidenced in all composite samples. These vibrations were absent in Nafion membrane. The peak signal located at 1729 cm^{-1} in mcl-PHA and PHB indicate the presence of ester group –C=O. Similar peaks between 1730 – 1740 cm^{-1} were observed in the blended membranes (PHB5%, PHB10% and PHB15%) with sharper peaks as the PHB content increases, indicating successful incorporation of PHB within PHA matrix. The stretching vibrations between 1160 – 1210 cm^{-1} and at 759 cm^{-1} in mcl PHA-PHB samples represent the C-O-C stretch and CH_2 from PHA side chains, respectively. The intensity of the peaks was more pronounced in 15% sample due to higher PHB content present. In Nafion sample, two distinct peaks at 1152 cm^{-1} and 1050 cm^{-1} represent the sulfones (S=O) and the sulfoxides (-SO_3). The findings are in accordance with earlier literature (Abid et al., 2016; Biradar et al., 2018; Gumel et al., 2012).
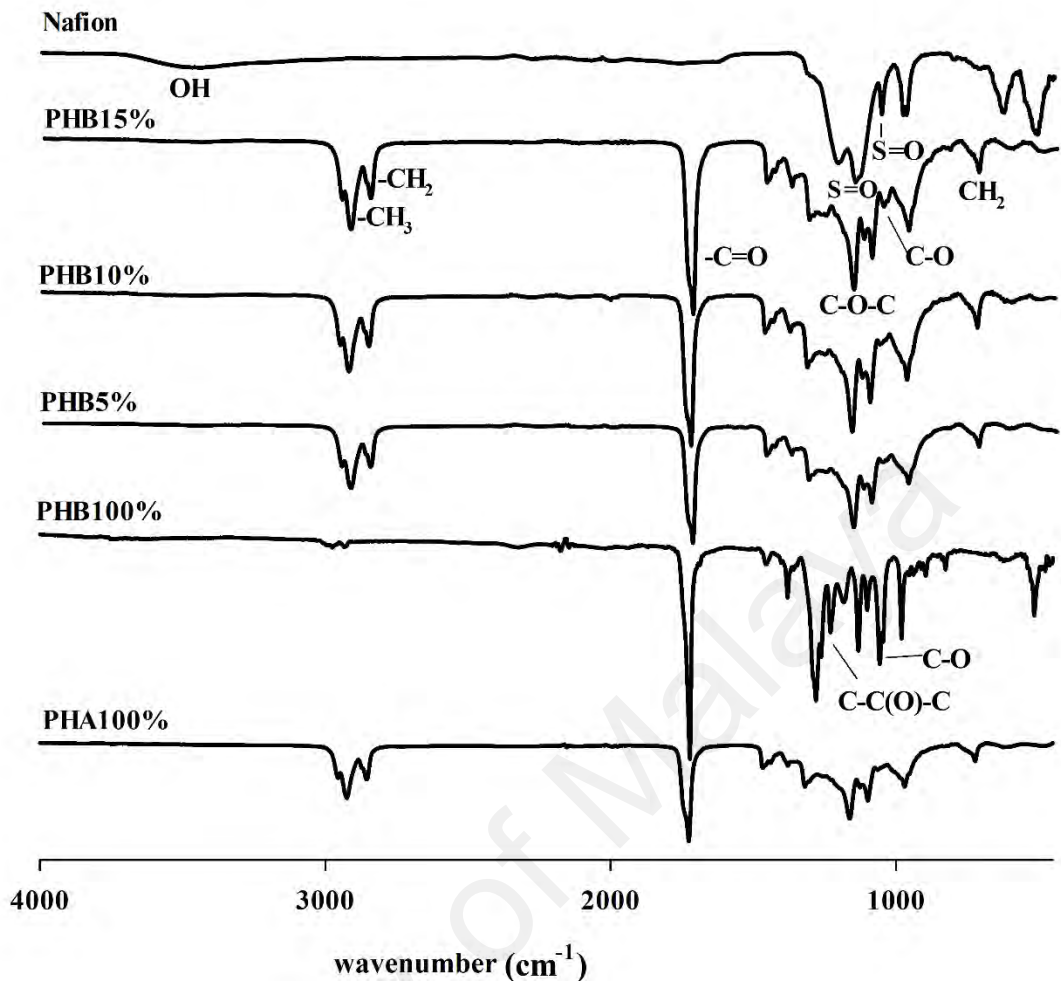
Figure 4.13: FTIR spectra of PHA100%, PHB100%, PHB5%, PHB10%, PHB15% and Nafion membranes

Figure 4.14 shows the XRD patterns of Nafion, pure mcl-PHA and its composites with PHB. The two broad peaks on Nafion located at 16.8° and 38.8° represent the backbone of polyfluorocarbon chains (Dai et al., 2019; Maiti et al., 2018; Ozden et al., 2017). Mcl-PHA and its composites showed two distinct diffraction peaks appearing at 19.1° and 20.7°, corresponding to (021) and (111) reflections. The appearance of new peaks in all PHB composites at 2θ values of 13.5, 16.9, and 25.5 with respective reflections of (020), (110) and (121) evidenced. The assignments are in agreement with earlier reports (Anbukarasu et al., 2015; Liau et al., 2014).
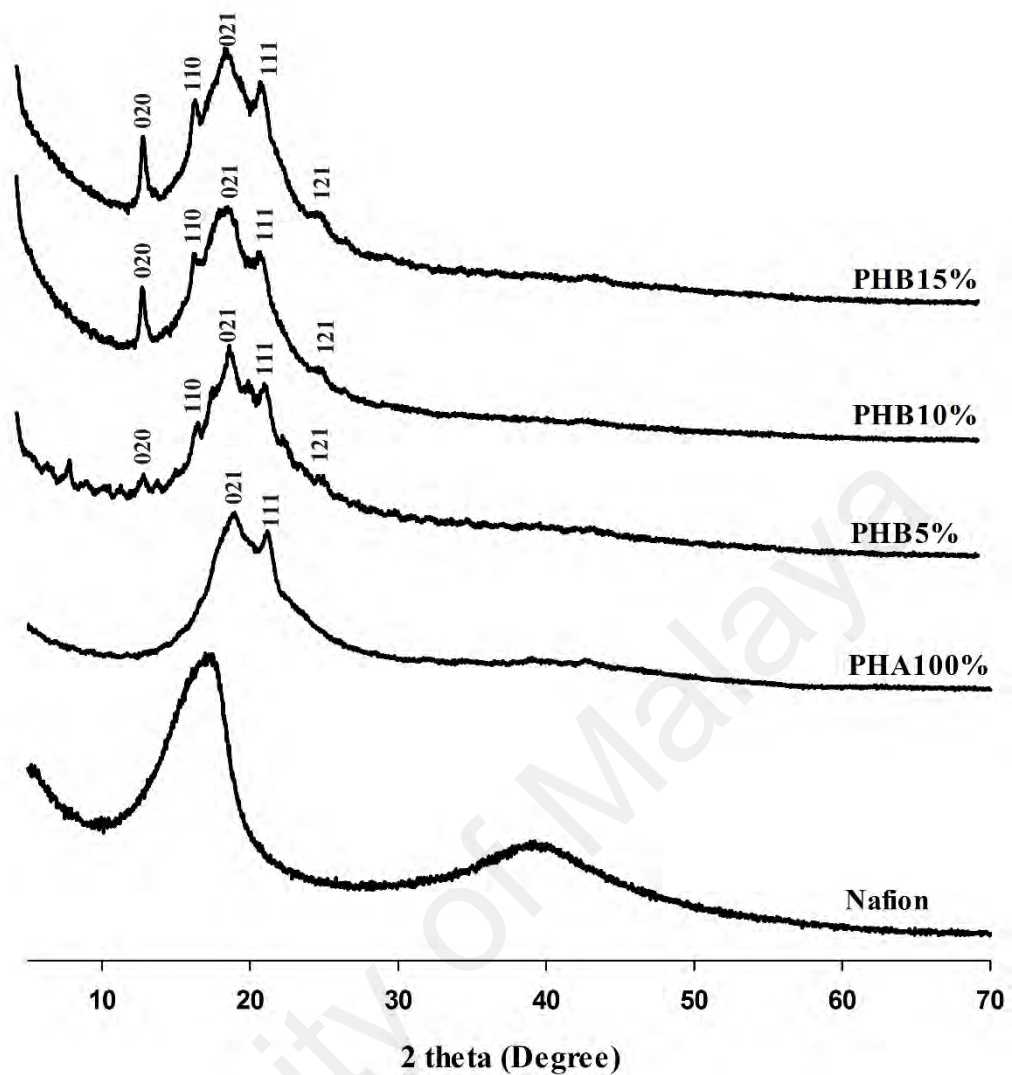
Figure 4.14: X-ray diffractogram of Nafion, PHA100%, PHB5%, PHB10%, and PHB15% membranes

4.3.2 FESEM

Figure 4.15 shows the surface and cross-sectional morphology of all membranes at different magnifications. The surface morphology of all membranes appeared smooth (Figure 4.15 (*a*1,*b*1,*c*1,*d*1,*e*1)) even after PHB incorporation. On the other hand, the cross-sectional view shows different morphologies. Nafion appeared cracked at higher and lower magnifications (Figure 4.15 (*a*2 and *a*3). Similar observation was reported by (Xue & Chan, 2015; Yusuf et al., 2018). The incorporation of PHB into mcl-PHA matrix introduced irregularities that roughened the membranes as shown in Figure 4.15 (*c*2,*c*3,*d*2,*d*3,*e*2,*e*3). These observations were absent in pristine PHA morphology. Higher

73

fraction of rough morphologies was observed in PHB15% membrane compared to PHB5% and PHB10%. The observed morphologies of the composited materials could explain the efficiency of the membrane to function as PEM in MFC.
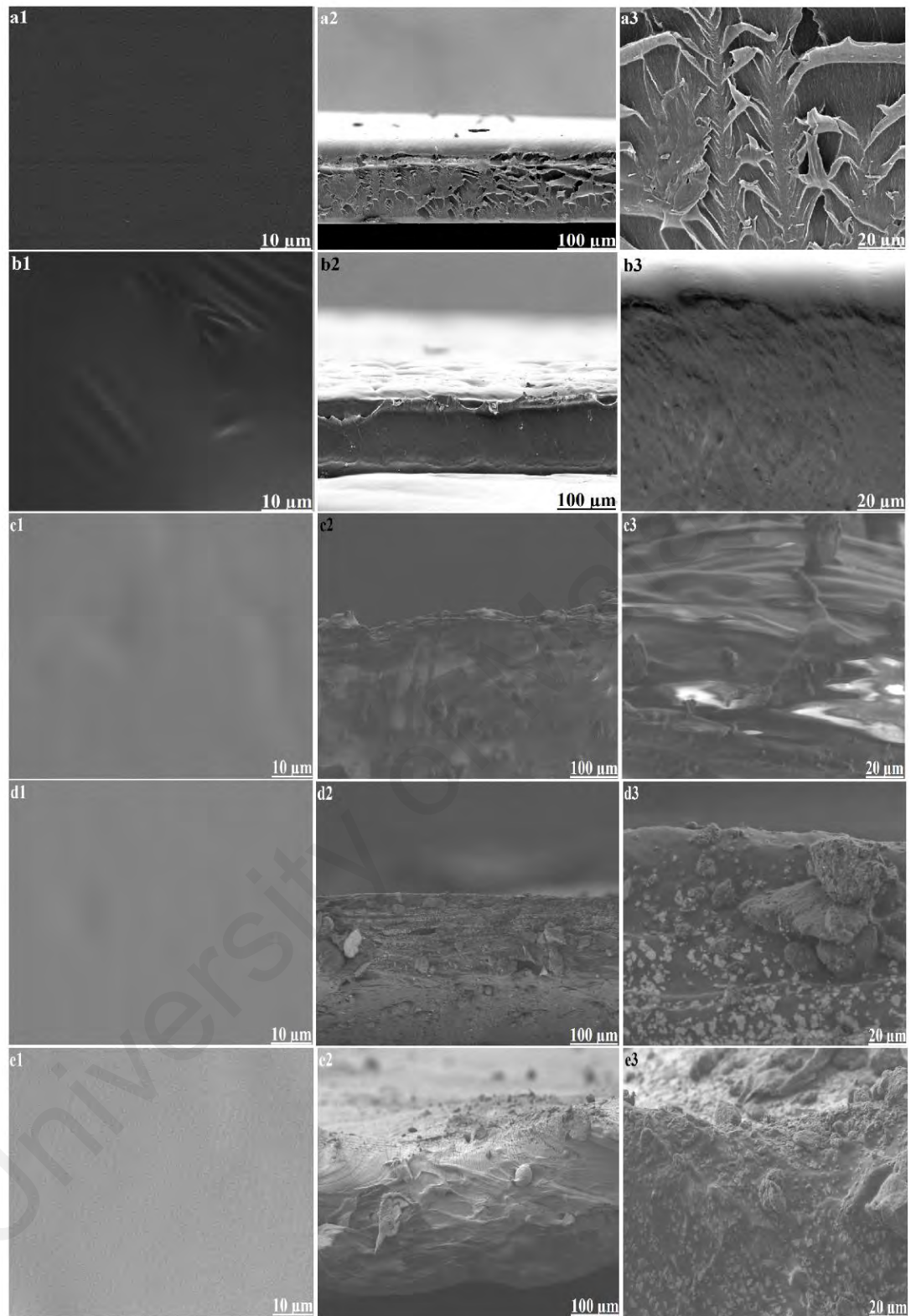
Figure 4.15: FESEM images of the surface morphologies at 10 μm (× 10,000) of *a*1 Nafion; *b*1 PHA100%; *c*1 PHb5%; *d*1 PHB10%; *e*1 PHB15%. The cross-sectional morphologies at 100 μm (× 1,000) of *a*2 Nafion; *b*2 PHA100%; *c*2 PHB5%; *d*2 PHB10%; *e*2 PHB15% and cross-sectional morphologies at higher magnification of 20 μm (× 5,000) of *a*3 Nafion; *b*3 PHA100%; *c*3 PHB5%; *d*3 PHB10%; *e*3 PHB15%

4.3.3 Oxygen diffusion test and water uptake by membrane

Oxygen flux from the cathode chamber to anode chamber is known to decrease coulombic efficiencies, reduce anaerobes population inside anode chamber and subsequently affect the overall MFC performance. An ideal membrane must be very much less conducive to oxygen diffusion (Logan, 2008). The rate of oxygen diffusion over time in all tested membranes is shown in Figure 4.16. The decreasing order of resistivity to oxygen flux is as follows: PHA100% < PHB15% < PHB10% < Nafion < PHB5%. The inability of oxygen to diffuse through PHA100% membrane could be attributed to its hydrophobic nature thereby making it difficult for dissolve oxygen in water to pass through. The composition of PHB crystals into PHA matrix allowed oxygen passage to some extent, most likely related to the observed roughness of the membrane as shown by FESEM earlier (Figure 4.15). Nevertheless, PHB10% and PHB15% membranes showed better resistivity to oxygen diffusion than the control, Nafion. Similar trend was observed in the oxygen mass transfer coefficient (K_o) and diffusion coefficient (D_o) as shown in Table 4.5 with PHB10% and PHB15% showing better D_o and K_o values than Nafion.
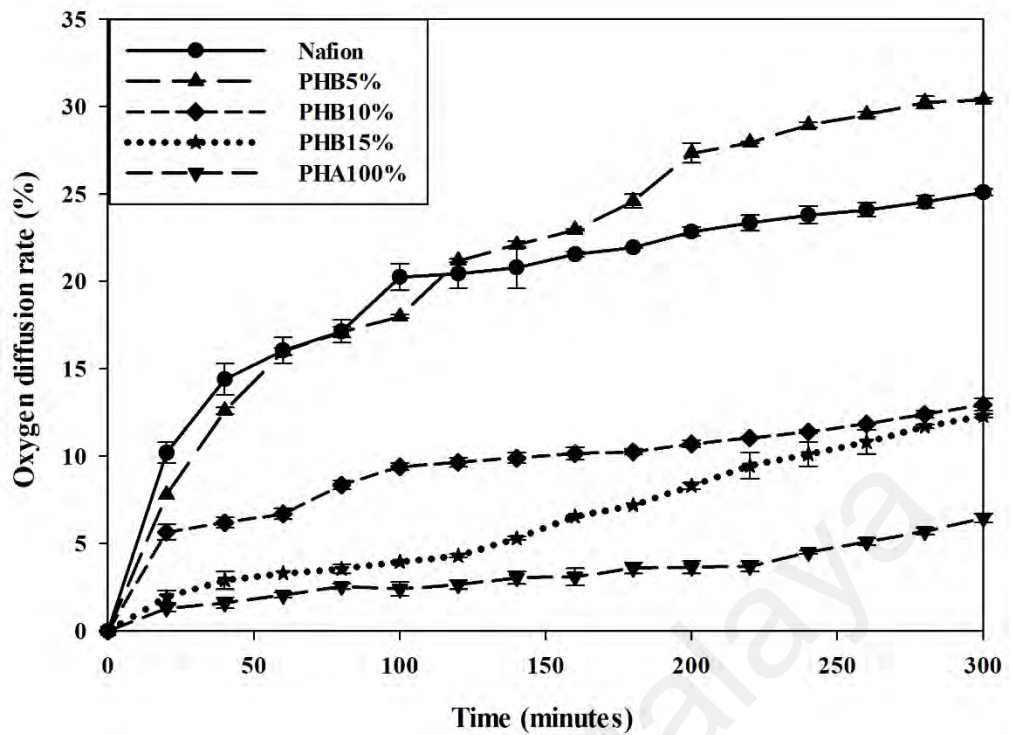
Figure 4.16: Oxygen gas flux from cathode chamber to anode chamber over time for Nafion, PHA100%, PHB5%, PHB10% and PHB15% membranes

Table 4.5: Membrane thickness (M_t), oxygen mass transfer coefficient (K_o) and diffusion coefficient (D_o) of Nafion, PHA100%, PHB5%, PHB10%, and PHB15% membranes

Membrane	M_t (cm)	K_o ($\times 10^{-5}$ cm/s)	D_o ($\times 10^{-6}$ cm^2/s)
Nafion	0.0179 ± 0.001	16.7 ± 0.2	3.1 ± 0.04
PHA100%	0.0152 ± 0.002	3.9 ± 0.2	0.6 ± 0.03
PHB5%	0.0125 ± 0.001	20.9 ± 0.1	2.7 ± 0.02
PHB10%	0.0128 ± 0.002	8.0 ± 0.3	1.0 ± 0.04
PHB15%	0.0149 ± 0.001	7.6 ± 0.1	1.1 ± 0.01

Values are average of duplicate ± standard deviation

Proton conductivity is in direct proportion with the amount of water held by a polymer matrix. Two phenomena are employed for proton movement in solution. The first is known as proton hopping *via* protonated sulfonate groups (-SO₃H), transferring protons from one water molecule to another by means of hydrogen bonding. The other phenomenon known as vehicle diffusion contributed about 22 % of the total proton passage *via* protonated water molecules in form of H_3O^+ or H_9O^{4+} (Rangel-Cárdenas & Koper, 2017). Figure 4.17 shows the percentage water uptake of different membranes. PHA100% has the lowest water uptake owing to its hydrophobic nature. Composition of hydrophobic mcl-PHA with PHB crystals improved the water uptake significantly (Figure 4.17) supposedly through water capillary action, with PHB15% showing the highest swollen percentage (22 %) compared to Nafion (16 %). It is hypothesized that the hydrophobic part of the composited membranes allows for morphological stability and oxygen diffusion resistivity, while the incorporated PHB crystals plays important role in facilitating proton passage.
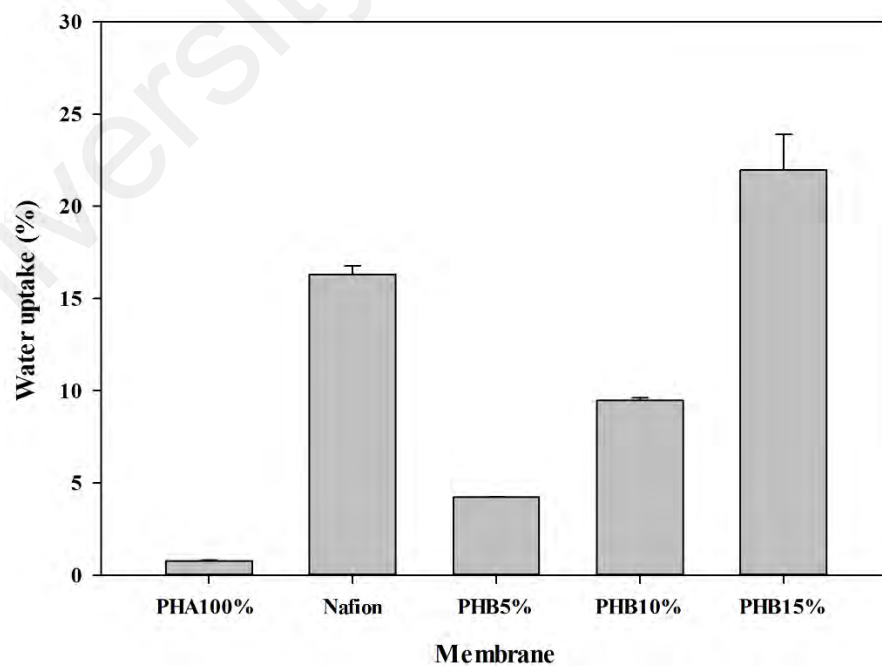
Figure 4.17: Percentage of water uptake for Nafion, PHA100%, PHB5%, PHB10%, and PHB15% membranes

4.4   MFC fabrication and operation

The six MFC set-ups contained composite membranes, Nafion and PHA100% as control were operated in a batch mode MFC cycle. Figure 4.18 shows the voltage-time curve of the MFC set-ups. PHA100% serving as negative control showed an initial voltage of 16 mV at 0th hour. The voltage remained level with maximum voltage of 19 mV generated at 192nd hour. This suggests the inability of proton to efficiently pass through the matrix due to its highly hydrophobic nature, and since proton conduction occurs mainly in association with water molecules, insignificant voltage generation is expected in PHA100% membrane. On the other hand, the incorporation of PHB crystals into mcl-PHA matrix showed significant voltage generation (Figure 4.18). For PHB5% membrane, an initial voltage of 24 mV was recorded. The voltage steadily increased to a maximum and stable potential of 403 ± 15 mV at 54th hour. The voltage remained steady till 90th hour prior to declination. Nafion membrane initially recorded a voltage of 119 mV with a gradual increase until a stable current of 594 ± 10 mV at 70th hour was achieved (Figure 4.18*a*). Longevity in the stability of maximum current generation (59 hours) was more pronounced in Nafion than in PHB5% membrane (34 hours). PHB10% and PHB15% membranes outperformed Nafion membrane both in the initial current generated and maximum voltage potential. An initial voltage of 364 mV was recorded for PHB10% and 436 mV for PHB15%. The maximum voltage potential of 988 ± 21 mV for PHB10% was achieved at 17th hour while PHB15% attained its maximum voltage potential of 1001 ± 9 mV at 11th hour of MFC operation. The initial voltage at start-up time recorded by PHB10% (364 mV) and PHB15% (436 mV) were far superior to the control, Nafion (119 mV). The ability of PHB10% and PHB15% membranes to achieved better start-up time voltage, and huge maximum voltage potentials at shorter time could be attributed to increased PHB crystals present as seen by FESEM cross-sectional images (Figure 4.15), better water uptake percentage (Figure 4.17) which allowed for better

proton conduction, and minimal gas diffusion to anode chamber (Figure 4.16), which translated to efficient biofilm growth and colonization on anode surface. Importantly, PHB has been reported to channel ions by forming pore structures and selectively allowing ion passage in mammals (Das et al., 1999; Elustondo et al., 2013; Reusch, 2014). Interestingly, these attributes could also be responsible for observed proton passage in composite membrane set-ups used in this study. Measured pHs, optical densities and conductivities in anode chambers for all membranes studied were obtained (Figures 4.19, 4.20, 4.21 respectively). Significant H^+ generation in anode chamber within the first 24 hours is indicated by a clear decrease in pH value (Figure 4.19). PHB10% and PHB15% membranes were able to conduct much of the proton than Nafion, which later translated to elevated generation of maximum voltage potential.
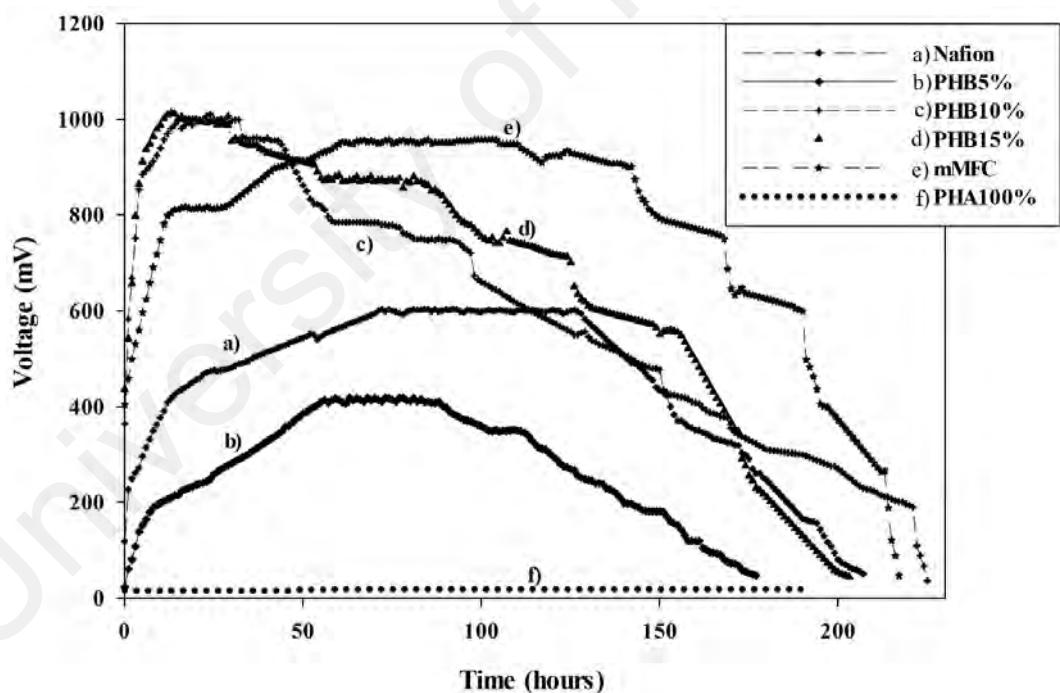
Figure 4.18: Voltage-time curve of MFC set-ups operated with *a* Nafion *b* PHB5% *c* PHB10% *d* PHB15% *e* mMFC *f* PHA100% membranes

Although, PHB10% and PHB15% membranes were far superior in maximum voltage potential compared to other membranes, instability of generated voltage necessitates

electrode modification. Both anode and cathode electrodes were modified with composites of mcl-PHA-*co*-methyl acrylate carbon nanotube (details provided in *section 3.3.1*). The modified electrodes together with PHB15% as PEM were utilized in MFC designated as mMFC. The mMFC recorded a stable maximum voltage of 958 ± 7 mV which lasted for 88 hours as evidenced in Figure 4.18*e*. The stability and longevity in maximum voltage potential was attributed to efficient colonization of the anode electrode by biocatalyst and superior reduction of oxygen at the cathode. The results obtained were demonstrated to be far superior to earlier reports (Ayyaru & Dharmalingam, 2011; Kim et al., 2007; Sevda et al., 2013; Yusuf et al., 2018).
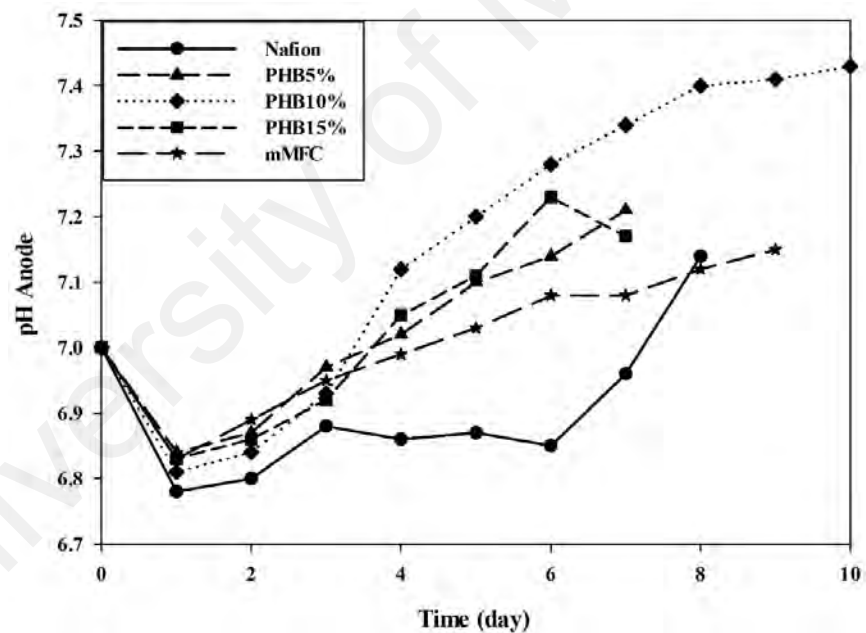
Figure 4.19: Measured pH values of anolytes during the MFC operation for Nafion, PHB5%, PHB10%, PHB15% and mMFC membranes
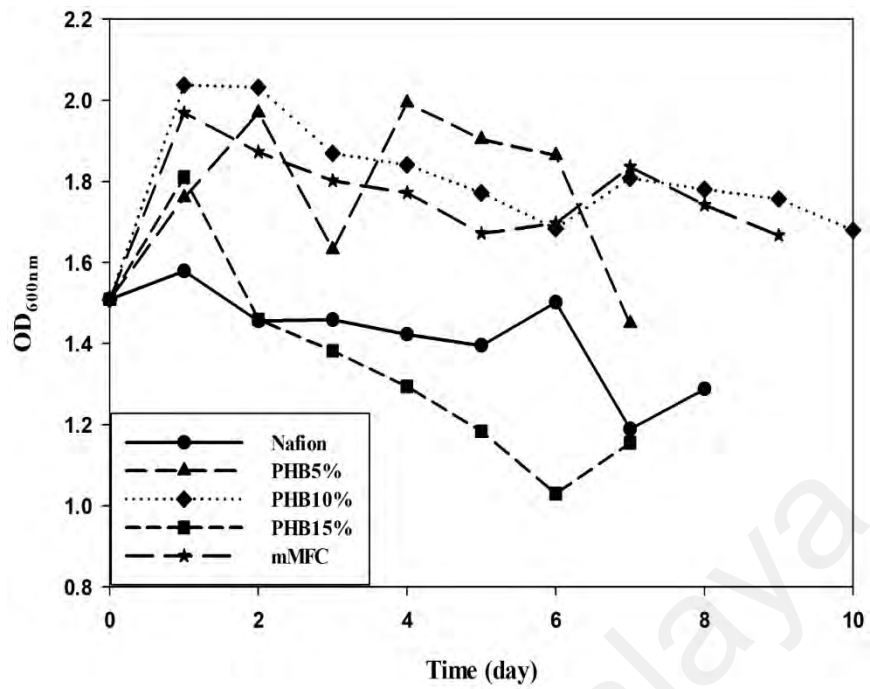
Figure 4.20: Optical densities at 600 nm (OD_{600nm}) of anolytes during the MFC operation for Nafion, PHB5%, PHB10%, PHB15% and mMFC membranes
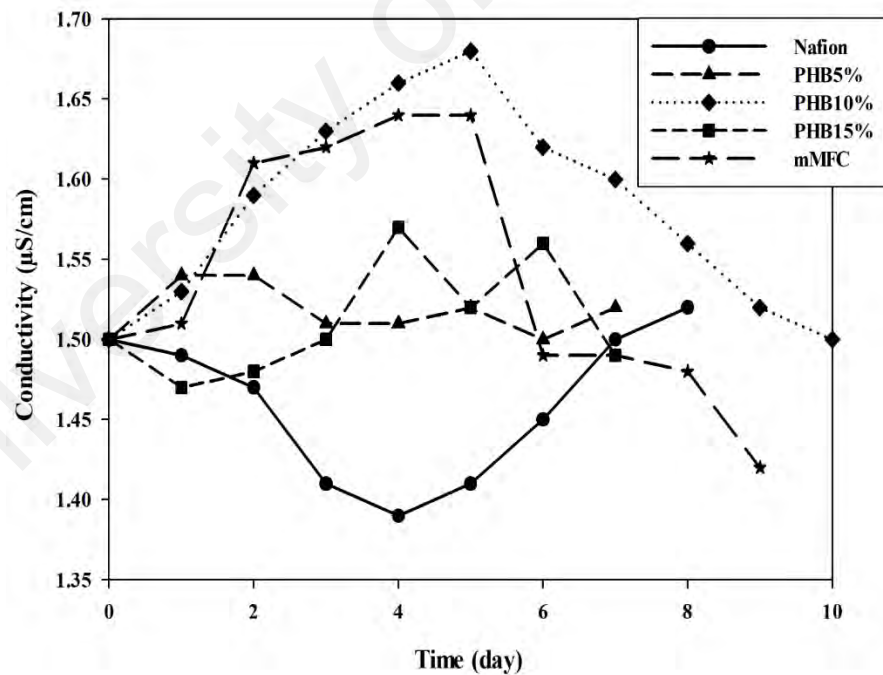
Figure 4.21: Conductivities (μS/cm) of anolytes during the MFC operation for Nafion, PHB5%, PHB10%, PHB15% and mMFC membranes

The determination of polarization data provides an insight into the MFC potential to maintain a voltage at a specific current. The data were recorded for different resistances at maximum voltage potential during MFC operation (Figure 4.22). The power densities for all tested membranes were in the following decreasing order: mMFC > PHB15% > Nafion > PHB10% > PHB5%. The lowest power density of 265 mW/m^2 was recorded by PHB5% at a current density of 665 mA/m^2. This was attributed to low PHB content in the hydrophobic mcl-PHA matrix, translating to low voltage potential (Figure 4.18b) and subsequently low power density. PHB10% recorded a power density of 322 mW/m^2 at current density of 733 mA/m^2 (Figure 4.22c), which was still lower than Nafion membrane (520 mW/m^2 at current density of 931 mA/m^2) (Figure 4.22a). PHB15% and mMFC were superior in both power and current densities compared to Nafion. PHB15% recorded a power density of 601 mW/m^2 at current density of 1402 mA/m^2 (Figure 4.22d) while mMFC recorded a power density of 912 mW/m^2 at a current density of 1233 mA/m^2 (Figure 4.22e). At lower currents, sharp decline in voltage were observed in all MFC set-ups except in mMFC set-up (Figure 4.22). The observation is attributed to activation loss (Logan, 2008). The absence of voltage loss in mMFC at higher and lower currents stemmed from improved electron transfer at the anode and improved oxygen reduction at the cathode. The maximum power densities recorded in this study were higher than that reported by (Ayyaru & Dharmalingam, 2011; Ghasemi et al., 2012; Rudra et al., 2017; Sevda et al., 2013) and comparable to that reported by Leong et al., (2015) (902 mW/m^2).
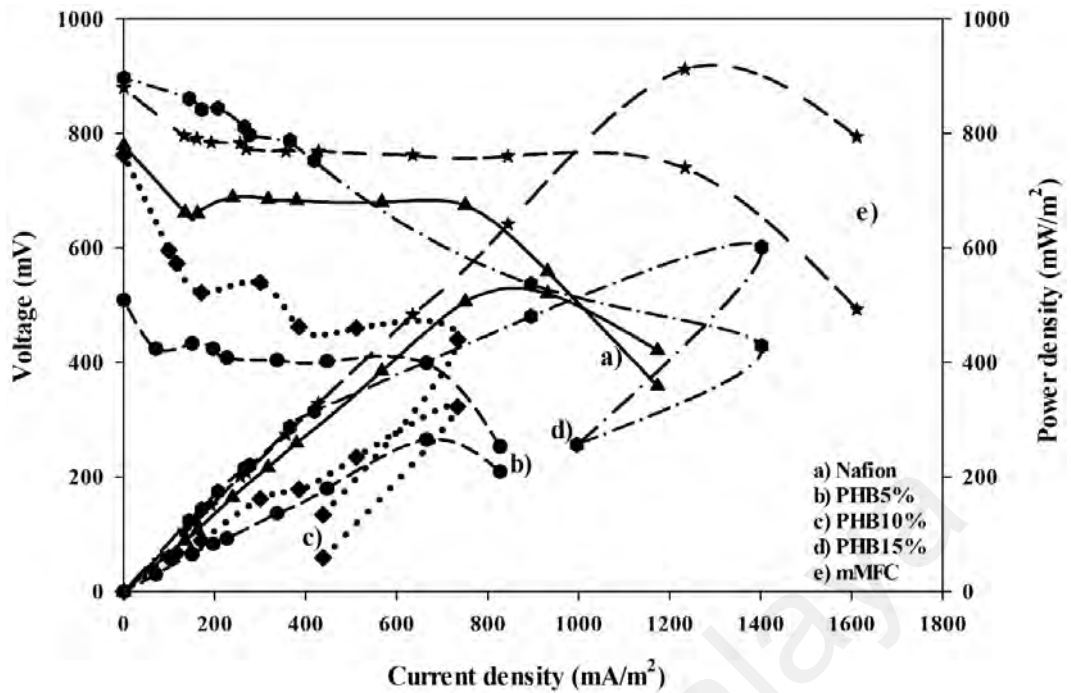
Figure 4.22: Polarization data and power density of MFC set-ups operated with *a* Nafion *b* PHB5% *c* PHB10% *d* PHB15% *e* mMFC *f* PHA100% membranes

4.4.1 Wastewater characterization during MFC operation

Although food wastewater can be characterized as non-hazardous since it contained little toxic compound, its high organic matter content calls for effective treatment prior to discharge (Oh & Logan, 2005). Table 3.2 shows the characteristics of the raw and supplemented wastewater. About seven-fold increase in the conductivity of wastewater was observed after the addition of supplements. Figure 4.23 shows the COD removal efficiencies, coulombic efficiencies (CE) and ammoniacal nitrogen (NH_3-N) removal rate of all MFC set-ups. The COD removal rate were in the following decreasing order: PHB15% (76.3 %) > PHB10% (72.7 %) > mMFC (70 %) > PHB5% (65.6 %) > Nafion (64.3 %). The observed order is expected since the composite membranes allow for better passage of proton from anode chamber to cathode chamber as shown earlier by voltage-time curve (Figure 4.18) and polarization curve (Figure 4.22). Electron recovery, known as coulombic efficiency (CE) is crucial to overall power output of MFC. The CE

was highest in both PHB15% (63 %) and mMFC (64 %) (Figure 4.22). Nafion recorded CE of 50 % while PHB10% and PHB5% recorded 38 % and 20 % CE respectively. When the CE is greater than 50 %, it is a good indicator that most of the substrate in anode chamber goes to cell respiration with efficient energy generation (Logan, 2008). The composite membranes helped to recover energy far superior than earlier reports (Angioni et al., 2016; Angioni et al., 2017; Ghasemi et al., 2012) and close to that reported by Kim et al. (2007) (72 %).

Organic compounds that are rich in protein, nucleic acid etc. could lead to ammonia accumulation, which could hinder the growth of the biocatalyst at anode (Chen et al., 2016). The ability of the MFC set-ups to degrade ammoniacal nitrogen (NH_3-N) during current generation was investigated. Nafion and mMFC membranes were superior in NH_3-N removal percentage at 59.8 % and 58.5 % respectively (Figure 4.23). PHB10% and PHB15% recorded similar NH_3-N removal of 37.8 % and 39.0 %, respectively. The lowest NH_3-N removal was recorded by PHB5% at 31.7 %. Ammonia, sulfate together with other species could diffuse through ion exchange membrane to the cathode chamber, resulting in increased electricity generation (Kim et al., 2008). Since PHB5% recorded the lowest maximum voltage potential, low NH_3-N removal percentage is expected.
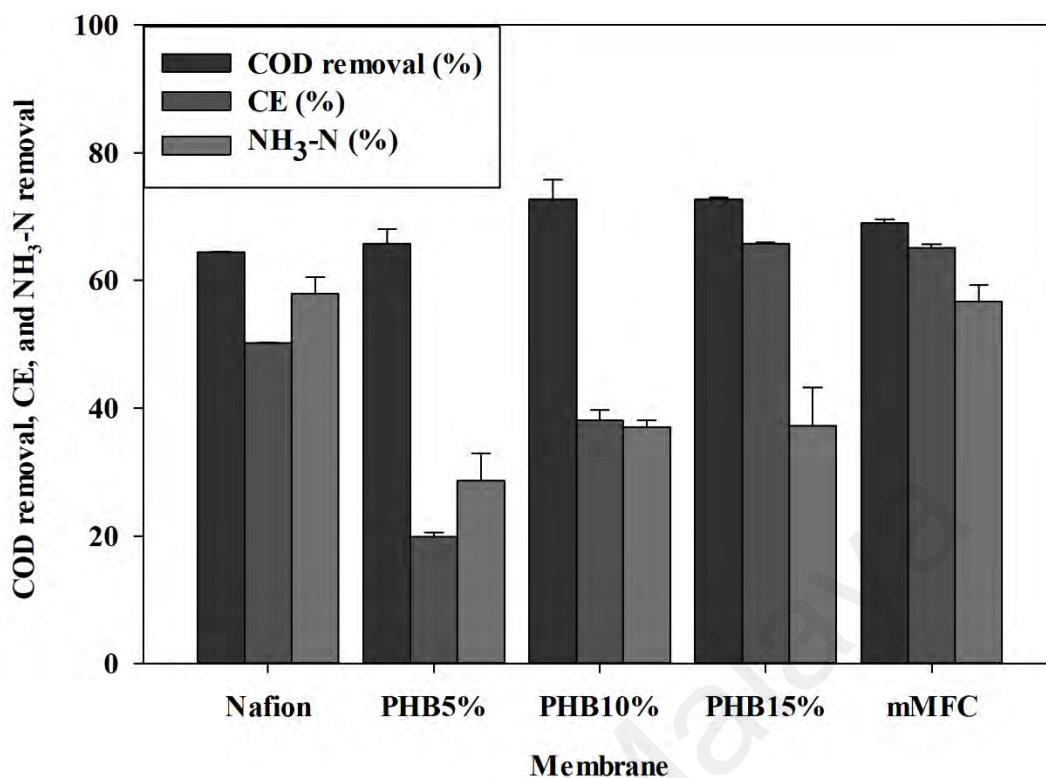
Figure 4.23: Percentage of COD removal, CE recovery and percentage of NH_3-N removal of the MFC set-ups with Nafion, PHB5%, PHB10%, PHB15% and mMFC membranes

4.4.2 Comparison studies of membranes

The results obtained in current study were compared with previously reported membrane composite in MFC (Table 4.6). In terms of maximum voltage potential and power density, results reported in this study were far superior to other literatures (Table 4.6). On the other hand, COD removal efficiency was comparable to that reported by Di Palma et al. (2018) and lesser than other studies. Apart for the CE reported by Elongovan & Dharmalingam (2016), the composite membrane in present study was superior to earlier studies (Table 4.6). It should be pointed out that unbiased comparison between different MFC studies is almost impossible due to wide variation in applied MFC size, type, configuration, membrane thickness, and environmental conditions amongst other factors.

Table 4.6: Comparison of results in the current study with reported literatures on membrane modification

Membrane composite	Maximum voltage potential (mV)	Maximum power density (mW/m^2)	COD removal (%)	CE (%)	Reference
mcl-PHA/PHB	958	912	70	64	**Current study**
Nafion/silica	26	750	95	34	(Angioni et al., 2016)
PEEK	765	603	-	76	(Elongovan & Dharmalingam 2016)
mcl-PHA/MWCNT	760	361	91	26	(Yusuf et al., 2018)
Polysulfone/SPEEK	800	68.64	91	26	(Ghasemi et al., 2016b)
Polybenzimidazole/SBA-15 mesostructured silica	600	110	90	31	(Angioni et al., 2017)
Chitosan/montmorillonite	832	119	88.5	43.64	(Yousefi et al., 2018)
Fe$_3$O$_4$/PES	552	9.59	75	11.36	(Di palma et al., 2018)
Graphene oxide/SPEEK	757	902	83	16.88	(Leong et al., 2015)

CHAPTER 5: CONCLUSION

5.1   Conclusion

The present study investigated the utilization of renewable biopolymer for innovative anode/cathode/proton exchange membrane (PEM) modifications in microbial fuel cell (MFC).

Investigation on the utilization of radical-mediated copolymerized medium chain length-polyhydroxyalkanoates-*co*-methyl acrylate (mcl-PHA-*co*-MA) graft as electrode modifier material in MFC was carried out. Spectroscopic analyses revealed extensive copolymerization of MA monomers with the mcl-PHA. Its utilization in MFC set-ups as both anode and cathode electrode modifier when composited with carbon nanotubes outperformed the control MFC in terms of maximum power and current densities, protracted voltage generation, low internal resistance and superior biofilm formation. Negligible bio(degradation) of the copolymer after 60 days of MFC operation was evidenced by slight decrease (11 %) in the weight-averaged molecular weight (M_w). The decrease is attributed to utilization of copolymer material by microbial colonizers as potentially assimilable carbon source.

Polyhydroxybutyrate (PHB) crystals at different weight percentages were composited into mcl-PHA matrix and utilized as PEM in MFC. The composite membrane with 15% PHB and mMFC (modified anode/cathode electrodes together with 15% PHB membrane) set-ups exhibited superior water uptake, high proton passage, maximum voltage potentials and improved power densities. The resistivity of composite membranes to oxygen gas flux resulted in almost complete anaerobic environment in anode chamber, thereby improving chemical oxygen demand (COD) removal and better coulombic efficiency (CE) recovery.

In summary, the study demonstrated that renewable biopolymer mcl-PHA plays a crucial role in enhancing power density and sustained voltage generation when utilized as an integral component of MFC. The use of environmental-friendly biopolymer eliminates the green disposal concern and serves as effective alternative towards practical MFC application. The important findings from this study open up a new research dimension for bringing MFC practical applications closer to reality.

5.2   Future studies

Composite nanomaterials of MA-PHA/CNT as electrodes modifier proved to be superior in enhancing MFC performance in a fed-batch mode MFC operation. Future work should focus on continuous mode of MFC operation for higher and stable current generation over a longer period of time.

Further grafting of MA-PHA/CNT with conducting polymer such as polypyrrole (PPy) or polyaniline (PANI) should be investigated to increase its conductivity, reduce the internal resistance and enhance its resistivity to bio(degradation) for prolonged reusability.

Multifunctional free-standing three-dimensional hydrogel electrode of MA-PHA/CNT should also be investigated. This can be achieved through radical polymerization with cross-linker such as acrylic acid.

Whilst mcl PHA-PHB composite membrane as PEM effectively prevents gas diffusion from cathode compartment to anode compartment over 6 hours of operation, long-term oxygen flux across the composite membrane should be investigated. In addition, the conduction of other ions apart from protons across the membrane should also be studied since native PHB is known to be permeable to them *in vivo*. Equally important to investigate is the composite membrane operation-dependent mechanical stability,

biofouling effect and its long-term utilization focusing on biodegradability effects towards the overall MFC performance.

REFERENCES

Abid, S., Raza, Z. A., & Hussain, T. (2016). Production kinetics of polyhydroxyalkanoates by using *Pseudomonas aeruginosa* gamma ray mutant strain EBN-8 cultured on soybean oil. *3 Biotech, 6*(2), Article#142.

Abidin, S. N. J. S. Z., Mamat, M. S., Rasyid, S. A., Zainal, Z., & Sulaiman, Y. (2018). Electropolymerization of poly (3, 4-ethylenedioxythiophene) onto polyvinyl alcohol-graphene quantum dot-cobalt oxide nanofiber composite for high-performance supercapacitor. *Electrochimica Acta, 261*, 548-556.

Abu-Elreesh, G., Zaki, S., Farag, S., Elkady, M. F., & Abd-El-Haleem, D. (2011). Exobiopolymer from polyhydroxyalkanoate-producing transgenic yeast. *African Journal of Biotechnology, 10*(34), 6558-6563.

Ahmed, J., Kim, H. J., & Kim, S. (2012). Polyaniline nanofiber/carbon black composite as oxygen reduction catalyst for air cathode microbial fuel cells. *Journal of the Electrochemical Society, 159*(5), B497-B501.

Akhtar, S. (1990). Physicomechanical properties of bacterial P(HB-HV) polyesters and their uses in drug delivery. Doctoral dissertation, University of Bath, UK.

Alatraktchi, F. A. a., Zhang, Y., & Angelidaki, I. (2014). Nanomodification of the electrodes in microbial fuel cell: Impact of nanoparticle density on electricity production and microbial community. *Applied Energy, 116*, 216-222.

Albuquerque, M., Concas, S., Bengtsson, S., & Reis, M. (2010). Mixed culture polyhydroxyalkanoates production from sugar molasses: The use of a 2-stage CSTR system for culture selection. *Bioresource Technology, 101*(18), 7112-7122.

Almatouq, A., & Babatunde, A. O. (2018). Identifying optimized conditions for concurrent electricity production and phosphorus recovery in a mediator-less dual chamber microbial fuel cell. *Applied Energy, 230*, 122-134.

Anbukarasu, P., Sauvageau, D., & Elias, A. (2015). Tuning the properties of polyhydroxybutyrate films using acetic acid via solvent casting. *Scientific Reports, 5*, Article#17884.

Angioni, S., Millia, L., Bruni, G., Ravelli, D., Mustarelli, P., & Quartarone, E. (2017). Novel composite polybenzimidazole-based proton exchange membranes as efficient and sustainable separators for microbial fuel cells. *Journal of Power Sources, 348*, 57-65.

Angioni, S., Millia, L., Bruni, G., Tealdi, C., Mustarelli, P., & Quartarone, E. (2016). Improving the performances of Nafion (TM)-based membranes for microbial fuel cells with silica-based, organically-functionalized mesostructured fillers. *Journal of Power Sources, 334*, 120-127.

Anis, S. N. S., Mohamad Annuar, M. S., & Simarani, K. (2017). *In vivo* and *in vitro* depolymerizations of intracellular medium-chain-length poly-3-hydroxyalkanoates produced by *Pseudomonas putida* BET001. *Preparative Biochemistry and Biotechnology, 47*(8), 824-834.

Annuar, M., Tan, I. K., & Ramachandran, K. (2008). Evaluation of nitrogen sources for growth and production of medium-chain-length poly-(3-hydroxyalkanoates) from palm kernel oil by *Pseudomonas putida* PGA1. *Asia Pacific Journal of Molecular Biology and Biotechnology*, *16,* 11-15.

Aris, M. H., Annuar, M. S. M., & Ling, T. C. (2016). Lipase-mediated degradation of poly-ε-caprolactone in toluene: Behavior and its Action Mechanism. *Polymer Degradation and Stability, 133*, 182-191.

Ates, M., Eker, A. A., & Eker, B. (2017). Carbon nanotube-based nanocomposites and their applications. *Journal of Adhesion Science and Technology, 31*(18), 1977-1997.

Ayyaru, S., & Dharmalingam, S. (2011). Development of MFC using sulphonated polyether ether ketone (SPEEK) membrane for electricity generation from waste water. *Bioresource Technology, 102*(24), 11167-11171.

Bajestani, M. B., & Mousavi, S. A. (2016). Effect of casting solvent on the characteristics of Nafion/TiO_2 nanocomposite membranes for microbial fuel cell application. *International Journal of Hydrogen Energy, 41*(1), 476-482.

Baudler, A., Schmidt, I., Langner, M., Greiner, A., & Schröder, U. (2015). Does it have to be carbon? Metal anodes in microbial fuel cells and related bioelectrochemical systems. *Energy & Environmental Science, 8*(7), 2048-2055.

Berezina, N., & Martelli, S. M. (2014). Polyhydroxyalkanoates: Structure, properties and sources. *Polyhydroxyalkanoate (PHA) based Blends, Composites and Nanocomposites, 30*, 18-36.

Biradar, G. G., Shivasharana, C., & Kaliwal, B. B. (2018). Characterization of polyhydroxybutyrate (PHB) produced by novel bacterium *Lysinibacillus sphaericus* BBKGBS6 isolated from soil. *Journal of Polymers and the Environment, 26*(4), 1685-1701.

Bond-Watts, B. B., Bellerose, R. J., & Chang, M. C. (2011). Enzyme mechanism as a kinetic control element for designing synthetic biofuel pathways. *Nature Chemical Biology, 7*(4), Article#222.

Bouten, C., Dankers, P., Driessen-Mol, A., Pedron, S., Brizard, A., & Baaijens, F. (2011). Substrates for cardiovascular tissue engineering. *Advanced Drug Delivery Reviews, 63*(4-5), 221-241.

Bugnicourt, E., Cinelli, P., Lazzeri, A., & Alvarez, V. A. (2014). Polyhydroxyalkanoate (PHA): Review of synthesis, characteristics, processing and potential applications in packaging. *Express Polymer Letters*, *8*(11), 791-808.

Chae, K. J., Kim, K. Y., Choi, M. J., Yang, E. T., Kim, I. S., Ren, X. H., & Lee, M. (2014). Sulfonated polyether ether ketone (SPEEK)-based composite proton exchange membrane reinforced with nanofibers for microbial electrolysis cells. *Chemical Engineering Journal, 254*, 393-398.

Chanprateep, S., Buasri, K., Muangwong, A., & Utiswannakul, P. (2010). Biosynthesis and biocompatibility of biodegradable poly (3-hydroxybutyrate-*co*-4-hydroxybutyrate). *Polymer Degradation and Stability, 95*(10), 2003-2012.

Chen, H., Wang, W., Xue, L., Chen, C., Liu, G., & Zhang, R. (2016). Effects of ammonia on anaerobic digestion of food waste: Process performance and microbial community. *Energy & Fuels, 30*(7), 5749-5757.

Chen, J. Y., Xie, P., & Zhang, Z. P. (2019). Reduced graphene oxide/polyacrylamide composite hydrogel scaffold as biocompatible anode for microbial fuel cell. *Chemical Engineering Journal, 361*, 615-624.

Cheng, S., Liu, H., & Logan, B. E. (2006). Increased performance of single-chamber microbial fuel cells using an improved cathode structure. *Electrochemistry Communications, 8*(3), 489-494.

Chou, H.-T., Lee, H.-J., Lee, C.-Y., Tai, N.-H., & Chang, H.-Y. (2014). Highly durable anodes of microbial fuel cells using a reduced graphene oxide/carbon nanotube-coated scaffold. *Bioresource Technology, 169*, 532-536.

Cui, H.-F., Du, L., Guo, P.-B., Zhu, B., & Luong, J. H. (2015). Controlled modification of carbon nanotubes and polyaniline on macroporous graphite felt for high-performance microbial fuel cell anode. *Journal of Power Sources, 283*, 46-53.

Dai, Z., Aboukeila, H., Ansaloni, L., Deng, J., Baschetti, M. G., & Deng, L. (2019). Nafion/PEG hybrid membrane for CO_2 separation: Effect of PEG on membrane micro-structure and performance. *Separation and Purification Technology, 214*, 67-77.

Das, S., Kurcok, P., Jedlinski, Z., & Reusch, R. N. (1999). Ion channels formed by biomimetic oligo-(R)-3-hydroxybutyrates and inorganic polyphosphates in planar lipid bilayers. *Macromolecules, 32*(26), 8781-8785.

Daud, S. M., Daud, W. R. W., Kim, B. H., Somalu, M. R., Abu Bakar, M. H., Muchtar, A., . . . Chang, I. S. (2018). Comparison of performance and ionic concentration gradient of two-chamber microbial fuel cell using ceramic membrane (CM) and cation exchange membrane (CEM) as separators. *Electrochimica Acta, 259*, 365-376.

Daud, S. M., Kim, B. H., Ghasemi, M., & Daud, W. R. W. (2015). Separators used in microbial electrochemical technologies: Current status and future prospects. *Bioresource Technology, 195*, 170-179.

De Schryver, P., Dierckens, K., Bahn Thi, Q. Q., Amalia, R., Marzorati, M., Bossier, P., . . . Verstraete, W. (2011). Convergent dynamics of the juvenile European sea bass gut microbiota induced by poly-β-hydroxybutyrate. *Environmental Microbiology, 13*(4), 1042-1051.

Defoirdt, T., Sorgeloos, P., & Bossier, P. (2011). Alternatives to antibiotics for the control of bacterial disease in aquaculture. *Current Opinion in Microbiology, 14*(3), 251-258.

Di Palma, L., Bavasso, I., Sarasini, F., Tirillo, J., Puglia, D., Dominici, F., & Torre, L. (2018). Synthesis, characterization and performance evaluation of Fe_3O_4/PES nano-composite membranes for microbial fuel cell. *European Polymer Journal, 99*, 222-229.

Dicks, A., & Rand, D. A. J. (2018). Fuel cell systems explained. Wiley, New York.

Doyle, C., Tanner, E., & Bonfield, W. (1991). *In vitro* and *in vivo* evaluation of polyhydroxybutyrate and of polyhydroxybutyrate reinforced with hydroxyapatite. *Biomaterials, 12*(9), 841-847.

Elangovan, M., & Dharmalingam, S. (2016). Comparative study of microbial fuel cell performance using poly ether ether ketone-based anion and cation exchange membranes. *Journal of Polymer Research, 23*(12), Article#250.

Elustondo, P. A., Angelova, P. R., Kawalec, M., Michalak, M., Kurcok, P., Abramov, A. Y., & Pavlov, E. V. (2013). Polyhydroxybutyrate targets mammalian mitochondria and increases permeability of plasmalemmal and mitochondrial membranes. *PLoS ONE, 8*(9), Article#e75812.

Filippou, P. S., Koini, E. N., Calogeropoulou, T., Kalliakmani, P., Panagiotidis, C. A., & Kyriakidis, D. A. (2011). Regulation of the *Escherichia coli* AtoSC two component system by synthetic biologically active 5; 7; 8-trimethyl-1; 4-benzoxazine analogues. *Bioorganic & Medicinal Chemistry, 19*(16), 5061-5070.

Fraiwan, A., Adusumilli, S. P., Han, D., Steckl, A. J., Call, D. F., Westgate, C. R., & Choi, S. (2014). Microbial power-generating capabilities on micro-/nano-structured anodes in micro-sized microbial fuel cells. *Fuel Cells, 14*(6), 801-809.

Fu, L., You, S. J., Yang, F. L., Gao, M. M., Fang, X. H., & Zhang, G. Q. (2010). Synthesis of hydrogen peroxide in microbial fuel cell. *Journal of Chemical Technology and Biotechnology, 85*(5), 715-719.

Gajda, I., Greenman, J., Melhuish, C., Santoro, C., & Ieropoulos, I. (2016). Microbial fuel cell-driven caustic potash production from wastewater for carbon sequestration. *Bioresource Technology, 215*, 285-289.

Gajda, I., Greenman, J., Melhuish, C., Santoro, C., Li, B., Cristiani, P., & Ieropoulos, I. (2015). Electro-osmotic-based catholyte production by microbial fuel cells for carbon capture. *Water Research, 86*, 108-115.

Gajda, I., Greenman, J., Santoro, C., Serov, A., Melhuish, C., Atanassov, P., & Ieropoulos, I. A. (2018). Improved power and long term performance of microbial fuel cell with Fe-N-C catalyst in air-breathing cathode. *Energy, 144*, 1073-1079.

Gao, X., Chen, J.-C., Wu, Q., & Chen, G.-Q. (2011). Polyhydroxyalkanoates as a source of chemicals, polymers, and biofuels. *Current Opinion in Biotechnology, 22*(6), 768-774.

Gao, Z., Yang, W., Wang, J., Wang, B., Li, Z., Liu, Q., . . . Liu, L. (2012). A new partially reduced graphene oxide nanosheet/polyaniline nanowafer hybrid as supercapacitor electrode material. *Energy & Fuels, 27*(1), 568-575.

Ghasemi, M., Daud, W. R. W., Alam, J., Ilbeygi, H., Sedighi, M., Ismail, A. F., . . . Aljlil, S. A. (2016a). Treatment of two different water resources in desalination and microbial fuel cell processes by poly sulfone/sulfonated poly ether ether ketone hybrid membrane. *Energy, 96*, 303-313.

Ghasemi, M., Daud, W. R. W., Alam, J., Jafari, Y., Sedighi, M., Aljlil, S. A., & Ilbeygi, H. (2016b). Sulfonated poly ether ether ketone with different degree of sulphonation in microbial fuel cell: Application study and economical analysis. *International Journal of Hydrogen Energy, 41*(8), 4862-4871.

Ghasemi, M., Shahgaldi, S., Ismail, M., Yaakob, Z., & Daud, W. R. W. (2012). New generation of carbon nanocomposite proton exchange membranes in microbial fuel cell systems. *Chemical Engineering Journal, 184*, 82-89.

Gnana Kumar, G., Kirubaharan, C. J., Udhayakumar, S., Ramachandran, K., Karthikeyan, C., Renganathan, R., & Nahm, K. S. (2014). Synthesis, structural, and morphological characterizations of reduced graphene oxide-supported polypyrrole anode catalysts for improved microbial fuel cell performances. *Acs Sustainable Chemistry & Engineering, 2*(10), 2283-2290.

Grillo, R., Santo Pereira, A. d. E., de Melo, N. F. S., Porto, R. M., Feitosa, L. O., Tonello, P. S., . . . Fraceto, L. F. (2011). Controlled release system for ametryn using polymer microspheres: Preparation, characterization and release kinetics in water. *Journal of Hazardous Materials, 186*(2-3), 1645-1651.

Grothe, E., Moo-Young, M., & Chisti, Y. (1999). Fermentation optimization for the production of poly (*β*-hydroxybutyric acid) microbial thermoplastic. *Enzyme and Microbial Technology, 25*(1-2), 132-141.

Gumel, A., Annuar, M., & Chisti, Y. (2013). Recent advances in the production, recovery and applications of polyhydroxyalkanoates. *Journal of Polymers and the Environment, 21*(2), 580-605.

Gumel, A., Annuar, M., & Heidelberg, T. (2012). Effects of carbon substrates on biodegradable polymer composition and stability produced by *Delftia tsuruhatensis* BET002 isolated from palm oil mill effluent. *Polymer Degradation and Stability, 97*(8), 1224-1231.

Gumel, A., Annuar, M., Ishak, K., & Ahmad, N. (2014). Carbon nanofibers-poly-3-hydroxyalkanoates nanocomposite: ultrasound-assisted dispersion and thermostructural properties. *Journal of Nanomaterials, 2014*, Article#123.

Gumel, A. M., & Annuar, M. S. M. (2014). Poly-3-hydroxyalkanoates-*co*-polyethylene glycol methacrylate copolymers for pH responsive and shape memory hydrogel. *Journal of Applied Polymer Science, 131*(23), Article#41149.

Gumel, A. M., Annuar, M. S. M., & Heidelberg, T. (2012). Biosynthesis and characterization of polyhydroxyalkanoates copolymers produced by *Pseudomonas putida* BET001 isolated from palm oil mill effluent. *PLoS ONE, 7*(9), Article#e45214.

Han, T. H., Parveen, N., Shim, J. H., Nguyen, A. T. N., Mahato, N., & Cho, M. H. (2018). Ternary composite of polyaniline graphene and TiO_2 as a bifunctional catalyst to enhance the performance of both the bioanode and cathode of a microbial fuel cell. *Industrial & Engineering Chemistry Research, 57*(19), 6705-6713.

Harewood, A. J. T., Popuri, S. R., Cadogan, E. I., Lee, C. H., & Wang, C. C. (2017). Bioelectricity generation from brewery wastewater in a microbial fuel cell using chitosan/biodegradable copolymer membrane. *International Journal of Environmental Science and Technology, 14*(7), 1535-1550.

He, Z., Huang, Y., Manohar, A. K., & Mansfeld, F. (2008). Effect of electrolyte pH on the rate of the anodic and cathodic reactions in an air-cathode microbial fuel cell. *Bioelectrochemistry, 74*(1), 78-82.

He, Z., Wagner, N., Minteer, S. D., & Angenent, L. T. (2006). An upflow microbial fuel cell with an interior cathode: Assessment of the internal resistance by impedance spectroscopy. *Environmental Science & Technology, 40*(17), 5212-5217.

Hernandez-Fernandez, F. J., de los Rios, A., Mateo-Ramirez, F., Juarez, M. D., Lozano-Blanco, L. J., & Godinez, C. (2016). New application of polymer inclusion membrane based on ionic liquids as proton exchange membrane in microbial fuel cell. *Separation and Purification Technology, 160*, 51-58.

Hernandez-Flores, G., Poggi-Varaldo, H. M., & Solorza-Feria, O. (2016). Comparison of alternative membranes to replace high cost Nafion ones in microbial fuel cells. *International Journal of Hydrogen Energy, 41*(48), 23354-23362.

Hernandez, L. A., Riveros, G., Gonzalez, D. M., Gacitua, M., & del Valle, M. A. (2019). PEDOT/graphene/nickel-nanoparticles composites as electrodes for microbial fuel cells. *Journal of Materials Science-Materials in Electronics, 30*(13), 12001-12011.

Hindatu, Y., Annuar, M., & Gumel, A. (2017a). Mini-review: Anode modification for improved performance of microbial fuel cell. *Renewable and Sustainable Energy Reviews, 73*, 236-248.

Hindatu, Y., Annuar, M., Subramaniam, R., & Gumel, A. (2017b). Medium-chain-length poly-3-hydroxyalkanoates-carbon nanotubes composite anode enhances the performance of microbial fuel cell. *Bioprocess and Biosystems Engineering, 40*(6), 919-928.

Hoegh-Guldberg, O., Jacob, D., Taylor, M., Bindi, M., Brown, S., Camilloni, I., . . . Engelbrecht, F. (2018). Chapter 3: Impacts of 1.5 ºC global warming on natural and human systems. Intergovermental Panel on Climate Change, Switzerland.

Holder, S. L., Lee, C. H., & Popuri, S. R. (2017). Simultaneous wastewater treatment and bioelectricity production in microbial fuel cells using cross-linked chitosan-graphene oxide mixed-matrix membranes. *Environmental Science and Pollution Research, 24*(15), 13782-13796.

Hou, J., Liu, Z., & Li, Y. (2015). Polyaniline modified stainless steel fiber felt for high-performance microbial fuel cell anodes. *Journal of Clean Energy Technologies, 3*(3), 165-169.

Hu, L., & Cui, Y. (2012). Energy and environmental nanotechnology in conductive paper and textiles. *Energy & Environmental Science, 5*(4), 6423-6435.

Huggins, T., Wang, H., Kearns, J., Jenkins, P., & Ren, Z. J. (2014). Biochar as a sustainable electrode material for electricity production in microbial fuel cells. *Bioresource Technology, 157*, 114-119.

Jafary, T., Ghasemi, M., Alam, J., Aljlil, S. A., & Yusup, S. (2018). 15 - Carbon-based polymer nanocomposites as electrodes for microbial fuel cells. In A. F. Ismail & P. S. Goh (Eds.), *Carbon-Based Polymer Nanocomposites for Environmental and Energy Applications*, *Elsevier*, 361-390.

Jian, J., Zhang, S.-Q., Shi, Z.-Y., Wang, W., Chen, G.-Q., & Wu, Q. (2010). Production of polyhydroxyalkanoates by *Escherichia coli* mutants with defected mixed acid fermentation pathways. *Applied Microbiology and Biotechnology, 87*(6), 2247-2256.

Jie, X., Gonzalez-Cortes, S., Xiao, T., Wang, J., Yao, B., Slocombe, D. R., . . . Edwards, P. P. (2017). Rapid production of high-purity hydrogen fuel through microwave-promoted deep catalytic dehydrogenation of liquid alkanes with abundant metals. *Angewandte Chemie International Edition, 56*(34), 10170-10173.

Jung, S. P., Yoon, M. H., Lee, S. M., Oh, S. E., Kang, H., & Yang, J. K. (2014). Power generation and anode bacterial community compositions of sediment fuel cells differing in anode materials and carbon sources. *International Journal of Electrochemical Science, 9*(1), 315-326.

Kang, Y. L., Ibrahim, S., & Pichiah, S. (2015). Synergetic effect of conductive polymer poly (3, 4-ethylenedioxythiophene) with different structural configuration of anode for microbial fuel cell application. *Bioresource Technology, 189*, 364-369.

Kanimozhi, S., & Perinbam, K. (2013). Biodesel production from *Pseudomonas fluorescens* Lp1 lipase immobilized on amino-silane modified super paramagnetic Fe_3O_4 nanoparticles. *Journal of Physics*: Conference Series, Volume 431, Conference 1, 5-7 December, 2012.

Kaur, A., Ibrahim, S., Pickett, C. J., Michie, I. S., Dinsdale, R. M., Guwy, A. J., & Premier, G. C. (2014). Anode modification to improve the performance of a microbial fuel cell volatile fatty acid biosensor. *Sensors and Actuators B-Chemical, 201*, 266-273.

Kim, J. R., Cheng, S., Oh, S.-E., & Logan, B. E. (2007). Power generation using different cation, anion, and ultrafiltration membranes in microbial fuel cells. *Environmental Science & Technology, 41*(3), 1004-1009.

Kim, J. R., Premier, G. C., Hawkes, F. R., Dinsdale, R. M., & Guwy, A. J. (2009). Development of a tubular microbial fuel cell (MFC) employing a membrane electrode assembly cathode. *Journal of Power Sources, 187*(2), 393-399.

Kim, J. R., Zuo, Y., Regan, J. M., & Logan, B. E. (2008). Analysis of ammonia loss mechanisms in microbial fuel cells treating animal wastewater. *Biotechnology and Bioengineering, 99*(5), 1120-1127.

Kim, T., Kang, S., Sung, J. H., Kang, Y. K., Kim, Y. H., & Jang, J. K. (2016). Characterization of polyester cloth as an alternative separator to nafion membrane in microbial fuel cells for bioelectricity generation using swine wastewater. *Journal of Microbiology and Biotechnology, 26*(12), 2171-2178.

Knowles, J., Hastings, G., Ohta, H., Niwa, S., & Boeree, N. (1992). Development of a degradable composite for orthopaedic use: *in vivo* biomechanical and histological evaluation of two bioactive degradable composites based on the polyhydroxybutyrate polymer. *Biomaterials, 13*(8), 491-496.

Kumar, G. G., Hashmi, S., Karthikeyan, C., GhavamiNejad, A., Vatankhah-Varnoosfaderani, M., & Stadler, F. J. (2014a). Graphene oxide/carbon nanotube composite hydrogels-versatile materials for microbial fuel cell applications. *Macromolecular Rapid Communications, 35*(21), 1861-1865.

Kumar, G. G., Kirubaharan, C. J., Udhayakumar, S., Ramachandran, K., Karthikeyan, C., Renganathan, R., & Nahrn, K. S. (2014b). Synthesis, structural, and morphological characterizations of reduced graphene oxide-supported polypyrrole anode catalysts for improved microbial fuel cell performances. *Acs Sustainable Chemistry & Engineering, 2*(10), 2283-2290.

Kumar, V., Kumar, P., Nandy, A., & Kundu, P. P. (2016a). A nanocomposite membrane composed of incorporated nano-alumina within sulfonated PVDF-*co*-HFP/Nafion blend as separating barrier in a single chambered microbial fuel cell. *Rsc Advances, 6*(28), 23571-23580.

Kumar, V., Mondal, S., Nandy, A., & Kundu, P. P. (2016b). Analysis of polybenzimidazole and polyvinylpyrrolidone blend membranes as separating barrier in single chambered microbial fuel cells. *Biochemical Engineering Journal, 111*, 34-42.

Lee, S. H., Ban, J. Y., Oh, C.-H., Park, H.-K., & Choi, S. (2016). A solvent-free microbial-activated air cathode battery paper platform made with pencil-traced graphite electrodes. *Scientific Reports, 6*, Article#28588.

Lemoigne, M. (1926). Produits de deshydration et de polymerisation de l'acide *β*= oxybutyrique. *Bulletin de la Société Chimique de France, 8*, 770-782.

Li, C., Wang, L., Wang, X. D., Kong, M. X., Zhang, Q., & Li, G. Y. (2017). Synthesis of PVDF-g-PSSA proton exchange membrane by ozone-induced graft copolymerization and its application in microbial fuel cells. *Journal of Membrane Science, 527*, 35-42.

Li, H. Y., Ma, H. Z., Liu, T., Ni, J., & Wang, Q. H. (2019). An excellent alternative composite modifier for cathode catalysts prepared from bacterial cellulose doped with Cu and P and its utilization in microbial fuel cell. *Bioresource Technology, 289*, Article#121661.

Li, S., Cheng, C., & Thomas, A. (2017). Carbon-based microbial-fuel-cell electrodes: From conductive supports to active catalysts. *Advanced Materials, 29*(8), Article#1602547.

Li, X. H., Qian, J. S., Guo, X. G., & Shi, L. W. (2018). One-step electrochemically synthesized graphene oxide coated on polypyrrole nanowires as anode for microbial fuel cell. *3 Biotech, 8*(8), Article#375.

Li, Z., & Loh, X. J. (2015). Water soluble polyhydroxyalkanoates: future materials for therapeutic applications. *Chemical Society Reviews, 44*(10), 2865-2879.

Li, Z. L., Yang, S. K., Song, Y. N., Xu, H. Y., Wang, Z. Z., Wang, W. K., . . . Zhao, Y. Q. (2019). In-situ modified titanium suboxides with polyaniline/graphene as anode to enhance biovoltage production of microbial fuel cell. *International Journal of Hydrogen Energy, 44*(13), 6862-6870.

Liang, B. L., Li, K. X., Liu, Y., & Kang, X. W. (2019). Nitrogen and phosphorus dual-doped carbon derived from chitosan: An excellent cathode catalyst in microbial fuel cell. *Chemical Engineering Journal, 358*, 1002-1011.

Lianhua, L., Xiaoying, K., Yongming, S., Zhenhong, Y., & Ying, L. (2011). Performance of microbial fuel cell in different anode and cathode electrode sizes. *International Conference on Remote Sensing, Environment and Transportation Engineering*, RSETE, 24-26 June 2011 - Proceedings.

Liau, C. P., Bin Ahmad, M., Shameli, K., Yunus, W. M. Z. W., Ibrahim, N. A., Zainuddin, N., & Then, Y. Y. (2014). Preparation and characterization of polyhydroxybutyrate/polycaprolactone nanocomposites. *The Scientific World Journal, 2014*(1), 71-82.

Liu, B. C., Yao, X., Zhou, X. M., & Wu, X. C. (2011). Effect of cathode electrode and cation exchange membrane areas on electricity production of H-type MFCs. *Huanjing Kexue/Environmental Science, 32*(6), 1837-1842.

Liu, H., & Logan, B. E. (2004). Electricity generation using an air-cathode single chamber microbial fuel cell in the presence and absence of a proton exchange membrane. *Environmental Science & Technology, 38*(14), 4040-4046.

Liu, J., Liu, J., He, W., Qu, Y., Ren, N., & Feng, Y. (2014). Enhanced electricity generation for microbial fuel cell by using electrochemical oxidation to modify carbon cloth anode. *Journal of Power Sources, 265*, 391-396.

Liu, X., Wu, W., & Gu, Z. (2015). Poly (3, 4-ethylenedioxythiophene) promotes direct electron transfer at the interface between *Shewanella loihica* and the anode in a microbial fuel cell. *Journal of Power Sources, 277*, 110-115.

Liu, X. W., Huang, Y. X., Sun, X. F., Sheng, G. P., Zhao, F., Wang, S. G., & Yu, H. Q. (2014). Conductive carbon nanotube hydrogel as a bioanode for enhanced microbial electrocatalysis. *Acs Applied Materials & Interfaces, 6*(11), 8158-8164.

Logan, B. E. (2008). Microbial fuel cells: John Wiley & Sons, Inc., New York.

Logan, B. E. (2009). Exoelectrogenic bacteria that power microbial fuel cells. *Nature Reviews Microbiology, 7*, 375-381.

Logan, B. E., Hamelers, B., Rozendal, R., Schröder, U., Keller, J., Freguia, S., . . . Rabaey, K. (2006). Microbial fuel cells: methodology and technology. *Environmental Science & Technology, 40*(17), 5181-5192.

Lu, M., Guo, L., Kharkwal, S., Ng, H. Y., & Li, S. F. Y. (2013). Manganese–polypyrrole–carbon nanotube, a new oxygen reduction catalyst for air-cathode microbial fuel cells. *Journal of Power Sources, 221*, 381-386.

Lu, M., & Li, S. F. Y. (2012). Cathode reactions and applications in microbial fuel cells: A review. *Critical Reviews in Environmental Science and Technology, 42*(23), 2504-2525.

Luckarift, H. R., Sizemore, S. R., Farrington, K. E., Roy, J., Lau, C., Atanassov, P. B., & Johnson, G. R. (2012). Facile fabrication of scalable, hierarchically structured polymer/carbon architectures for bioelectrodes. *Acs Applied Materials & Interfaces, 4*(4), 2082-2087.

Luklinska, Z., & Bonfield, W. (1997). Morphology and ultrastructure of the interface between hydroxyapatite-polyhydroxybutyrate composite implant and bone. *Journal of Materials Science: Materials in Medicine, 8*(6), 379-383.

Luo, H., Liu, G., Zhang, R., & Jin, S. (2009). Comparison of power generation in microbial fuel cells of two different structures. *Huan Jing Ke Xue = Huanjing Kexue, 30*(2), 621-624.

Luo, S., & He, Z. (2016). Ni-coated carbon fiber as an alternative cathode electrode material to improve cost efficiency of microbial fuel cells. *Electrochimica Acta, 222*, 338-346.

Ma, Q., Pu, K. B., Cai, W. F., Wang, Y. H., Chen, Q. Y., & Li, F. J. (2018). Characteristics of poly(3,4-ethylenedioxythiophene) modified stainless steel as anode in air-cathode microbial fuel cells. *Industrial & Engineering Chemistry Research, 57*(19), 6633-6638.

Maiti, J., Kakati, N., Woo, S. P., & Yoon, Y. S. (2018). Nafion® based hybrid composite membrane containing GO and dihydrogen phosphate functionalized ionic liquid for high temperature polymer electrolyte membrane fuel cell. *Composites Science and Technology, 155*, 189-196.

Mani, P., Keshavarz, T., Chandra, T. S., & Kyazze, G. (2017). Decolourisation of acid orange 7 in a microbial fuel cell with a laccase-based biocathode: Influence of mitigating pH changes in the cathode chamber. *Enzyme and Microbial Technology, 96*, 170-176.

Merino-Jimenez, I., Santoro, C., Rojas-Carbonell, S., Greenman, J., Ieropoulos, I., & Atanassov, P. (2016). Carbon-based air-breathing cathodes for microbial fuel cells. *Catalysts, 6*(9), Article#127.

Modi, A., Singh, S., & Verma, N. (2017). Improved performance of a single chamber microbial fuel cell using nitrogen-doped polymer-metal-carbon nanocomposite-based air-cathode. *International Journal of Hydrogen Energy, 42*(5), 3271-3280.

Modi, S., Koelling, K., & Vodovotz, Y. (2011). Assessment of PHB with varying hydroxyvalerate content for potential packaging applications. *European Polymer Journal, 47*(2), 179-186.

Mottet, L., Le Cornec, D., Noel, J. M., Kanoufi, F., Delord, B., Poulin, P., . . . Bremond, N. (2018). A conductive hydrogel based on alginate and carbon nanotubes for probing microbial electroactivity. *Soft Matter, 14*(8), 1434-1441.

Muralidhar, C., & Pillai, P. (1988). XRD studies on barium titanate (BaTiO 3)/polyvinylidene fluoride (PVDF) composites. *Journal of Materials Science, 23*(2), 410-414.

Ng, K.-S., Wong, Y.-M., Tsuge, T., & Sudesh, K. (2011). Biosynthesis and characterization of poly (3-hydroxybutyrate-*co*-3-hydroxyvalerate) and poly (3-hydroxybutyrate-*co*-3-hydroxyhexanoate) copolymers using jatropha oil as the main carbon source. *Process Biochemistry, 46*(8), 1572-1578.

Nhan, D. T., Wille, M., De Schryver, P., Defoirdt, T., Bossier, P., & Sorgeloos, P. (2010). The effect of poly *β*-hydroxybutyrate on larviculture of the giant freshwater prawn *Macrobrachium rosenbergii*. *Aquaculture, 302*(1-2), 76-81.

Ni, Y.-Y., Chung, M. G., Lee, S. H., Park, H.-Y., & Rhee, Y. H. (2010). Biosynthesis of medium-chain-length poly (3-hydroxyalkanoates) by volatile aromatic hydrocarbons-degrading *Pseudomonas fulva* TY16. *Bioresource Technology, 101*(21), 8485-8488.

Oh, S.-E., & Logan, B. E. (2006). Proton exchange membrane and electrode surface areas as factors that affect power generation in microbial fuel cells. *Applied Microbiology and Biotechnology, 70*(2), 162-169.

Oh, S., & Logan, B. E. (2005). Hydrogen and electricity production from a food processing wastewater using fermentation and microbial fuel cell technologies. *Water Research, 39*(19), 4673-4682.

Ong, H. R., Woon, C. W., Ahmad, M. S., Yousuf, A., Cheng, C. K., & Khan, M. M. R. (2018). Facile synthesis of PVP-MnO_2/CNT composites as ORR electrocatalyst for an air-cathode microbial fuel cell. *International Journal of Electrochemical Science, 13*(8), 7789-7799.

Ortiz-Martínez, V., Salar-García, M., Hernández-Fernández, F., & De los Ríos, A. (2015). Development and characterization of a new embedded ionic liquid based membrane-cathode assembly for its application in single chamber microbial fuel cells. *Energy, 93*, 1748-1757.

Ozden, A., Ercelik, M., Ozdemir, Y., Devrim, Y., & Colpan, C. O. (2017). Enhancement of direct methanol fuel cell performance through the inclusion of zirconium phosphate. *International Journal of Hydrogen Energy, 42*(33), 21501-21517.

Papiya, F., Pattanayak, P., Kumar, P., Kumar, V., & Kundu, P. P. (2018). Development of highly efficient bimetallic nanocomposite cathode catalyst, composed of Ni:Co supported sulfonated polyaniline for application in microbial fuel cells. *Electrochimica Acta, 282*, 931-945.

Parmar, A., Singh, N. K., Pandey, A., Gnansounou, E., & Madamwar, D. (2011). Cyanobacteria and microalgae: a positive prospect for biofuels. *Bioresource Technology, 102*(22), 10163-10172.

Phukon, P., Saikia, J. P., & Konwar, B. K. (2011). Enhancing the stability of colloidal silver nanoparticles using polyhydroxyalkanoates (PHA) from *Bacillus circulans* (MTCC 8167) isolated from crude oil contaminated soil. *Colloids and Surfaces B: Biointerfaces, 86*(2), 314-318.

Prieto, M. A. (2007). From oil to bioplastics, a dream come true? *Journal of Bacteriology, 189*(2), 289-290.

Pu, K. B., Ma, Q., Cai, W. F., Chen, Q. Y., Wang, Y. H., & Li, F. J. (2018). Polypyrrole modified stainless steel as high performance anode of microbial fuel cell. *Biochemical Engineering Journal, 132*, 255-261.

Qiao, Y., Wu, X.-S., & Li, C. M. (2014). Interfacial electron transfer of Shewanella putrefaciens enhanced by nanoflaky nickel oxide array in microbial fuel cells. *Journal of Power Sources, 266*, 226-231.

Rabaey, K., & Verstraete, W. (2005). Microbial fuel cells: Novel biotechnology for energy generation. *Trends in Biotechnology, 23*(6), 291-298.

Rangel-Cárdenas, A., & Koper, G. (2017). Transport in proton exchange membranes for fuel cell applications—a systematic non-equilibrium approach. *Materials, 10*(6), Article#576.

Ren, Q., Ruth, K., Thöny-Meyer, L., & Zinn, M. (2010). Enatiomerically pure hydroxycarboxylic acids: current approaches and future perspectives. *Applied Microbiology and Biotechnology, 87*(1), 41-52.

Reusch, R. (2014). Biogenesis of ion channels. *Journal of Biochemistry and Biophysics, 1*, 1-24.

Rice, E. W., Baird, R. B., Eaton, A. D., & Clesceri, L. S. (2012). Standard methods for the examination of water and wastewater (Vol. 10), Washington DC, American Public Health Association.

Roh, S.-H., & Woo, H.-G. (2015). Carbon nanotube composite electrode coated with polypyrrole for microbial fuel cell application. *Journal of Nanoscience and Nanotechnology, 15*(1), 484-487.

Rout, S., Nayak, A. K., Varanasi, J. L., Pradhan, D., & Das, D. (2018). Enhanced energy recovery by manganese oxide/reduced graphene oxide nanocomposite as an air-cathode electrode in the single-chambered microbial fuel cell. *Journal of Electroanalytical Chemistry, 815*, 1-7.

Rudra, R., Kumar, V., Pramanik, N., & Kundu, P. P. (2017). Graphite oxide incorporated crosslinked polyvinyl alcohol and sulfonated styrene nanocomposite membrane as separating barrier in single chambered microbial fuel cell. *Journal of Power Sources, 341*, 285-293.

Sabirova, J., Golyshin, P., Ferrer, M., Lunsdorf, H., Abraham, W.-R., & Timmis, K. (2014). Extracellular polyhydroxyalkanoates produced by genetically engineered microorganisms: *U.S. Patent No. 8,623,632*. Washington, DC: U.S. Patent and Trademark Office.

Salih, A., Ahmad, M., Ibrahim, N., Dahlan, K., Tajau, R., Mahmood, M., & Yunus, W. (2015). Synthesis of radiation curable palm oil–based epoxy acrylate: NMR and FTIR spectroscopic investigations. *Molecules, 20*(8), 14191-14211.

Sánchez, R. J., Schripsema, J., da Silva, L. F., Taciro, M. K., Pradella, J. G., & Gomez, J. G. C. (2003). Medium-chain-length polyhydroxyalkanoic acids (PHAmcl) produced by *Pseudomonas putida* IPT 046 from renewable sources. *European Polymer Journal, 39*(7), 1385-1394.

Sarathi, V. S., & Nahm, K. S. (2013). Recent advances and challenges in the anode architecture and their modifications for the applications of microbial fuel cells. *Biosensors and Bioelectronics, 43*, 461-475.

Saravanan, N., & karthikeyan, M. (2017). Study of single chamber and double chamber efficiency and losses of wastewater treatment. *International Research Journal of Engineering and Technology, 5*(3), 1225-1230.

Sekar, N., & Ramasamy, R. P. (2013). Electrochemical impedance spectroscopy for microbial fuel cell characterization. *Journal of Microbial and Biochemical Technology, 5*(S6), Article#004.

Senthilkumar, N., Pannipara, M., Al-Sehemi, A. G., & Kumar, G. G. (2019). PEDOT/NiFe$_2$O$_4$ nanocomposites on biochar as a free-standing anode for high-performance and durable microbial fuel cells. *New Journal of Chemistry, 43*(20), 7743-7750.

Sevda, S., Dominguez-Benetton, X., Vanbroekhoven, K., Sreekrishnan, T., & Pant, D. (2013). Characterization and comparison of the performance of two different separator types in air–cathode microbial fuel cell treating synthetic wastewater. *Chemical Engineering Journal, 228*, 1-11.

Shishatskaya, E., Volova, T., Efremov, S., Puzyr', A., & Mogil'Naya, O. (2002). Tissue response to biodegradable suture threads made of polyhydroxyalkanoates. *Biomedical Engineering, 36*(4), 210-217.

Shishatskaya, E., Volova, T., Puzyr, A., Mogilnaya, O., & Efremov, S. (2004). Tissue response to the implantation of biodegradable polyhydroxyalkanoate sutures. *Journal of Materials Science: Materials in Medicine, 15*(6), 719-728.

Silva, T. C. D. E., Bhowmick, G. D., Ghangrekar, M. M., Wilhelm, M., & Rezwan, K. (2019). SiOC-based polymer derived-ceramic porous anodes for microbial fuel cells. *Biochemical Engineering Journal, 148*, 29-36.

Sivasankaran, A., Sangeetha, D., & Ahn, Y. H. (2016). Nanocomposite membranes based on sulfonated polystyrene ethylene butylene polystyrene (SSEBS) and sulfonated SiO$_2$ for microbial fuel cell application. *Chemical Engineering Journal, 289*, 442-451.

Theodorou, E. C., Theodorou, M. C., & Kyriakidis, D. A. (2011). AtoSC two-component system is involved in cPHB biosynthesis through fatty acid metabolism in *E. coli*. *Biochimica et Biophysica Acta (BBA)-General Subjects, 1810*(5), 561-568.

Tofighi, A., Rahimnejad, M., & Ghorbani, M. (2018). Ternary nanotube α-MnO$_2$/GO/AC as an excellent alternative composite modifier for cathode electrode of microbial fuel cell. *Journal of Thermal Analysis and Calorimetry, 135*(3), 1667-1675.

Venkatesan, P. N., & Dharmalingam, S. (2017). Characterization and performance study of phase inversed Sulfonated Poly Ether Ether Ketone - Silico tungstic composite membrane as an electrolyte for microbial fuel cell applications. *Renewable Energy, 102*, 77-86.

Wang, P., Li, H., & Du, Z. (2014). Polyaniline synthesis by cyclic voltammetry for anodic modification in microbial fuel cells. *International Journal of Electrochemical Science, 9*, 2038-2046.

Wang, X. Y., He, H. B., Zheng, C. C., & Guo, Q. J. (2014). Preparation and performance of PANI/MWNT composite films anode for microbial fuel cell. *Particle Science and Engineering, 347*, 62-74.

Ward, A. J., Lesic, R. A., Proschogo, N., Masters, A. F., & Maschmeyer, T. (2015). Strained surface siloxanes as a source of synthetically important radicals. *Rsc Advances, 5*(122), 100618-100624.

Wei, J., Liang, P., & Huang, X. (2011). Recent progress in electrodes for microbial fuel cells. *Bioresource Technology, 102*(20), 9335-9344.

Williams, S. F., Martin, D. P., Horowitz, D. M., & Peoples, O. P. (1999). PHA applications: Addressing the price performance issue: I. Tissue engineering. *International Journal of Biological Macromolecules, 25*(1-3), 111-121.

Winfield, J., Chambers, L. D., Rossiter, J., & Ieropoulos, I. (2013a). Comparing the short and long term stability of biodegradable, ceramic and cation exchange membranes in microbial fuel cells. *Bioresource Technology, 148*, 480-486.

Winfield, J., Ieropoulos, I., Rossiter, J., Greenman, J., & Patton, D. (2013b). Biodegradation and proton exchange using natural rubber in microbial fuel cells. *Biodegradation, 24*(6), 733-739.

Xia, B. Y., Yan, Y., Li, N., Wu, H. B., Lou, X. W. D., & Wang, X. (2016). A metal–organic framework-derived bifunctional oxygen electrocatalyst. *Nature Energy, 1*(1), Article#15006.

Xiao, L., Damien, J., Luo, J., Jang, H. D., Huang, J., & He, Z. (2012). Crumpled graphene particles for microbial fuel cell electrodes. *Journal of Power Sources, 208*, 187-192.

Xiao, L., & He, Z. (2015). Application of graphene-based materials to improve electrode performance in microbial fuel cells. Graphene-based Energy Devices, Wiley, *13*, 355-370.

Xue, Y., & Chan, S. (2015). Layer-by-layer self-assembly of CHI/PVS–Nafion composite membrane for reduced methanol crossover and enhanced DMFC performance. *International Journal of Hydrogen Energy, 40*(4), 1877-1885.

Yellappa, M., Sravan, J. S., Sarkar, O., Reddy, Y. V. R., & Mohan, S. V. (2019). Modified conductive polyaniline-carbon nanotube composite electrodes for bioelectricity generation and waste remediation. *Bioresource Technology, 284*, 148-154.

Yıldrım, A., & Seçkin, T. (2014). In situ preparation of polyether amine functionalized MWCNT nanofiller as reinforcing agents. *Advances in Materials Science and Engineering, 2014,* 1-6.

Yin, T., Zhang, H., Yang, G. Q., & Wang, L. (2019). Polyaniline composite TiO_2 nanosheets modified carbon paper electrode as a high performance bioanode for microbial fuel cells. *Synthetic Metals, 252*, 8-14.

Yousefi, V., Mohebbi-Kalhori, D., & Samimi, A. (2018). Application of layer-by-layer assembled chitosan/montmorillonite nanocomposite as oxygen barrier film over the ceramic separator of the microbial fuel cell. *Electrochimica Acta, 283*, 234-247.

Yu, F., Wang, C., & Ma, J. (2016). Applications of graphene-modified electrodes in microbial fuel cells. *Materials, 9*(10), Article#807.

Yuan, H., Deng, L., Tang, J., Zhou, S., Chen, Y., & Yuan, Y. (2015). Facile synthesis of MnO_2/polypyrrole/MnO_2 multiwalled nanotubes as advanced electrocatalysts for the oxygen reduction reaction. *ChemElectroChem, 2*(8), 1152-1158.

Yusuf, H., Annuar, M. S. M., Subramaniam, R., & Gumel, A. M. (2018). Amphiphilic biopolyester-carbon nanotubes anode enhances electrochemical activities of microbial fuel cell. *Chemical Engineering & Technology*, *42*(3), 566-574.

Yusuf, H., Annuar, M. S. M., Syed Mohamed, S. M. D., & Subramaniam, R. (2018). Medium-chain-length poly-3-hydroxyalkanoates-carbon nanotubes composite as proton exchange membrane in microbial fuel cell. *Chemical Engineering Communications*, *206*(6), 731-745.

Zhang, J., Shishatskaya, E. I., Volova, T. G., da Silva, L. F., & Chen, G.-Q. (2018). Polyhydroxyalkanoates (PHA) for therapeutic applications. *Materials Science and Engineering: C, 86*, 144-150.

Zhang, T., Cui, C., Chen, S., Yang, H., & Shen, P. (2008). The direct electrocatalysis of *Escherichia coli* through electroactivated excretion in microbial fuel cell. *Electrochemistry Communications, 10*(2), 293-297.

Zhang, X., Luo, R., Wang, Z., Deng, Y., & Chen, G.-Q. (2009). Application of (*R*)-3-hydroxyalkanoate methyl esters derived from microbial polyhydroxyalkanoates as novel biofuels. *Biomacromolecules, 10*(4), 707-711.

Zhang, X., Wei, C., He, Q., & Ren, Y. (2010). Enrichment of chlorobenzene and o-nitrochlorobenzene on biomimetic adsorbent prepared by poly-3-hydroxybutyrate (PHB). *Journal of Hazardous Materials, 177*(1-3), 508-515.

Zhao, F., Rahunen, N., Varcoe, J. R., Roberts, A. J., Avignone-Rossa, C., Thumser, A. E., & Slade, R. C. (2009). Factors affecting the performance of microbial fuel cells for sulfur pollutants removal. *Biosensors and Bioelectronics, 24*(7), 1931-1936.

Zhou, M., Wang, H., Hassett, D. J., & Gu, T. (2013). Recent advances in microbial fuel cells (MFCs) and microbial electrolysis cells (MECs) for wastewater treatment, bioenergy and bioproducts. *Journal of Chemical Technology & Biotechnology, 88*(4), 508-518.

Zhu, D. D., Liu, J. L., & Qiao, S. Z. (2016). Recent advances in inorganic heterogeneous electrocatalysts for reduction of carbon dioxide. *Advanced Materials, 28*(18), 3423-3452.

Zinadini, S., Zinatizadeh, A. A., Rahimi, M., Vatanpour, V., & Rahimi, Z. (2017). High power generation and COD removal in a microbial fuel cell operated by a novel sulfonated PES/PES blend proton exchange membrane. *Energy, 125*, 427-438.

LIST OF PUBLICATIONS AND PAPERS PRESENTED

LIST OF PUBLICATIONS

Sirajudeen, A. A. O., Annuar, M. S. M., & Subramaniam, R. (2020). Composite of medium-chain-length polyhydroxyalkanoates-co-methyl acrylate and carbon nanotubes as innovative electrodes modifier in microbial fuel cell. *Biotechnology and Applied Biochemistry,* doi: org/10.1002/bab.1928.

LIST OF PRESENTATIONS

Sirajudeen, A. A. O., Annuar, M. S. M. *Improved Performance of Microbial Fuel Cell with Nanocomposite of Medium-Chain-Length Polyhydroxyalkanoates-co-Methyl Acrylate Carbon Nanotubes as Electrodes Modifier*. Paper presented at 2nd International Postgraduate Symposium in Biotechnology 2019 (IPSB2019), 24th – 25th September 2019, Johor, Malaysia

Sirajudeen, A. A. O., *Polyhydroxyalkanoates for Innovative Electrodes and Proton Exchange Membrane Modification in Microbial Fuel Cell*. Seminar presentation on 10th June 2020, University of Malaya, Malaysia